

UC San Diego

UC San Diego Electronic Theses and Dissertations

Title

Topology, frustration, folding and function of the inflammatory cytokine Interleukin-1[beta]

Permalink

<https://escholarship.org/uc/item/3mv5d8q8>

Author

Capraro, Dominique T.

Publication Date

2008

Peer reviewed|Thesis/dissertation

UNIVERSITY OF CALIFORNIA, SAN DIEGO

**Topology, Frustration, Folding and Function of the
Inflammatory Cytokine Interleukin-1 β**

A Dissertation submitted in partial satisfaction of the
requirements for the degree of Doctor of Philosophy

in

Chemistry

by

Dominique T. Capraro

Committee in Charge:

Professor Patricia A. Jennings, Chair
Professor William S. Allison
Professor Doug Magde
Professor José N. Onuchic
Professor Shankar Subramaniam

Copyright

Dominique T. Capraro, 2008

All rights reserved.

The Dissertation of Dominique T. Capraro is approved, and it is acceptable in quality and form for publication on microfilm:

Chair

University of California, San Diego
2008

TABLE OF CONTENTS

	Signature Page.....	iii
	Table of Contents.....	iv
	List of Abbreviations.....	vi
	List of Figures.....	viii
	List of Tables.....	xi
	Dedication.....	xiii
	Acknowledgements.....	xiv
	Vita.....	xvii
	General Abstract.....	xviii
Chapter 1	General Introduction.....	1
Chapter 2	General Methods.....	11
Chapter 3	Circular Permutation of Interleukin-1 β Does Not Affect the Native Global Fold.....	25
	Abstract.....	26
	Introduction.....	26
	Specific Methods.....	28
	Results.....	31
	Discussion.....	49
Chapter 4	Circular Permutation of Interleukin-1 β Affects the Transition of the Folding Intermediate to the Native Ensemble.....	55
	Abstract.....	56
	Introduction.....	56

	Specific Methods.....	61
	Results.....	63
	Discussion.....	78
Chapter 5	Removal of the β -Bulge Functional Loop has No Affect on the Global Fold While Altering the Formation of the Kinetic Intermediate.....	83
	Abstract.....	84
	Introduction.....	84
	Specific Methods.....	86
	Results.....	90
	Discussion.....	110
Chapter 6	The Capturing the Folding Moment: Folding/Backtracking and the Refolding of Interleukin-1 β using Real-Time NMR.....	114
	Abstract.....	115
	Introduction.....	115
	Special Methods.....	119
	Results and Discussion.....	121
Chapter 7	Conclusions.....	129
References	135

LIST OF ABBREVIATIONS

AmSO ₄	Ammonium Sulfate
ANS	1, anilino-naphthalene 8-sulfonate
βME	β-mercaptoethanol
CO	contact order
DHFR	Dihydrofolate reductase
DTT	Dithiothreitol
E. coli	Escherichia coli
EDTA	ethylene diamine tetraacetic acid
Gnd-HCl	guanidine hydrochloride
H/D	hydrogen-deuterium
HDX	hydrogen-deuterium exchange
HSQC	heteronuclear single quantum coherence
IL-1β	Interleukin-1β
IL-1ra	Interleukin-1 receptor antagonist
IPTG	Isopropyl β-D-1-thiogalactopyranoside
LB	Luria Broth
MD	molecular dynamics
MES	2-(N-morpholino) ethanesulfonic acid
NMR	Nuclear magnet resonance
PCR	Polymer chain reaction
PM	permutation

PMSF	phenylmethysulphonyl fluoride
WT	wild type

LIST OF FIGURES

Figure 1-1:	Schematic of the 12 strands that form the β -trefoil fold of IL-1 β	6
Figure 1-2:	2D splay representation depicting (A) Pulse-labeling and (B) hydrogen/deuterium exchange (H/D) of WT IL-1 β	7
Figure 3-1:	Schematic of tandem-gene design for the construction of the IL-1 β permutations and linker variants.....	29
Figure 3-2:	Schematic indicating the location of the cut sited for permutant variants of IL-1 β	33
Figure 3-3:	Analysis of the fingerprint pattern of ^1H - ^{15}N -HSQC spectra of (A) PM52 and (B) PM100 indicate denatured protein.....	35
Figure 3-4:	Analysis of the fingerprint pattern of ^1H - ^{15}N -HSQC spectra of wild type and permutant IL-1 β strongly indicate similar tertiary structure and an intact β -trefoil fold.....	36
Figure 3-5:	Effects of the permutations on $^{13}\text{C}^\alpha$ chemical shifts of permutant IL-1 β residues indicate differences at turns and hinge-points of the molecules.....	38
Figure 3-6:	A representation of the similarity in the Ramachandran plot of PM23 (A) and PM142 (B) with respect to WT IL-1 β along with the effects of the changes mapped back onto the molecule.....	40
Figure 3-7:	A representation of the similarity in the Ramachandran plot of PM65 (A) and PM76 (B) with respect to WT IL-1 β along with the effects of the changes mapped back onto the molecule.....	41
Figure 3-8:	Time course of hydrogen-deuterium (HDX) exchange via NMR. ^1H - ^{15}N -HSQC at various time points during the H/D exchange experiment.....	44
Figure 3-9:	Representative comparisons of H^N solvent exchange rates between WT IL-1 β and permutant proteins.....	45
Figure 3-10:	Illustrations depicting hydrogen/deuterium exchange (H/D) for the IL-1 β permutations, (A) PM23 and (B) PM65.....	46
Figure 3-11:	Illustrations depicting hydrogen/deuterium exchange (H/D) for the 1 β permutations, (A) PM76 and (B) PM142.....	47

Figure 3-12:	The estimated protection factors show similar pattern of protection for all proteins with four β -strands showing less protection in the region located near the functional loop.....	48
Figure 4-1:	Schematic of tandem-gene design for the construction of the IL-1 β permutant linker variants.....	62
Figure 4-2:	Analysis of the fingerprint pattern of ^1H - ^{15}N -HSQC spectra of wild type and permutant IL-1 β strongly indicate similar tertiary structure and an intact β -trefoil fold.....	64
Figure 4-3:	Plots of F apparent (F_{app}) as a function of denaturant concentration for the equilibrium unfolding of wild type and permutant proteins at pH 6.5 and 25°C indicate destabilized protein variants.....	65
Figure 4-4:	Representative traces of the fast phase (t_2) of folding collected by stopped- flow fluorescence indicating the similarities in the observed rates of folding.....	68
Figure 4-5:	Representative traces of manual mixing fluorescence kinetics for wild type and circularly permuted IL-1 β showing the differences in the observed refolding kinetics.....	71
Figure 4-6:	Chevron plots of the log of the relaxation rates for the permutations of IL-1 β indicating the similarities and differences in determined folding rates.....	72
Figure 4-7:	Analysis of the fingerprint pattern of ^1H - ^{15}N -HSQC spectra of wild type IL-1 β and the respective linker variants strongly indicate similar tertiary structure to the parent permutant, PM76, and an intact β -trefoil fold.....	74
Figure 4-8:	Plots of the equilibrium titration showing no difference in equilibrium stability or cooperativity and chevron plot showing no variation in folding kinetics due to linker size.....	76
Figure 5-1:	2D splay diagrams of the secondary structure of (A) IL-1 β and (B) IL-1 β with the β -bulge removed and replaced with a loop to mimic IL-1ra.....	88
Figure 5-2:	Comparison spectra of the fingerprint pattern of ^1H - ^{15}N -HSQC spectra of the bulge-deletion construct (cyan) and wild type IL-1 β (black) indicate similar tertiary structure and an intact	

	β -trefoil fold.....	91
Figure 5-3:	Representative ^1H - ^{15}N HSQC spectra of bulge-deletion construct indicating assigned resonance peaks.....	93
Figure 5-4:	Affects of the bulge-deletion on $^{13}\text{C}^\alpha$ chemical shifts of the chimeric IL-1 β residues indicate differences at turns and hinge-points of the molecule.....	94
Figure 5-5:	Representation of (A) the Ramachandran plot of the bulge-less construct of IL-1 β overlaid with (B) the differences mapped onto the molecule indicating changes in the first turn of the first trefoil subunit, where differences moved into different regions of phi/psi space.....	96
Figure 5-6:	A series of ^1H - ^{15}N -HSQC spectra demonstrating the time course of hydrogen-deuterium (HDX) exchange monitored by NMR for the bulge-less IL-1 β variant.....	98
Figure 5-7:	Representative comparisons of H^N solvent exchange rates for bulge-less variant of IL-1 β	99
Figure 5-8:	Representation of the results from H/D exchange indicates a more dynamic protein with less sites of protection upon removal of the β -bulge.....	100
Figure 5-9:	Representation of the results from comparing the H/D solvent exchange data of the bulge-less construct with WT IL-1 β . Differences appear away from the site of the loop deletion.....	102
Figure 5-10:	Plots of F apparent (F_{app}) as a function of denaturant concentration for the equilibrium unfolding of IL-1 β and the β -bulge deletion construct showing similar stability.....	103
Figure 5-11:	Representative traces of the fast phase (t_2) of folding collected by stopped- flow fluorescence indicating the differences in the observed rates of folding.....	108
Figure 5-12:	Chevron Plot of the log of the relaxation rates for the construct of IL-1 β containing the bulge deletion showing effects in intermediate formation and in unfolding.....	109
Figure 6-1:	Representations of the IL-1 β and the theoretical folding routes of interleukin-1 β based on simulation data by Chavez et al., 2006.....	117

Figure 6-2:	A visual representation of the multiple folding routes of interleukin-1 β based on simulation data by Chavez et al., 2006.....	118
Figure 6-3:	2D representation of the final fold of WT IL-1 β in 0.8M Gnd-HCl....	122
Figure 6-4:	Schematic of serial 1D spectra representing the core resonances of the molecule during the refolding reaction for (A) WT IL-1 β and (B) the functional loop deletion construct of IL-1 β	124
Figure 6-5:	Time-dependent ^1H - ^{15}N spectral changes of representative regions in WT (blue) and in the bulge-less construct (orange) during the refolding.....	125
Figure 6-6:	Schematic of serial 1D spectra representing the core resonances of the molecule during the refolding reaction for a permutation of the IL-1 β protein.....	127
Figure 7-1:	Representation of IL-1 β bond to the IL-1R1 receptor with ^{13}C chemical shift deviations highlighted, showing the potential biological relevance for these changes in IL-1 β constructs.	132

LIST OF TABLES

Table 4-1:	Thermodynamic Parameters for WT and permutant IL-1 β	66
Table 4-2:	Thermodynamic Parameters for PM76 and Permutant Linker Variants.....	77
Table 5-1:	Thermodynamic Parameter Comparison for IL-1 β and the Deletion Construct.....	104

DEDICATION

I would like to dedicate this thesis to Gabriel and Stella who have given me the most to live for, their love. If it were not for their continued love and support, this journey that graduate school took us on may never have come to a joyous conclusion. Thank you for helping me push through and reach the end of this journey and embark on a new, more adventurous one. I love you both, very much!!

ACKNOWLEDGEMENTS

This has been an incredible, challenging journey. I would like to thank my advisor, Patricia Jennings, for having faith in my ability to be a good scientist, worthy of a Ph.D. I am grateful for her guidance and mentorship, not only in science but in life. She has been one of the sources of my inspiration to be a scientist and to be a good mother. I am also very thankful for her sense of humor. I think that humor is a great way to elevate stress and, let me tell you, there have been plenty of moments! I am grateful that nothing was taken too much to heart. It has been a pleasure to work with her and be challenged by her. I am very appreciative of the space and independence that she gave me to learn at my pace, and the patience that she has had in guiding me in the proper way to approach an answer. Thank you for all of your help!

I would like to thank my committee for their insightfulness and guidance throughout my graduate career. I would especially like to thank Dr. José Onuchic for opening my eyes to the theoretical world and for patiently demonstrating the significance in the shared views between experimentalists and theoreticians. The collaborations that we have shared have been very exciting and educational and I hope that they will continue.

I would like to thank all the current and past members of the Jennings lab including Dave Heidary, John Finke, Jaime Covalt, Ben Andrews, Michael Jamros, and John Zuris for all of their support. I would like to individually thank Melinda Roy for being instrumental in my growth as a scientist and for all of her help in getting me to

this point. I am certain that without her help, this journey may not have ended as well as it did. Her insight and perspective were fundamental in my growth and achievement. I would also like to thank Kendra Hailey for all of her scientific insight throughout our time together and her dedication and help in the final months, helping me push to get to the end. There are no words to describe my gratitude. I would like to also thank Jamie Mills and Andrea Schoenfish, my officemates, for all of their support and help, especially within the last few months, that was instrumental in my success and achievement. Their patience and compassion were very gracious.

I would like to acknowledge and thank my two former office mates, Ryan Bertsch, Lilly Wong and Yuki Horiuchi, for being great friends and accomplished scientists. They welcomed me into the lab and helped me build a solid scientific foundation. In particular, Lilly was instrumental in my growth as a leader in the lab by being a solid example of one herself. She was a excellent example of how the transition from graduate “newbie”, to senior graduate student, to post doc, includes a growth in guidance and mentoring of fellow students in lab. She patiently taught me to be meticulous and share that wealth with others. I aspire to be as good as her in the lab!

There are many friends and colleagues that I would like to thank for their love and support throughout the years, including Jason Fienberg, Sean Studer and Remi Merhi. I am very grateful for their friendship.

Finally, I would like to thank my family for all of their love and support in all of my years of education. I would like to thank my parents for instilling in me the importance of a work ethic and the value in the integrity in one's work. They have been true “lead-by-example” people, where day in and day out, they have shown that hard

work does pay off and that you can achieve what you set your mind to if you persevere. Thank you for being great teachers in life, I love you. I would also like to thank Gabriel for giving me all the intangibles in my quest to getting my doctorate, from food on the table to company in the wee hours of the morning, when I had to go back to lab, to a beautiful little girl!! I really cannot express enough how thankful and grateful I am for all that he has done. Thank you for all the dedication and support and love, and especially thank you for your patience. Getting here would not have been possible had it not been for him. This achievement is as much his as it is mine. Thank you for everything, ti amo!

Vita

- | | |
|------|--|
| 2001 | B.S Food Science and Nutrition, Chapman University
Minor: Chemistry |
| 2008 | Ph.D., Chemistry, University of California, San Diego |

Publications

Mark L Paddock, Sandra E Wiley, Herbert L Axelrod, Aina E Cohen, Melinda Roy, Edward C Abresch, **Dominique Capraro**, Anne N Murphy, Rachel Nechushtai, Jack E Dixon, Patricia A Jennings. MitoNEET is a uniquely folded 2Fe-2S outer mitochondrial membrane protein stabilized by pioglitazone. P Natl Acad Sci Usa (2007) vol. 104 (36) pp. 14342-14347

Honors

GAAN Fellowship 2001-2002

ABSTRACT OF DISSERTATION

**Topology, Frustration, Folding and Function of the
Inflammatory Cytokine Interleukin-1 β**

by

Dominique T. Capraro

Doctor of Philosophy in Chemistry

University of California, San Diego, 2008

Professor Patricia A. Jennings, Chair

One of the most intriguing problems in biology today continues to be centered on understanding the mechanism by which a newly synthesized linear polypeptide chain attains its functional three-dimensional native structure. Initially, it was thought that the fundamental problem arose because even a small protein has access to an enormous number of possible conformational states, which could not be searched through in a random way in any reasonable way in any reasonable length of time. This problem became known as the “Levinthal Paradox” because proteins do fold in a timely fashion

and people are interested in the mechanism by which the primary structure directs folding of the protein to the fully folded state. In real proteins, the interplay of chain connectivity with desired structure and function creates ruggedness on the folding landscape, making a rough or partially frustrated funnel. Interleukin-1 β (IL-1 β) is an ideal system for experimental determination of the role of topology on folding mechanisms. IL-1 β adopts a β -trefoil fold, where the tertiary fold is formed from six two-stranded hairpins, three of which form a barrel structure and the other three form a triangular array to “cap” one end of the barrel. The study of circular permuted proteins presents a particularly interesting way of testing this topology-based model. By changing the connectivity through the construction IL-1 β circular permutations, we studied the balance between topology and energetics on the formation of the intermediate and the overall folding mechanism. In this study, the role of topology and the affects circular permutations have on folding and the native state of IL-1 β was investigated. Using a combination of techniques, such as H/D, ^{13}C chemical shift analysis (CSI), stopped-flow and manual mixing fluorescence, we characterize the stability, the native state, and the folding mechanisms for several permutations. We also test the affects of the frustration of the β -bulge on the native state by engineering a loop swap from IL-1ra. These studies reveal topological similarities among the variants of engineered proteins.

Chapter 1

General Introduction

One of the most intriguing problems in biology today continues to be centered on understanding the mechanism by which a newly synthesized linear polypeptide chain attains its functional three-dimensional native structure (1). Initially, it was thought that the fundamental problem arose because even a small protein has access to an enormous number of possible conformational states, which could not be searched through in a random way in any reasonable way in any reasonable length of time (2). This problem became known as the “Levinthal Paradox” because proteins do fold in a timely fashion and people interested in the mechanism by which the primary structure directs folding of the protein to the fully folded state.

Proteins progress through a complex network of elementary reactions involving solvent influenced conformational changes as they fold, where simple empirical patterns (such as linear free energy relationships) can describe the experimentally observed reactions (3, 4). A major advance then, came when it was realized that this simplicity arises from the global organization of the energies of the possible conformations into a funneled folding landscape (4). In contrast, a random polypeptide chain samples many globally different structures within a few kT. The ground state of such a random polypeptide arises from competition between conflicting energy contributions and the resulting landscape can be described as “frustrated”. Even a minor change in sequence could cause an alternate structure to become the new ground state. Thus, the energy landscape for a random sequence would be “rugged” and the dynamics “glassy”. This type of landscape would be disastrous to an evolving organism, as random mutations could destroy structures that had evolved for a particular function.

However, it is hypothesized that protein structures evolved by selection of sequences where interactions are not in conflict as described above for the random polypeptide, but are supportive and cooperatively lead to a low-energy structure and the energy landscape is “funneled”. This funneling predicts simple kinetics for small single domain proteins, in agreement with experimental results (5-9).

Because energetic frustration is sufficiently small, geometrical effects become the dominant factor determining the structural heterogeneity of the transition state ensemble and possible intermediates during the folding event. Well-designed energy landscapes have minimal trapping. Thus, protein models that lack energetic “frustration” and encode only the native structure (Gō-type) can capture the main structural features of the transition states and intermediates found in experimental studies of small globular proteins (10-16). These models not only make computation faster but also give results that are easier to analyze. In real proteins, the interplay of chain connectivity with desired structure and function creates ruggedness on the folding landscape, making a rough or partially frustrated funnel. This frustration can be studied with the C α model in which all frustration is due to the native fold and to the interactions of functional loops across the protein.

While it is largely accepted that the landscape for the folding of small two-state folding proteins is funneled (17-25), it is clear that more complex, larger proteins and enzymes are subject to the competing pressures of efficient folding, maintaining function and avoiding toxic gain of function during evolution (26-32). Topologically driven models are not limited to small single-domain two-state folding proteins as work from the Onuchic and Jennings laboratories have demonstrated that such topology-

based folding models also correctly simulated the experimental folding mechanisms of the large systems dihydrofolate reductase (DHFR) and IL-1 β (33-35). In addition, the same holds true for the members of the β -trefoil family of proteins, IL-1 β , FGF-1 and hisactophilin (36). These proteins share similar topologies, low sequence homology, and folding mechanisms that includes the population of discrete intermediates under certain conditions (6, 15, 37-41).

IL-1 β is an ideal system for experimental determination of the role of topology on folding mechanisms. IL-1 β adopts a β -trefoil fold, which was first observed for the Kunitz inhibitor from soybean, and subsequently found in other protein families including the fibroblast growth factors, ricin-like toxins, and actin-binding hisactophilins (42). These families of proteins have distinct functions, occur in both intra- and extra-cellular space, and lack similarities in their binding partners (43). Thus, the proteins do not belong to the same superfamily, despite the striking structural similarities. Diagrams of the core structure of the β -trefoil of IL-1 β are shown in Figure 1-1 (36, 44). The core structure consists of 12 antiparallel β -strands connected by turns or loops. The tertiary fold is formed from six two-stranded hairpins, three of which form a barrel structure and the other three form a triangular array to “cap” one end of the barrel (Figure 1-1A). In the case of IL-1 β , one long loop in the protein (residues 30-39) contains 2.3 turns of a 3_{10} helix, but because the loop is surface exposed and lies outside the core of the protein, it is still considered an all β structure. The fold is characterized by a three-fold pseudo-symmetry consisting of three topological equivalent units with a repeating beta-beta-beta-Loop-beta ($\beta\beta\beta L\beta$) motif (Figure 1-1B) (44). These repeats are not detectable from sequence alignments, but are detectable with structural alignment

and superposition (42). In addition, patterns of residue-property conservation are apparent from structural alignment and are thought to define the fold (42). Throughout this study, a 2D splay diagram depicting the barrel and cap strands will be referred to in order to identify areas of the protein affected by the various experiments (Figure 1-1C).

IL-1 β is a slow folding protein. Experimental and theoretical studies agree that IL-1 β folds via early formation of a central core that is a well-populated kinetic intermediate (which is associated with the τ_2 phase) that forms on the millisecond timescale followed by turnover to the native structured state (which is associated with the τ_1 phase) that occurs on the seconds timescale (33, 38, 45, 46)(Figure 1-2A). Native hydrogen-deuterium solvent exchanges shows areas of solvent protection within the β -strands involved in the formation of the β -barrel and the cap (Figure 1-2B). Real-time NMR kinetic experiments of the denaturant-induced unfolding of IL-1 β revealed a rugged unfolded landscape where the native-like turns were important in creating the topology and the arrangement of the β -strands (47).

Experimentalists and theorists have shown that the folding rates for small two-state folding proteins correlate well with the topological parameter referred to as the relative contact order (*CO*) (7, 48-51). The parameter *CO* compares the difference in topology between proteins of different lengths. The parameter is small for proteins where local contacts are favored and large when residues in a protein interact with partners far away in the protein sequence. (7, 48). Relative contact order has been usefully captured the features of protein folding, where proteins with many local contacts (e.g. α -helices) fold faster than those with predominately non-local contacts (β -sheet proteins) (7, 52). While this simple topological parameter is effective in predicting

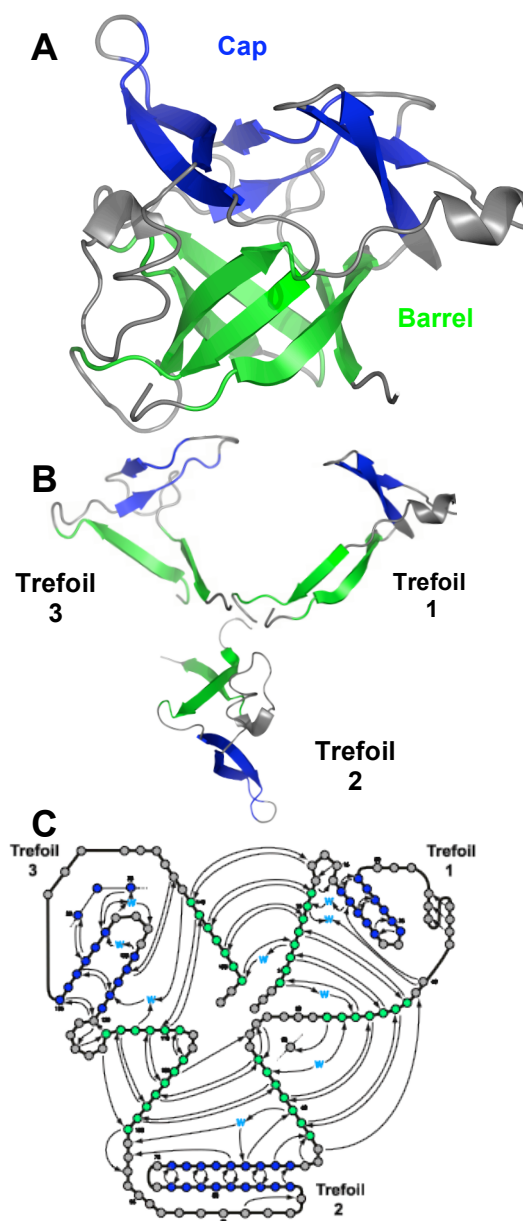


Figure 1-1: Schematic of the 12 strands that form the β -trefoil fold of IL-1 β .

(A) The molecule of IL-1 β (PDB ID 6I1B) colored to depict the strands forming the hairpin cap (**blue**) and those that form the β -barrel (**green**). (B) Following the same color scheme, a representation of the individual trefoils that comprise the overall pseudo trefoil fold of IL-1 β . (C) The 2D splay diagram depicting the barrel and cap strands in the same orientation as Figure 1B. This diagram is used throughout the publication in order to identify areas of the proteins affected by the various experiments. These illustrations were adapted from Chavez et al., 2006.

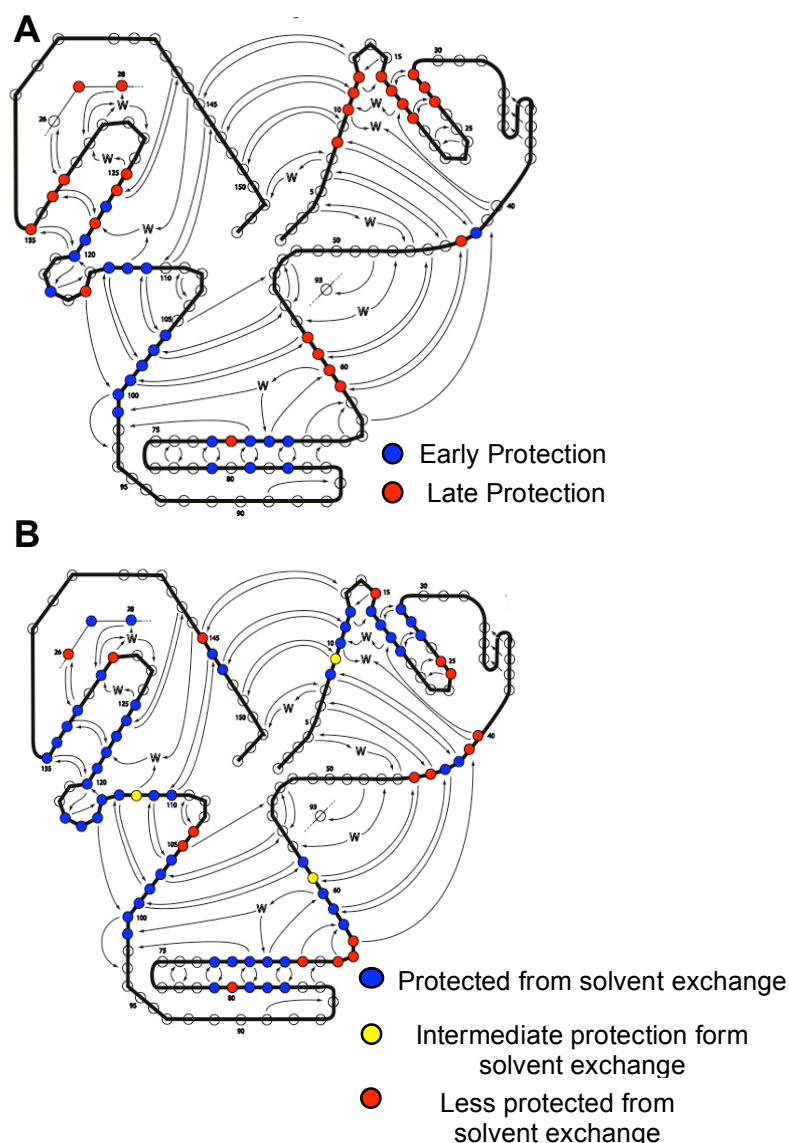


Figure 1-2: 2D splay representation depicting (A) Pulse-labeling and (B) hydrogen/deuterium exchange (H/D) of WT IL-1 β .

Results from pulse-labeling refolding NMR experiments reveal areas of early and late protection in WT IL-1 β during refolding. (B) NMR detected H/D exchange studies of WT IL-1 β were conducted to determine local or global differences in the native state stability of the secondary structure. Circles in the figure represent each amino acid in the polypeptide chain. Blue circles represent amide backbone residues that are stable, or protected, from deuterium exchange. Yellow circles represent residues that show some protection from exchange, or intermediate exchange, while red circles represent those residues that exchange away rapidly. Circles that are not colored represent amide backbone residues that could not be detected.

folding rates for small two-state folding proteins, it fails to predict the folding rates of larger, multi-state proteins (51). Therefore, changes in the contact order of larger proteins should have an affect on the rate of folding.

While changes in the contact order may affect the rate of folding for larger proteins, it does not affect the overall topology. The study of circular permuted proteins presents a particularly interesting way of testing this topology-based model. A circular permutation of bovine pancreatic trypsin inhibitor was first designed to investigate the role of chain connectivity on protein folding (53). Application of the same topology-based theoretical model to the study of circular permuted proteins for two simple two-state folding proteins, SH3 and CI2 was also in very good agreement with the experimental observations (49, 54, 55). The differences between the folding mechanisms of the permuted and wild type protein are correlated to the change in transition state. Based on simulated data, topology is an important determinant in the transition state and intermediate ensemble (15, 33, 48). In IL-1 β , experimental results indicate side-chain interactions also change the energetics of the folding funnel where the transition state has been altered for the rate-determining step in folding (34). By changing the connectivity through the construction IL-1 β circular permutations, we can study the balance between topology and energetics on the formation of the intermediate and the overall folding mechanism.

Proteins, however, do not have one landscape for folding and a different one for function. The challenge is generalizing these ideas to accommodate both folding and function. Since the minimally frustrated, funnel-like, landscape that has been successful

in understanding the folding mechanism, the question has turned to if it is sufficient to also explain function? Minimally frustrated landscapes have gone beyond protein folding and have characterized protein-protein recognition and binding mechanisms (56).

There is some speculation that functional residues are a hindrance to folding (57-60). Mutations in active and/or binding site residues cause reduced function. These residues need to be conserved for the protein to function correctly and therefore cannot be optimized for folding. However, the rest of the protein can evolve to make folding more efficient by making the energy landscape more funneled. Thus, it is possible that the most “frustrated” parts of the protein are the functional sites within the native structure of the protein.

In the case of the IL-1 family, the connecting loops provide the functional binding sites for protein-protein interactions (61, 62). These loops increase contact order (48) within the backbone structure. Interestingly, our recent studies indicate that the residues within and contacting the functionally significant β -bulge in IL-1 β may introduce “frustration” into the folding of this β -trefoil (36, 63). The bulge region is directly involved in receptor binding and cell signaling. This is consistent with the hypothesis that slow folding is often related to the functional necessity of conserving protein-protein or protein-ligand interaction sites (57-60). As the β -bulge is not conserved across the trefoil family and other surfaces are involved in their respective interaction sites (44, 64-66).

In this study, the role of topology and the affects circular permutations have on folding and the native state of IL-1 β will be investigated. Using a combination of

techniques, such as H/D, ^{13}C chemical shift analysis, stopped-flow and manual mixing fluorescence, we characterize the stability, the native state, and the folding mechanisms for several permutations. We also test the affects of the frustration of the β -bulge on the native state by engineering a loop swap from IL-1ra. These studies reveal topological similarities among the variants of engineered proteins.

Chapter 2

General Materials and Methods

Introduction

The structure and folding of permutant and deletion variants of IL-1 β is studied with a number of biophysical techniques. In order to successfully conduct experiments probing structural changes as result of modifying the WT protein and how those changes affect the folding mechanism, the proteins of interest must be isolated in high concentrations. The use of a bacterial expression system to grow and express large amounts of soluble protein becomes necessary for success. The proteins must also be purified in conditions that maximize the yield and maintain the integrity of the protein. For experiments using heteronuclear NMR, the requirement of isotope enrichment and hence the use of a minimal media becomes an additional challenge. In addition, NMR samples require greater amounts of protein versus fluorescence. Purified proteins are then used in a number of spectroscopic techniques to acquire raw data for processing, analysis and interpretation.. All these steps are important and vital for the progress of science and the integrity of the work gathered here. To avoid redundancy in the thesis, general methods are listed and described here.

GENERAL METHODS

Cloning of WT and Variant IL-1 β and Protein

The PCR amplified permutant sequence was digested with *NdeI* and *BamHI* and purified from agarose gels using Qiagen Gel Extraction Kits. The gene fragment was then ligated into the bacterial expression vector pET24d(+) (New England Biolabs). This vector was then transformed into E. coli host strain BL-21 (DE3).

Expression and Protein Purification

Cells were grown in a 2X LB media to and O.D.₆₀₀ between 0.8 and 1.0, and protein expression was induced with IPTG at a final concentration of 1mM. Four hours after induction, cells were harvested by centrifugation at 4300xg for 30 minutes (Sorvall RC-3). Uniform ¹⁵N enrichment (>95%) of IL-1 β permutant protein was performed by growing cells on minimal media with 2.0g l⁻¹ [¹⁵N] ammonium sulfate (Cambridge Isotopes) as the sole nitrogen source. Uniform ¹⁵N/ ¹³C enrichment (>95%) was performed by growing cells on minimal media with 2.0 g l⁻¹ [¹⁵N] ammonium sulfate and 2.0 g l⁻¹ [¹³C] glucose (Cambridge Isotopes) in order to obtain isotopically enriched IL-1 β permutant protein for NMR spectroscopy.

The protein was purified according to methods previously described(38, 67, 68). Pelleted cells were resuspended in 10 ml of 10 mM KPO₄, 0.2 mM EDTA, 5mM DTT and 1mM PMSF at pH 8.0 and then lysed by sonication at 4°C for 10 minutes of total on-time (20 minutes total time) followed by centrifugation at 7000xg for 15 minutes (Sorvall RC-5C Plus). The supernatant was decanted from the cellular debris and then was 80% saturated with ammonium sulfate (AmSO₄) at 4°C and over a period of 30 minutes. Precipitated was achieved by centrifugation as before. The AmSO₄ pellet which contains the IL-1 β protein was then dissolved in ca. 20 ml of 24 mMNH₄OAc, 2mM EDTA and 1 mM β ME at pH 5.2 (buffer A) and dialyzed overnight with three changes of buffer with at least three hours between changes.

The dialysate was centrifuged as before, filtered with 0.45 μ m cutoff and applied to a cation exchange column (Pharmacia) equilibrated in buffer A. IL-1 β permutant was eluted in a 40 column volume linear gradient of buffer B (750 mM NH₄Oac, pH 5.2) at a flow rate of 3 ml/min. The purity of the protein was assessed by SDS Polyacrylamide

Gel Electrophoresis (PAGE). Purity was judged to be greater than 95%. If the IL-1 β permutant protein solution contained impurities, it was applied to a Superdex 75 FPLC gel filtration column (Pharmacia), for additional purification.

To recover insoluble IL-1 β proteins from the cellular debris, the pellet was dissolved in minimal amounts of 5.4 M guanidine isothiocyanate, 25mM Tris-HCl, 1mM EDTA and 1mM DTT at pH 7.5. It stood stirring for one hour at room temperature. The protein was then refolded by adding 9 volumes of refolding buffer containing 50 mM KH₂PO₄ (pH 9.0), 1mM EDTA, 1mM DTT and 50 mM NaCl. It was allowed to stir at room temperature for 30 minutes. The solution was then centrifuged for 15 minutes at 5000 rpm (Sorvall RC-3). The supernatant was then dialyzed overnight into 4 liters of buffer A with 5 changes separated by a minimum of 3 hours. The dialysate was then centrifuged again. The resulting supernatant was then purified by ion exchange and size-exclusion chromatography as previously described. We assessed protein concentration by measuring the UV absorbance at 280nm using a Pharmacia Biotech Ultraspec 3000 UV/Visible Spectrometer using an experimentally determined ϵ_{280} = 11.26mM⁻¹cm⁻¹ for WT IL-1 β , ϵ_{280} = 11.4mM⁻¹cm⁻¹ for permutant protein and ϵ_{280} = 11.26mM⁻¹cm⁻¹ for the bulge-less construct.

Equilibrium Fluorescence

Equilibrium denaturation titrations were measured using average fluorescence wavelength (69, 70). Protein samples were prepared at multiple concentrations (0.2-0.4 mg/ml) in a buffer solution (MES) containing varying concentrations of denaturant ranging from 0 to 5M (Gnd-HCl). The protein solutions were allowed to denature for

~24 hours prior to measurement. Fluorescence emission spectra were collected from 300 to 450 nm using the Flouromax-2 spectrofluorimeter (Jobin Yvon-Spex) with an excitation wavelength of 293 nm (67, 71, 72). Fitting of the acquired data is described below in **Data Fitting and Analyses**.

Stopped-Flow Fluorescence-Detected Refolding

Relaxation times faster than 10 seconds were measured using stopped-flow methods. Stopped-flow fluorescence studies were performed with an Applied Photophysics SX.17MV instrument. The experiments were carried out as previously described (35, 67, 72) using asymmetric mixing with protein at various initial concentrations (2.2-4.4 mg/ml) in 2.2M and 3.3M Gnd-HCl (MES buffer, pH 6.5) followed by an 11-fold dilution with MES (pH 6.5) to give a final concentration of ~0.2-0.4 mg/ml protein in 0.2M and 0.3M Gnd-HCl in MES (pH 6.5). For refolding to higher final Gnd-HCl concentrations an appropriate amount of Gnd-HCl was added to the MES buffer in the refolding syringe so that the data was collected with a final concentration of Gnd-HCl varying from 0.3 M to 1.1 M. Data was collected in logarithmic mode with an excitation wavelength of 293 nm, and the emission was collected using a 320 nm cutoff filter. Typical refolding spectra were averaged over a minimum of 7 runs and a maximum of 14.

The refolding kinetics of wild-type IL-1 β is characterized by an initial biphasic increase in fluorescence intensity followed by a slow decay of the fluorescent intensity to the native state. The wild-type IL-1 β exhibited three exponential phases during refolding. Stopped-flow fluorescence refolding kinetic traces exhibit a rapid increase in

signal, which is best fit by two exponential time constants: τ_3 , that occurs on the millisecond timescale, and τ_2 , that occurs on the millisecond to second timescale. Fitting of the acquired data is described below in **Data Fitting and Analyses**.

Manual-Mixing Fluorescence-Detected Refolding/Unfolding

Relaxation times greater than 10 seconds were measured using manual-mixing methods. Manual-mixing kinetics were carried out as previously described (35, 67, 71, 72) on the Flouromax-2 spectrofluorimeter (Spex) with the excitation wavelength set at 293nm and the emission intensity monitored at 343nm. The dead time for the manual mixing experiments was approximately 20 seconds. For refolding experiments, the protein was unfolded in 2.2M Gnd-HCl at varying concentrations (2-4 mg/ml) in MES buffer (pH 6.5) and was allowed to equilibrate for 24 hours at 4°C. Refolding was initiated by dilution of the unfolded protein with the appropriate amount of buffer and denaturant to a final concentration ranging from 0.2 to 1.1 M. The final protein concentration was 0.2-0.4 mg/ml. For unfolding studies, the native protein was at an initial concentration of 2 and 3 mg/ml in MES (pH 6.5). Unfolding experiments were initiated by dilution of the native protein to a final Gnd-HCl concentrations ranging from 1.5 to 5.0M (MES, pH 6.5) and final protein concentrations of 0.2 and 0.4mg/ml.

Manual mixing refolding generate a rapid increase in fluorescent signal is followed by a slow decrease of fluorescence to the native state is described as a single exponential phase, τ_1 , which is on the tens of seconds timescale. This non-monotonic change in intensity as a function of time is indicative of the population of a highly

fluorescent intermediate species prior to the formation of the native protein (38, 67, 71). The amplitude of the slowest phase changes from negative to positive at increasing final denaturant concentration when refolding. This observation is consistent with the changes in equilibrium fluorescence measurements as denaturant concentrations changes from 0 to 1.0M Gnd-HCl for wild-type IL-1 β (67). Manual mixing unfolding generate a signal of decreasing fluorescence under strong denaturing conditions. The intensity change was fit to a single-exponential, τ_{unf} . Fitting of the acquired data is described below in **Data Fitting and Analyses**.

8-Anilino-1-naphthalenesulphonic acid (ANS) Stopped-flow Fluorescence-Detected Refolding

Protein refolding prior to 20 seconds was monitored using stopped-flow methods. Stopped-flow fluorescence studies were performed with an Applied Photophysics Pi-Star SX.17MV instrument (Applied Photophysics, London) with a path length of 0.1 cm. The experiments were carried out similarly to as previously described (35, 67, 72, 73) using asymmetric mixing of protein at 1.1 mg/ml in a with a solution of 2.2M Gnd-HCl (MES buffer, pH 6.5) and 1mM ANS, diluted 11-fold with MES (pH 6.5) to give a final concentration of ~0.1 mg/ml protein in 0.3M Gnd-HCl, 100 μ M ANS in MES (pH 6.5). For refolding to 0.3M final Gnd-HCl concentration, an appropriate amount of Gnd-HCl was added to the MES buffer in the refolding syringe so that the data was collected with a final concentration of Gnd-HCl varying from 0.3 M. Data was collected for 250 seconds at 25°C in logarithmic mode with an excitation wavelength of 365nm, and the emission was collected using a >420 nm cutoff filter. Typical refolding

spectra were averaged over a minimum of 7 runs and a maximum of 14. Fitting of the acquired data is described below in **Data Fitting and Analyses**.

NMR Spectroscopy

^1H - ^{15}N heteronuclear single quantum coherence (HSQC) experiments (74, 75) were performed on the DMX 500 NMR Spectrometer (Bruker) for WT, permutant, and bulge-less IL-1 β variants. All NMR experiments were performed similar to previous experiments (47, 76) on a Bruker DMX500 spectrometer, using a triple-resonance gradient probe. The ^1H chemical shifts were referenced directly to sodium 2,2-dimethyl-2-silapentane-5-sulfonate (DSS), and the ^{13}C and ^{15}N chemical shifts were referenced indirectly. Protein samples consisted of approximately 1mM of protein in 100 mM deuterated ammonium acetate (Aldrich) and 10% D_2O (Isotech) at pH 5.4. Experiments were run at 36°C. These experiments were acquired with 128 real t_1 (^{15}N) and 512 complex t_2 (^1H) points with a spectral width corresponding to 1517.72 Hz (30 ppm) and 3005 Hz (6 ppm), respectively. The ^{15}N carrier was set to 121ppm, and the ^1H carrier was set to water during the ^{15}N evolution and placed at 8.5ppm during acquisition.

Three-dimensional CBCA(CO)NH (77, 78) and HNCA (79) spectra were collected for permutated IL-1 β protein samples that were approximately 0.5-0.7mM in 100mM sodium acetate- d_3 , pH 5.4, 10%/90% $\text{D}_2\text{O}/\text{H}_2\text{O}$ at 36°C. The CBCA(CO)NH spectra were collected with constant time in t_1 and t_2 . For the ^1H - ^{15}N - ^{13}C dimensions, a total of 64 complex t_1 (^{13}C), 32 complex t_2 (^{15}N), and 512 complex t_3 (^1H) points were collected. The spectral widths were 4024Hz (32ppm) (t_1), 1520Hz (30ppm) (t_2), and 3004.808Hz (6ppm)(t_3). Points in the indirectly-detected dimensions were linear

predicted and zero-filled. The HNCA spectra were collected as described (76) with constant time in t_1 . For the ^1H - ^{15}N - ^{13}C dimensions, a total of 32 complex t_1 (^{15}N), 70 complex t_2 (^{13}C) and 512 complex t_3 (^1H) points were collected. The spectral widths were 1520.513 Hz (30ppm) (t_1), 4024.469 Hz (32ppm) (t_2) and 3004.808 Hz (6ppm) (t_3). Points in the indirectly detected dimensions were linear-predicted and zero-filled. Water suppression was achieved using a 3-9-19 train pulse sequence with gradients. When needed, broadband ^{15}N decoupling during acquisition was accomplished using a WALTZ16 decoupling scheme. All experiments were processed using Felix 95.0 software (MSI, San Diego, CA).

Amide H^{N} Solvent Exchange of IL-1 β

Solvent amide NH exchange was measured as described previously (76) by following the change in intensity/volume of cross-peaks in the ^1H - ^{15}N -HSQC spectra as a function of time. Concentrated permutant IL-1 β protein was applied to a Quick-Spin buffer-exchange column (Boehringer Mannheim) that was equilibrated in 100 mM sodium acetate- d_3 acid in 99.9% D_2O , pD 5.0. Elution by centrifugation at 1900xg took three minutes. Following elution of the protein, the first HSQC experiment for each H/D experiment was acquired uniformly at 26 minutes. A total of 80 HSQC spectra were collected in series, with 12 minutes for each spectrum at 36°C. The amide proton signal decay was plotted as a function of time for each individual amide resonance. A total of 67 residues were used for comparison between WT, permutant and bulge-less IL-1 β variants. The change in intensity/volume of individual amino acid cross-peaks over time was compared to WT IL-1 β amide exchange results previously published (46,

47, 80). Fitting of the resulting time curves is described below in **Data Fitting and Analyses**.

NMR Processing and Analysis

The program FELIX 95.0 (MSI, San Diego, CA) was used for processing and analyzing the NMR spectral data acquired. The NMR spectral data were apodized with a sinebell squared function shifted by 70° in all dimensions before applying the Fourier transformation. Linear prediction was applied before apodization in T_1 and to an additional 1/3 of the number of points collected in the indirect detected dimension. Backbone resonance assignments of WT IL-1 β were previously published (80). The resonances were assigned and the peak volume/intensity calculated and normalized with respect to the protein concentration as determined by the optical density at 280nm. Assignments for ^{13}C , ^{15}N and ^1H resonances are based on comparison to previously published work (80, 81).

Residue-specific ^{13}C Chemical Shifts

Chemical shifts of the α -carbons in amino acid residues have been empirically correlated to the secondary structure of folded and unfolded proteins at the level of individual residues (82). The deviations of the $^{13}\text{C}^\alpha$ chemical shifts from random coil values are dependent on the ϕ, ψ backbone dihedral angles of the peptide bonds. The relative deviation from random coil in the $^{13}\text{C}^\alpha$ ppm for each specific amino acid residue in permutant IL-1 β was calculated as described (76) from the following equation:

$$\text{Relative } \Delta\delta_{^{13}\text{C}} = (\delta_{^{13}\text{C}} \text{ WT IL-1}\beta - \delta_{^{13}\text{C}} \text{ mutant IL-1}\beta) / (\delta_{^{13}\text{C}} \text{ WT IL-1}\beta - \delta_{^{13}\text{C}}) \quad (1)$$

where δ_{13C} refers to the chemical shift of the $^{13}C^{\alpha}$ of the individual amino acid in a random coil, δ_{13C} permutant IL-1 β is the chemical shift of the specific amino acid residue in the permutation, and δ_{13C} WT IL-1 β is the chemical shift of the specific amino acid residue in wild-type IL-1 β . Random coil ^{13}C chemical shifts for C^{α} atoms were taken from the literature. (82, 83) For differences of 0 ± 2 ppm, chemical shifts of specific residues are taken to be similar to wild-type.

Ramachandran Plots

Ramachandran plots of each permutation containing the TAQT linker and for the bulge-less variant were generated using the $^{13}C^{\alpha}$ chemical shift data acquired from the HNCA and CACB(CO)NH experiments. The torsion angles for WT IL-1 β were generated from PDB ID 6I1B. Data were compiled and input into the PREDITOR web server (84), generating torsion angles for each residue in the polypeptide chain of each permutation. The torsion angles were then graphed in Excel and overlaid with those of WT IL-1 β for comparison.

Data Fitting and Analyses

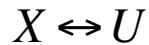
Fitting of the fluorescence-detected equilibrium data to a two-state model as described previously, (35, 67, 71). Equilibrium data were fit as described previously, assuming a two-state model of unfolding (85). The equilibrium denaturation process was monitored by changes in the tryptophan fluorescence spectrum as a function of denaturant. Due to the existence of the unusual increase in fluorescence at low concentrations of Gnd-HCl, we fit the data using the average wavelength (45). The single tryptophan residue in the IL-1 β sequence was used to monitor the unfolding

reaction. Trp 120 has been shown to be a useful probe of the global unfolding reaction (85). The average wavelength, λ_{average} was determined by the center of mass of the fluorescence spectra given in equation 1:

$$\lambda_{\text{average}} = \frac{\sum \lambda * I_{\lambda}}{\sum I_{\lambda}} \quad (2)$$

where λ is the wavelength of light in nanometers at each point in the spectra and I_{λ} is the intensity of the light at wavelength λ .

Equilibrium denaturation fluorescence data was fit with in-house software to the two-state model shown in Scheme 1:



where X is the folded species, either intermediate or native state, (70) and the U is the unfolded protein. The apparent fraction of unfolded form, F_{XU}^{app} , populated at a given Gnd-HCl concentration [D], is measured and determines the apparent free energy of the unfolded species X ($\Delta G_{XU}^{\text{app}}$) with equation 2:

$$F_{XU}^{\text{app}} = \frac{e^{-\frac{\Delta G_{XU}^{\text{app}}}{RT}}}{1 + e^{-\frac{\Delta G_{XU}^{\text{app}}}{RT}}} \quad (3)$$

To calculate the free energy of stabilization (ΔG) and the denaturant concentration-dependence of the transition, m , for WT, permuted and bulge-less IL-1 β proteins the following equation was used. The transition value, m , is defined by the equation:

$$\Delta G = \Delta G_{H_2O}^0 - m[\text{denaturant}] \quad (4)$$

where $\Delta G_{H_2O}^0$ is the y-intercept that corresponds to the free energy change of unfolding at zero concentration denaturant, while the denaturant concentration-dependence of ΔG is described by the slope, m .

Manual mixing and stopped flow fluorescence kinetic data were fit to equation 4 using the Marquardt algorithm (86) and globally (87) using GraphPad and Matlab software.

$$A(t) = \sum_i A_i e^{\frac{-t}{\tau_i}} + A(\infty) \quad (5)$$

The number of kinetic processes i , relaxation time, τ_i , signal amplitude, A_i , of each exponential kinetic process i , and the final signal value $A(\infty)$ at equilibrium were calculated using the fit quality represented in the χ^2 (chi-squared) values, the random dispersion of residuals, and the logical consistency of the generated fitting parameters (45). The relaxation time τ equals the inverse of the observed rate constant and is not directly equivalent to the intrinsic rate constant k for a kinetic process (88, 89).

Solvent amide NH exchange NMR spectra data following the decay in intensity/volume (I) of amino acid cross-peaks over time for each permutant were compared to WT IL-1 β . The individual amino acid backbone NH resonance signal was measured was fit to a single-exponential function:

$$I = I_o \exp(-k_{ex} t) + C \quad (6)$$

where I_o is the initial intensity (or volume), k_{ex} is the rate constant of exchange, and C is the final amplitude. The calculated rates for the permutations were compared with

those obtained for WT protein. The protection factor (P) for various amide protons in the proteins was estimated using equation:

$$P = \frac{k_{\text{int}}}{k_{\text{ex}}} \quad (7)$$

where k_{int} and k_e represent the intrinsic exchange rate and k_{ex} is the observed rate, respectively.

All the data analyses were conducted with Matlab and/or GraphPad software.

Molecular Visualization

All molecular representations generated within this thesis were with MacPyMOL (90).

Chapter 3

Circular Permutation of Interleukin-1 β Does Not Affect the Native Global Fold

Abstract

Circular permutations of proteins have been found to fold into functional, native-like conformations. The variety of global structural motifs represented by these proteins demonstrates that the propensity to fold is not limited or defined by the type of secondary structure or the distribution of amino acids in the sequence. Circular permutant variants have led to extensive studies on the effect of chain connectivity on folding for different proteins without introducing additional variables that mutations introduce and demonstrates to what extent a protein can tolerate changes in the order of the secondary structures as well as allow the identification of the regions in a protein that are essential for folding. Six permutations of IL-1 β were generated to study the effects on the global fold of the protein. Two permutations, near functionally relevant loops, did not fold while four variants folded into a similar global fold. $^{13}\text{C}^\alpha$ chemical shift analysis shows changes at structural stress points within the native fold. Native solvent amide hydrogen-deuterium exchange reveals similar areas of loosening within the native fold, where protons exchanged faster compared to WT.

Introduction

Circular permutations of proteins is the result of covalent linkage of the N- and C-termini and subsequent linearization of the circular protein by cleavage between residues i and $i + 1$, so that i and $i + 1$ becomes the new N- and C- termini of the circularly permuted protein(53). This works best when the N- and C-termini are close in space. The first circular permutation experiment of a protein was reported for bovine pancreatic trypsin inhibitor, in which the termini were linked chemically and the

inhibitor was subsequently cleaved by trypsin at its reactive peptide bond (53). Several proteins have been viable systems for generating permuted variants including aspartate transcarbamolase (91), the SH3 domain of α -spectrin (49), chymotrypsin inhibitor 2 (55) and interleukin-1 β (92). The new termini generated in all these circular permuted proteins were designed by rational means and placed in surface-exposed loop regions. The common result of these studies is that the circularly permuted variants are capable of folding into a functional, native-like confirmation. (93) Experiments on dihydrofolate reductase (DHFR) (94), identified essential folding elements by creating permutations at each amino acid position. The variety of global structural motifs represented by these proteins demonstrates that the propensity to fold is not limited or defined by the type of secondary structure nor the distribution of amino acids in the sequence (95).

Circular permutant variants have led to extensive studies on the effect of chain connectivity on folding (49, 92, 95-99) and on function (100) for different proteins without introducing additional variables that mutations introduce, such as steric clashes, and demonstrates to what extent a protein can tolerate changes in the order of the secondary structures as well as allow the identification of the regions in a protein that are essential for folding. We generated six circular permutant variants of interleukin-1 β (IL-1 β), in order to study the effects on the global fold. The β -trefoil native fold consists of 12 antiparallel β -strands connected by turns and loops. The tertiary fold is formed from six two-stranded hairpins, three of which form the β -barrel and the other three form the “cap” at one end of the barrel. The β -bulge, which is functionally relevant for bioactivity (61), is located between strands 4 and 5 of the protein. Experiments on the unfolding of IL-1 β monitored by NMR spectroscopy revealed that native-like turns

were the last to unfold and were the most persistent structure within the β -trefoil topology of the protein (47). Additional studies showed that surface residues contribute significantly to structural stability and also modulate long-range coupling between the two separate docking sites for the IL-1 receptor (35). The first permutant variant of IL-1 β was designed to test the technique and to test its functional viability (92). We have designed five additional permutations, to add to the one first generated by (92). New N- and C- termini are in various turns and loops throughout the protein, to assess the structural effects, if any, of permutation on the overall fold of the protein.

Permutant variants of IL-1 β were checked for changes in the native global fold. Chemical shift analysis (CSI) of the $^{13}\text{C}^\alpha$ amino acid chemical shifts, HSQC (^{15}N - ^1H) spectra and hydrogen-deuterium solvent exchange (HDX) experiments were used to identify any differences in terms of topology have relative to WT. The tertiary fold is conserved for all the permutant variants while HDX highlighted β -strand areas of the proteins that were less protected from solvent exchange, relative to WT.

Special Methods

Construction of Permutants

To construct the various permutants of IL-1 β , we used the four-primer PCR method (92) with the modifications as described below. We used the same biologically active amino acid linker, TAQT (92), unless indicated. Primers for construction of the template consisting of two IL-1 β genes in tandem were designed as follows (Figure 3-1):

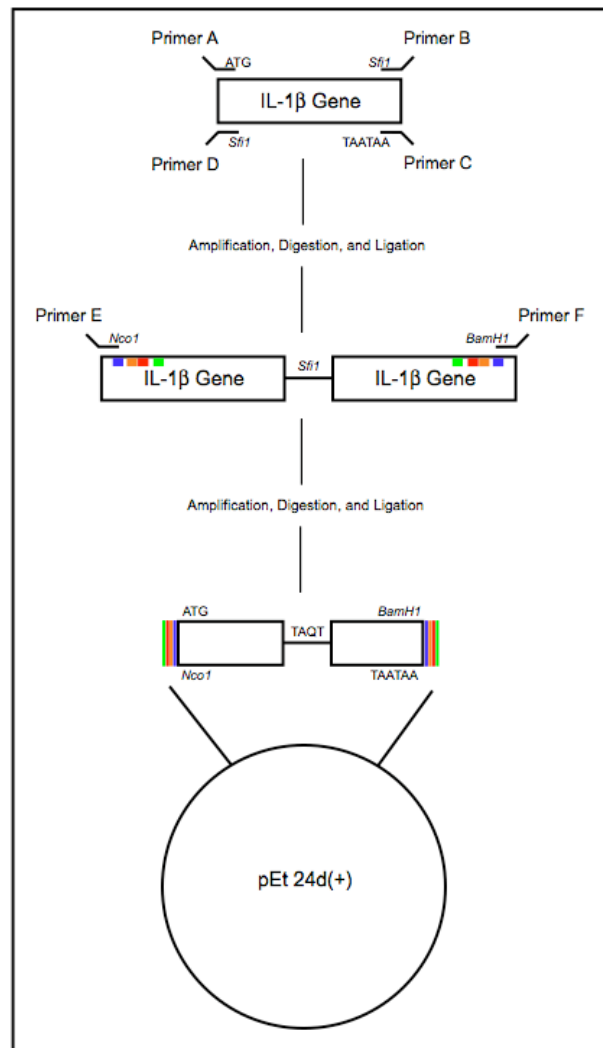


Figure 3-1: Schematic of tandem-gene design for the construction of the IL-1 β permutations and linker variants.

Representation of the design of the individual permutations of IL-1 β , adapted from (92). The colored squares represent the starting and stopping positions of the respective permutants, pm 23 (**blue**), pm65 (**orange**), pm 76 (**red**), and pm 142 (**green**). This color scheme will be referred to throughout the thesis.

Primer A: 5' AAACC**ATG**GCACCGGTACGATCGCTGAACTGC 3'

Primer B: 3' AGTGGTACGTAAACACAGAAGG**TGCCGGGTCTGCCGG** 5'

Primer C: 5' **C[GGCCCAGACGGCC]**CCTGTACGATCGCTGAACTGCACT 3'

Primer D: 3' TTGACTGAAGTGGTACGTAAACACAGAAGG**ATTATT**CAGCTGCT 5'

Primer E: 5' AAA/CC**ATG**G/AGAATCTGTACCTGTCC 3'

Primer F: 3' CGGAACCCGGAGTTCCTT**ATTATT**/CCTAGG/GATA 5'

Primer A incorporates an ATG start codon and the first 8 codons of the IL-1 β gene. Primer B includes the last 7 2/3 codons of the IL-1 β gene, the sequence encoding the four amino acid linker region, and the first codon of the second IL-1 β gene. An interrupted palindromic restriction site (*Sfi*I) was incorporated into the nucleotide sequence of the four amino acid linker region. Primer C includes most of the sequence encoding the four amino acid linker region, the same *Sfi*I restriction site as found in primer B, and the first 9 codons of the IL-1 β gene. Primer D contains two TAA stop codons and the last 12 codons of the IL-1 β gene. The PCR conditions used for the construction of the IL-1 β permutants were:

1. 94°C for 5 minutes
2. 94°C for 30 seconds
3. 50°C for 30 seconds
4. 72°C for 45 seconds (repeat steps 2-4 24 consecutive times)
5. 72°C for 7 minutes
6. 4°C for ∞

Primer A and B were used in one PCR reaction to yield an IL-1 β gene, and primers C and D were used in another PCR reaction to yield the other IL-1 β gene. The resulting two DNA fragments representing IL-1 β genes 1 and 2 were purified by gel electrophoresis on a 1% agarose gel using Qiagen kits. The isolated fragments were digested with the restriction enzyme SfiI (New England Biolabs) followed by gel electrophoresis and purification as described above. The two IL-1 β gene fragments were then ligated at 16°C overnight with T4 ligase, and this product served as the initial template for construction of all subsequent permutants.

Primer E and F were used to construct the various permutants. The primers changed depending on the desired permutant. Primer E incorporates an *Nde*I restriction site, an ATG codon, and the first 6 amino acids of the IL-1 β gene sequence starting wherever the desired permutant begins. For example, for PM65/64, the sequence will begin at the position on the IL-1 β gene sequence coding for amino acid 65. Primer F incorporates a *Bam*HI restriction site, two TAA stop codons, and the last six amino acids of the IL-1 β gene sequence ending with the codon encoding for the amino acid prior to the first amino acid encoded in primer E. For example, for PM65/64, primer F codes for 6 amino acids of the IL-1 β sequence ending with the codon encoding amino acid 64.

Results

Construction of IL-1 β permutant variants

The circular permutations that were created and used in this investigation were located at various turns and loops within the protein relative to the structure formed in

the experimentally observed refolding intermediate (37, 38). These turns and loops are important because they appear to be important determinants in unfolding and folding (47). Circular permutations of IL-1 β were constructed to study the structural effects of the permutations on the folding of the pseudo-trefoil fold of IL-1 β . The sites of the cuts in the primary sequence to create the permutant variants are indicated in various turns and loops throughout the protein (Figure 3-2A). Permutant 64/65 (PM65) was constructed by removing the peptide bond between glutamate 64 and lysine 65 at the turn between β -strand 5 and 6 on the interface between the barrel and the cap. Permutant 75/76 (PM76) was constructed by removing the peptide bond between aspartate 75 and aspartate 76 at the turn between strand 6 and strand 7, which is one of the three hairpin turns involved in formation of the hairpin cap. β -strands 5, 6 and 7 showed protection against hydrogen exchange/deuterium exchange early in the folding reaction(38, 46) (Figure 3-2B). Permutant 22/23 (PM23) was constructed by removing the peptide bond between glycine 22 and proline 23 at the first hairpin turn between strands 2 and 3, and permutant 141/142 (PM142) was constructed by removing the peptide bond between glutamine 141 and aspartate 142 in the 8 residue loop between strand 11 and 12. β -strands 2, 3, 11, and 12 all showed late protection in the folding reaction(38, 46) (Figure 3-2B). Additionally, two permutants 51/52 (PM52) and 99/100 (PM100) were constructed by removing the peptide bond between glutamate 51 and serine 52, and phenylalanine 99 and valine 100, respectively. PM52 is located at the beginning of the β -bulge, the loop between strands 4 and 5 that is responsible for function. PM99 is located at the end of the end of the 90's loop, a 16-residue loop that

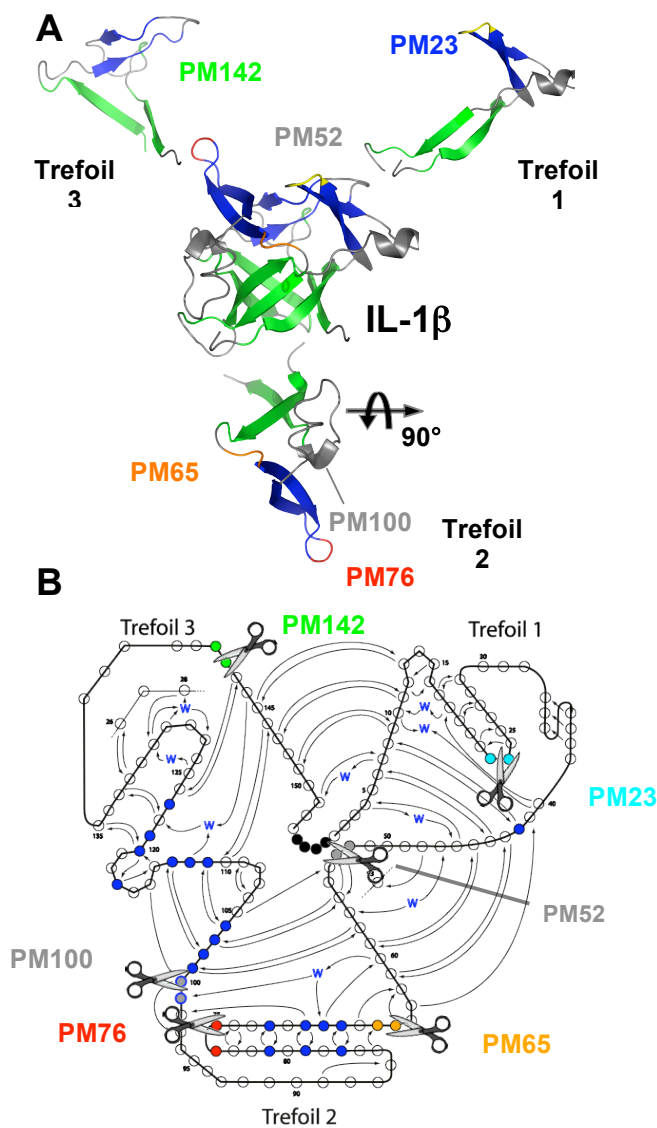


Figure 3-2: Schematic indicating the location of the cut sited for permutant variants of IL-1β.

(A) The molecule of IL-1β has been colored to indicate the strands involved in the formation of the cap (blue) and those that contribute to the β-barrel (green). Each trefoil subunit has been separated out to further indicate the spatial reference of the cut sites that form the new N- and C- termini for each permutant. PM142 is located in the long loop region of the third trefoil and is indicated in green. PM23 is located in a hairpin turn in the first trefoil and is highlighted in yellow. PM52 is located in trefoil 1 in the region prior to the β-bulge. PM 76 is located in trefoil 2 in a tight turn between two strands that form a β-sheet involved in the cap and is highlighted in red. PM65 is also located in trefoil 2 and is in an interface between the cap and barrel strands. The cut site location is in orange. PM100 is located in the second trefoil at the end of the 90's loop. (B) 2D splay indicating the location and of the permutations of IL-1β and the area of the molecule that showed early protection (●) in pulse-labeling experiments and theoretical simulations that were identified as the part of the kinetic folding intermediate. Figure A was generated using MacPyMOL (90) and PDB ID 6I1B.

contributes to the packing of the β -bulge, between strands 7 and 8. The overall global fold of four of these permutant proteins (PM23, PM65, PM76, PM142) remains relatively similar to that of WT IL-1 β based on and protein behavior during bacterial expression and protein purification. Two permutant variants did not fold, PM52 and PM100, based on NMR spectral evidence as indicated by Figure 3-3.

^1H - ^{15}N HSQC spectra of IL-1 β permutant variants

^1H - ^{15}N HSQC spectra were acquired for the permutants are shown in Figure 3-4. The similarity in chemical shift pattern and dispersion relative to WT indicate an intact β -trefoil for four permutants (Figure 3-4). Backbone amide resonances seen in the ^1H - ^{15}N spectra of the IL-1 β variants have a unique chemical shift dispersion and pattern that are correlated to the secondary structure and tertiary interactions (35, 47). The ^1H - ^{15}N HSQC spectra of PM23 (**blue**), PM65 (**orange**), PM76 (**red**) and PM142 (**green**) were essentially identical to WT (**black**), except for perturbations at the cut sites in each permutant as well as the four additional cross-peaks in the four permutant spectra attributed to the TAQT linker. Triple resonance ^1H - ^{13}C - ^{15}N spectroscopy was performed to confirm confirm-specific resonance assignments for each permutant.

$^{13}\text{C}^\alpha$ chemical shifts

Deviations of the $^{13}\text{C}^\alpha$ backbone chemical shifts from random coil values are dependent on the ϕ, ψ backbone dihedral angles of the peptide bonds. Chemical shifts of the α -carbons in amino acid residues have been empirically correlated to the secondary structure of folded and unfolded proteins at the level of individual residues (82). Especially compared to the ^1H and ^{15}N resonances of the peptide backbone, variations in

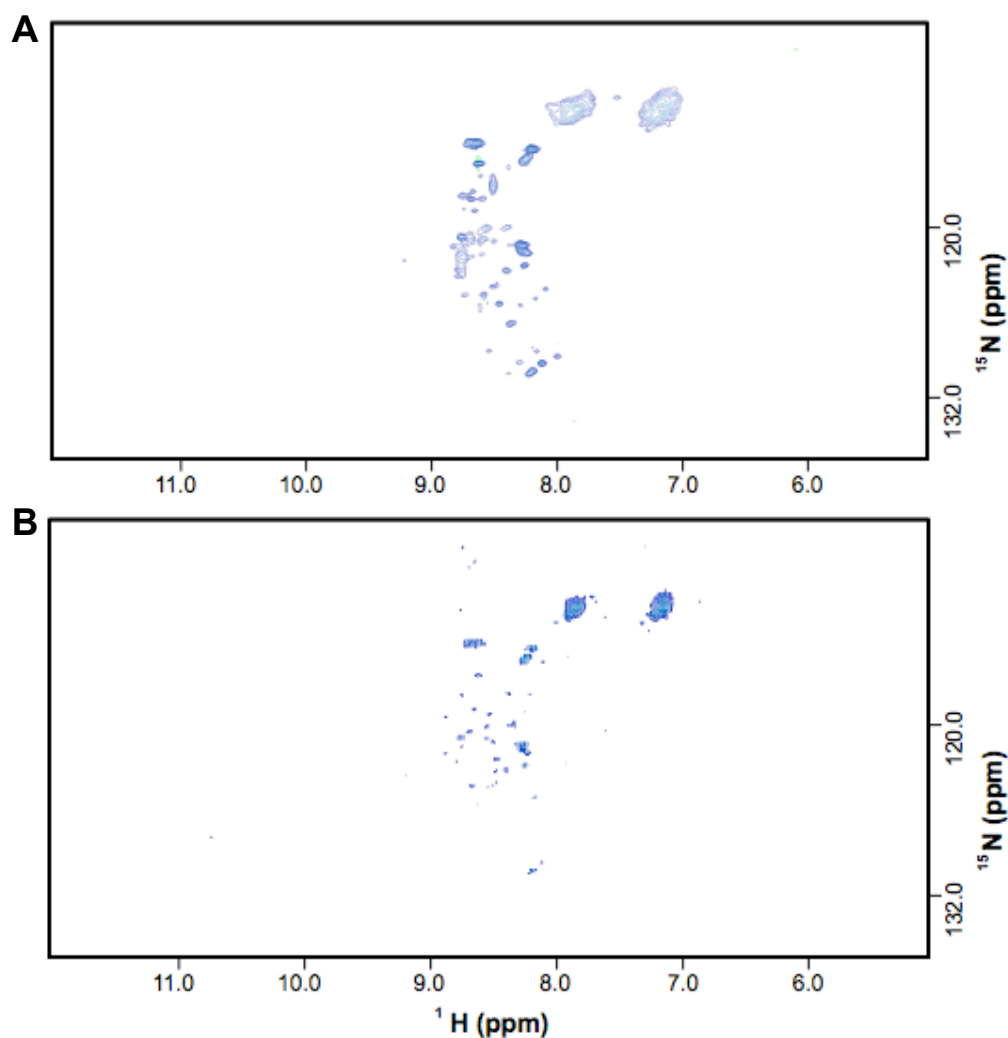


Figure 3-3: Analysis of the fingerprint pattern of ^1H - ^{15}N -HSQC spectra of (A) PM52 and (B) PM100 indicate denatured protein.

These representative spectra were acquired to determine if the proteins could fold and be isolated and purified similar to WT IL-1 β . The lack of chemical shift dispersion and the collapsed appearance of the backbone amides are indicative of denatured protein.

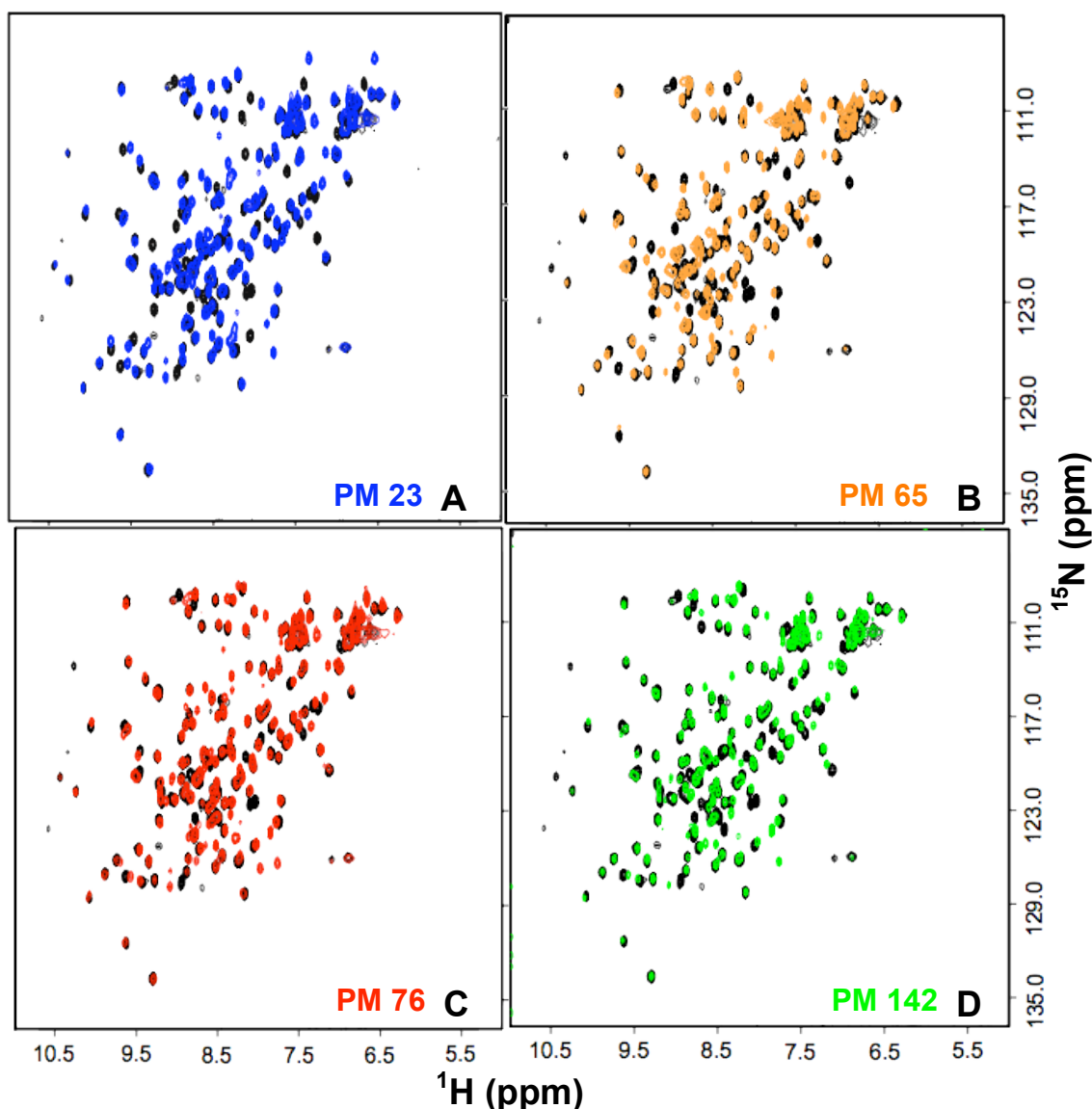


Figure 3-4: Analysis of the fingerprint pattern of ^1H - ^{15}N -HSQC spectra of wild type and permutant IL-1 β strongly indicate similar tertiary structure and an intact β -trefoil fold.

Each permutant spectrum is overlaid with a spectrum of WT IL-1 β (in **black**). (A) PM 23 overlaid in **blue**. (B) PM 65 overlaid in **orange**. (C) PM 76 overlaid in **red**. (D) PM 142 overlaid in **green**. The similarity in chemical shift pattern and dispersion relative to WT indicate an intact β -trefoil for the four permutants except for perturbations attributed to the cut sites in each permutant as well as the four additional cross-peaks in the four permutant spectra attributed to the TAQT linker. Triple-resonance NMR experiments (HNCA and CBCA(CO)NH) confirmed resonance assignments.

$^{13}\text{C}^\alpha$ carbon chemical shifts correlate quite well empirically to the ϕ , ψ backbone dihedrals. Carbon chemical shifts are relatively unaffected by salt, pH, ionic strength and other solvent parameters and are primarily affected by bonding and bond angles. A particular observed $^{13}\text{C}^\alpha$ chemical shift for an amino acid type indicates a preferred population of the ϕ , ψ angles of the polypeptide backbone.

Changes in α -carbon chemical shift upon destabilization can be interpreted as a changes in the average conformation of the ϕ , ψ backbone bond angles (76). For permutant variants of IL-1 β , relative $^{13}\text{C}^\alpha$ chemical shift deviations were derived from HNCA spectral data. Differences between the WT and permutant $^{13}\text{C}^\alpha$ chemical shifts of individual amino acid residues were analyzed. The relative $\Delta\delta_{^{13}\text{C}}$ shift was calculated using equation 1 (See **GENERAL METHODS**). Figure 3-5A is a plot of the average relative $\Delta\delta_{^{13}\text{C}}$ for each amino acid in the permutants. Changes greater than $\pm 2\text{ppm}$ were deemed significant.

Most of the changes in backbone dihedral angles between permutants and WT are seen at turns and hinge points of the β -strands (Figure 3-5B and C). In addition, approximately 80% of residue-specific deviations were seen in the first and third trefoil subunits of the permutants. The residues that exhibit stabilization in β -structure, G22, V40, V41, F42, N89, K103, W120, S123, G136 and K138, were predominately located in the β -strands that contribute to the β -barrel and the hairpin cap of the protein and are colored blue. A destabilization in native structure was seen in residues L29, Q38, Q39, Q48, E51, D54, F99, V100, E128, V132, G136 and G140 that are found in loops leading into turns and are colored red (Figure 3-5C).

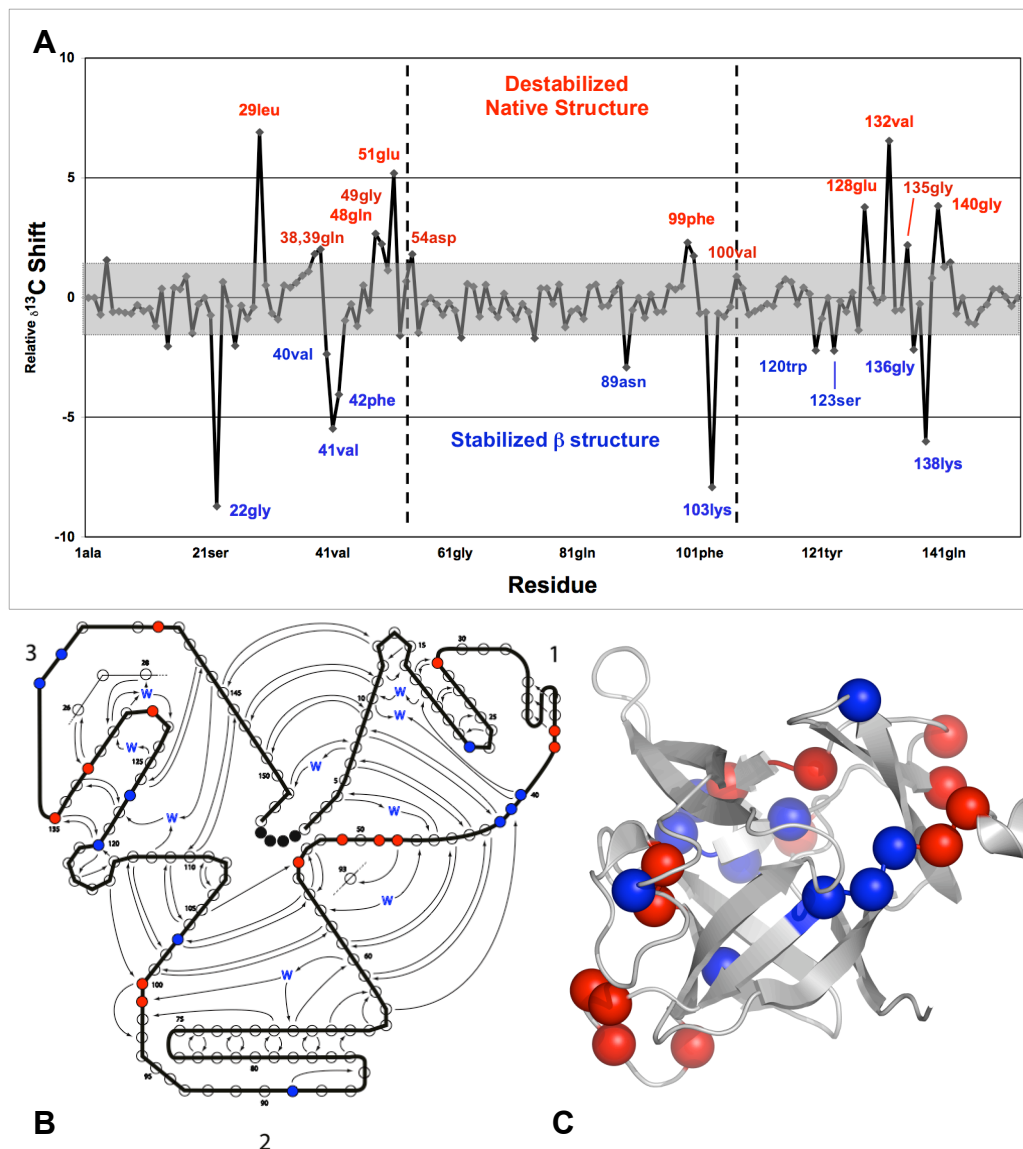


Figure 3-5: Effects of the permutations on $^{13}\text{C}^\alpha$ chemical shifts of permutant IL-1 β residues indicate differences at turns and hinge-points of the molecules.

(A) Graphical representation of the relative $\Delta \delta_{13C}$ for $^{13}\text{C}^\alpha$ chemical shifts of permutant IL-1 β residues. The black line represents the average deviation for the permutations at each amino acid. Numbering for the polypeptide chain for each permutant followed that of WT. The vertical dashed lines indicate the location of the 2nd and 3rd trefoil subunits. Residues with the most significant shifts are indicated. The grey area indicates shifts that are similar to WT protein. (B) The residues with the most significant differences found in common with each permutation mapped onto the 2D splay of WT IL-1 β . Red circles (●) represent $\text{C}\alpha$ shifts that are destabilized β -structure while the blue circles (●) represent stabilized β -structure. (C) $\text{C}\alpha$ shift differences indicated in the 2D splay mapped onto the molecule following the same red and blue color scheme. This figure was made with MacPyMOL (90) using PDB ID 6I1B.

Ramachandran Plots

To further investigate changes in the population distribution of ϕ, ψ backbone dihedral Ramachandran plots were generated using the $^{13}\text{C}^\alpha$, $^{13}\text{C}^\beta$, $^{15}\text{N}^H$ and $^1\text{H}^N$ chemical shifts determined from the HNCA and the CBCA(CO)NH NMR experiments and the PREDITOR web server (84). The dihedral angle distributions demonstrates the strong preference for the low energy core α and β regions of the Ramachandran plot as defined by Morris *et al.*, 1992. Figure 3-6 presents the Ramachandran plots for PM23 (Figure 3-6A, left) and PM142 (Figure 3-6B, left) overlaid on that of WT IL-1 β . Overall, the torsion angle distribution for both permutant variants appears to be similar to WT, as indicated by the overlapping points. Differences are identified as backbone torsion angles that shift into sampling another quadrant. For example residue 15 samples β -core in WT now samples α -core in a permutant. Differences seen in PM23 (Figure 3-6A, right) reside in the first and third trefoil subunit of the protein, as indicated by the red region along one side of the protein molecule. For PM142, variations from WT are in the region of the third trefoil following the cut site and the tight turn in the first trefoil of the protein, which is near by in space (Figure 3-6B, right). Differences are significant because the backbone torsion angles sample the core α region of the plot, rather than the core β region.

Figure 3-7 presents the Ramachandran plots for the two permutant variants within the region associated with the kinetic intermediate (residues 58-123), PM 65 (Figure 3-7A, left) and PM76 (Figure 3-7B, left) respectively, overlaid on that of WT IL-1 β . Although the plots appear different compared to WT, the overall scatter of the

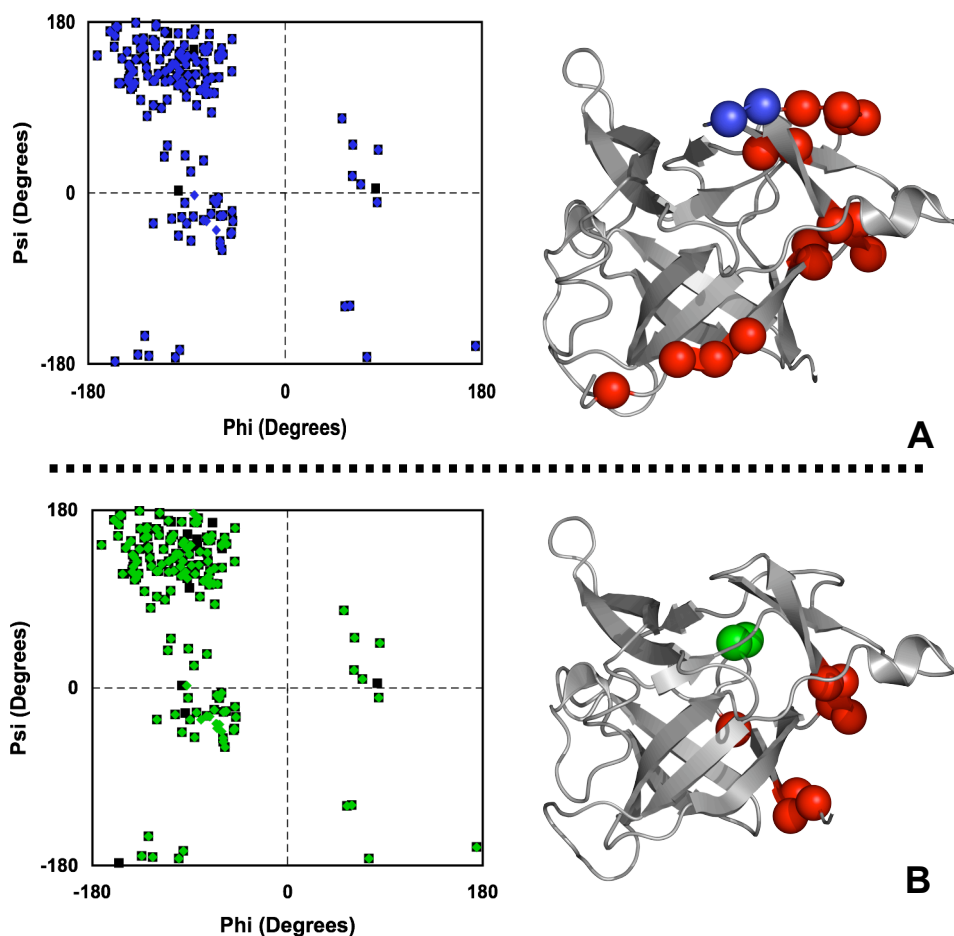


Figure 3-6: A representation of the similarity in the Ramachandran plot of PM23 (A) and PM142 (B) with respect to WT IL-1 β along with the effects of the changes mapped back onto the molecule.

On the left, the Ramachandran plot illustrates the overall similarities in phi and psi angles between WT (■) and the PM23 and PM142. (A) The plot of PM23 (◆) overlaid onto WT. The overall distribution of the torsion angles for the permutation is similar to WT. Most of the differences reside in the first trefoil subunit of the protein. (B) Plot of PM142 (◆) overlaid with WT. The overall distribution of torsion angles for the permutation is similar to WT. Changes appeared in the region following the cut-site in the third trefoil subunit and a turn in the first trefoil subunit of the protein. On the right, the **red** spheres highlighted the change in torsion angles, while the location of the cut site was highlighted in the permutant color scheme. The torsion angles were generated from PREDITOR (84) by combining sequence alignment methods with chemical shift data. The ribbon structure was generated using MacPyMOL (90) and PDB ID 6I1B.

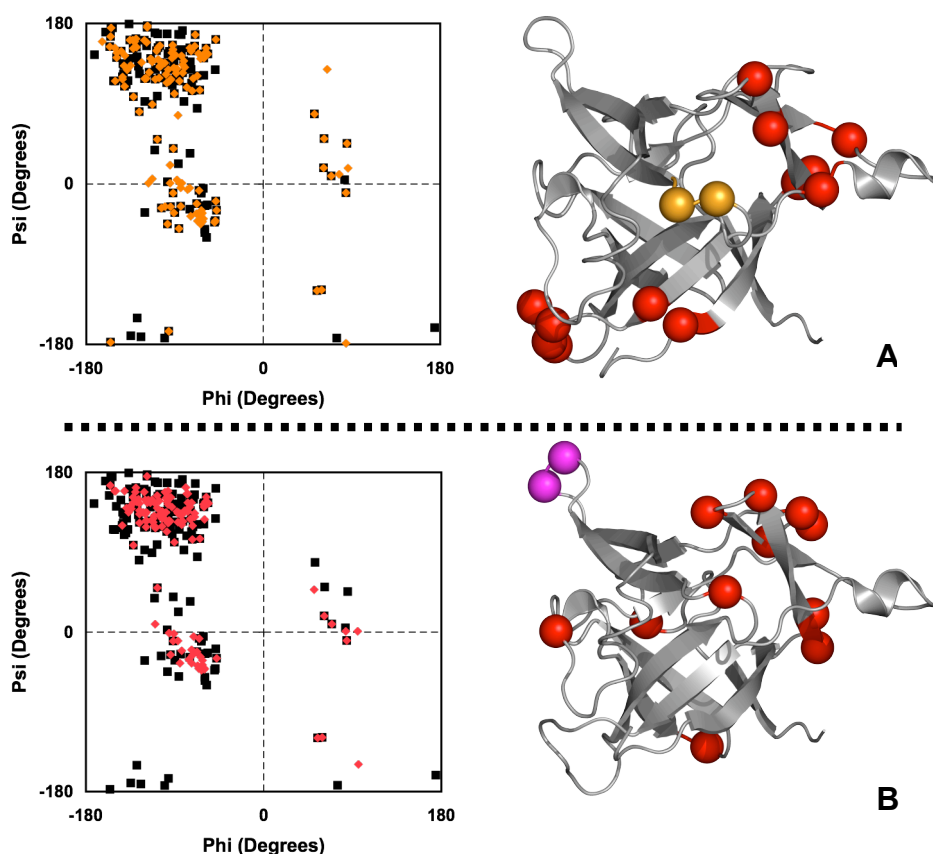


Figure 3-7: A representation of the similarity in the Ramachandran plot of PM65 (A) and PM76 (B) with respect to WT IL-1 β along with the effects of the changes mapped back onto the molecule.

On the left, the Ramachandran illustrates the similarities and differences in phi and psi angles between WT (■) and the respective permutations. (A) The plot of PM65 (◆) overlaid with WT. Differences appear in residues in the first trefoil subunit of the protein and the β -bulge region. (B) Schematic of PM76 (◆) overlaid with WT. Differences appear in the first trefoil subunit, a interface point between the cap and the barrel in trefoil subunit two, and the loops in the $\beta\beta\text{L}\beta$ motif in trefoil subunit two and three. Although the plots appear different compared to WT, the overall scatter of the torsion angles for both permutations sample the same core α and β regions with respect to WT and are shifted within error of the WT plot. On the right, the **red** spheres highlight the changes in torsion angles, while the location of the cut site is highlighted in the permutant color scheme. The torsion angles were generated from PREDITOR (84) by combining sequence alignment methods with chemical shift data. The ribbon structure was generated using MacPyMOL (90) and PDB ID 6I1B.

torsion angles for both permutations sample the same core α and β regions with respect to WT and are shifted within error of the WT plot. Differences in PM65 (Figure 3-7A, right) predominately appear in residues residing in the first trefoil subunit of the protein and the region encompassing the functional loop between the first and second trefoil subunit (β -bulge). This is just prior to the location of the cut site, as indicated by the red regions of the molecule. Differences in PM76 (Figure 3-7B, right) appear in residues in the first trefoil subunit of the protein in the a interface point between the cap and the barrel in trefoil subunit two, as well as the loops between strands 7 and 8 and between strands 11 and 12. The structural alterations in subunit two are a result of the cut site location. For both sets of data, all residues that sample the β -core region of the Ramachandran plot in WT and are different in the permutants, sample the α -core region of the plot.

Native-State Hydrogen-Deuterium Exchange (HDX)

The ^1H - ^{15}N HSQC spectra of all four permutations are well-resolved and the cross-peaks in each respective spectrum have been assigned to a sequence-specific residue (Figure 3-3). Native-state hydrogen-deuterium solvent exchange (HDX) detects the rate of solvent exchange of individual backbone amide hydrogen atoms. The H/D exchange rates can be determined by fitting the time-dependent rate of exchange for individual amino acid residues detected in the collection of series of ^1H - ^{15}N HSQC spectra. The H/D exchange rate for ~70 of 153 amide protons in WT and ~60 of 157 amide protons in each permutation (the four additional amino acids coming from the linker) was fitted and calculated at pD 5.4 at 36°C. Figure 3-8 shows overlapping ^1H -

^{15}N HSQC spectra of the time-course of H/D exchange for each permutant (PM23 in **blue**, PM65 in **orange**, PM76 in **red** and PM142 in **green**) and WT IL-1 β (in **black**) overlaid together. Residues that were slow to exchange are similar for all proteins (Figure 3-8).

Globally, the IL-1 β variants behave similarly but there are differences at the level of individual residues. In Figure 8, residues from selected areas of the molecule with well-resolved ^1H - ^{15}N resonances were chosen as representative time courses. Figure 3-9A is a representative plot of slow amide proton exchange for all proteins. Figure 3-9B and C indicate amide protons that have intermediate (3-9B) and fast (3-9C) exchange, respectively. The H/D exchange rates of the backbone amides were determined by fitting the observed intensity to equation 6 in **GENERAL METHODS**. Figures 3-10 and 3-11 are schematics depicting the H/D exchange for all the permutations as a 2D splay (top), and mapped back onto a ribbon diagram of the individual trefoil subunits in the same orientation as the splay diagram (bottom). The fitted exchange rates were plotted as protected (**blue** data points) for slow exchange rates, intermediate protection (**yellow** data points) for rates of intermediate exchange, and less protected (**red** data points) for fast exchange. The schematic of each permutation highlights regions of similar solvent exchange to WT in proteins that are generally destabilized. The majority of the changes in protection are in β -strands 1-3 located in the first trefoil subunit, β -strand 5, which follows the functional loop of IL-1 β , and β -strand 11 that has hydrogen-bonding partners with β -strand 3. The permutant variants are more prone to solvent exchange, compared to WT IL-1 β , as demonstrated

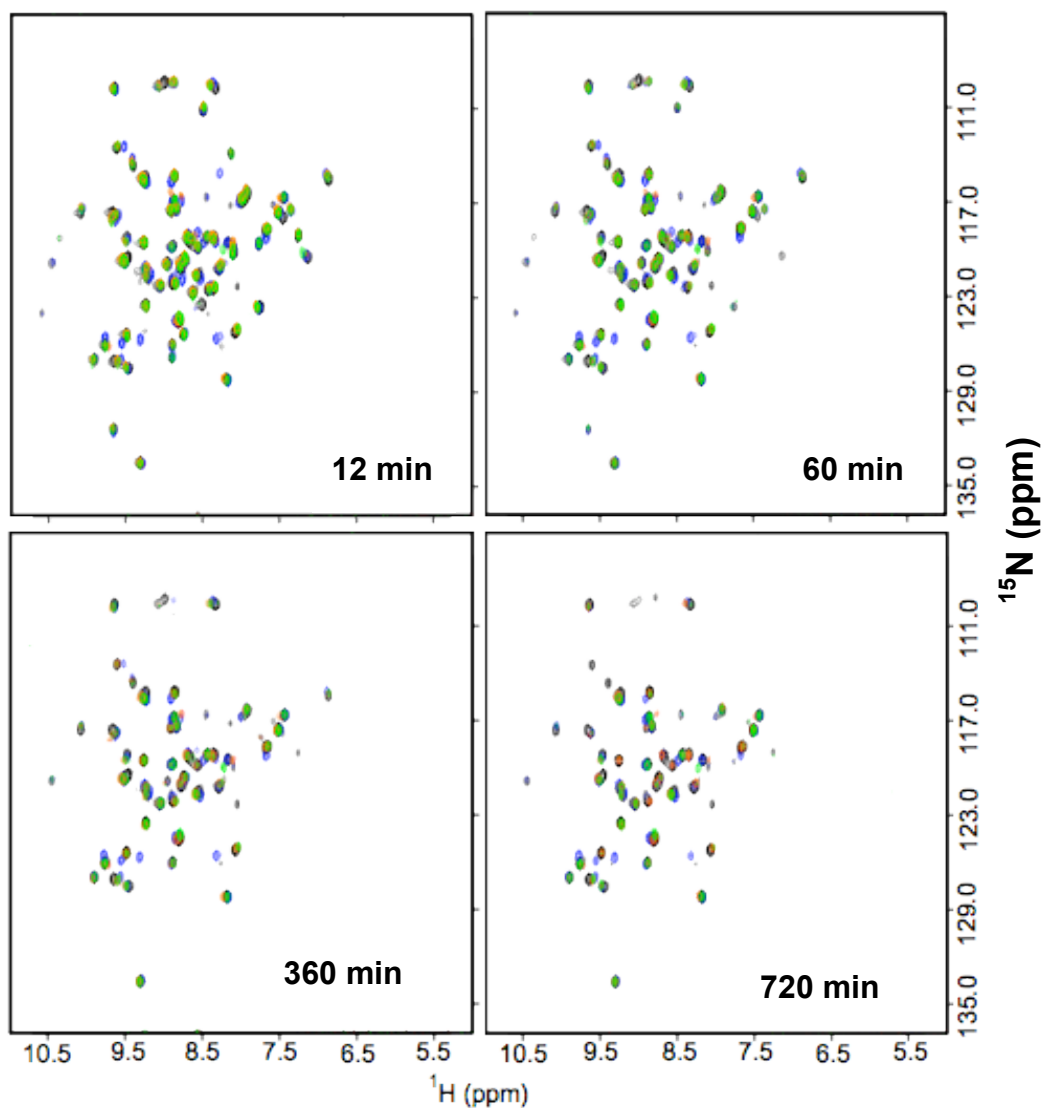


Figure 3-8: Time course of hydrogen-deuterium (HDX) exchange via NMR. ^1H - ^{15}N -HSQC at various time points during the H/D exchange experiment.

Each permutant (PM23 **blue**, PM65 **orange**, PM76 **red**, PM142 **green**) is overlaid together with WT (in **black**). These representative HSQC spectra indicate the initial probes available at initiation of the experiment and gradual disappearance of peaks over time. Residues in permutants slow to exchange were similar to those in WT IL-1 β . The experiment was initiated by exchanging protein into 100mM NaOAc- d_3 , in D_2O , pD 5.4.

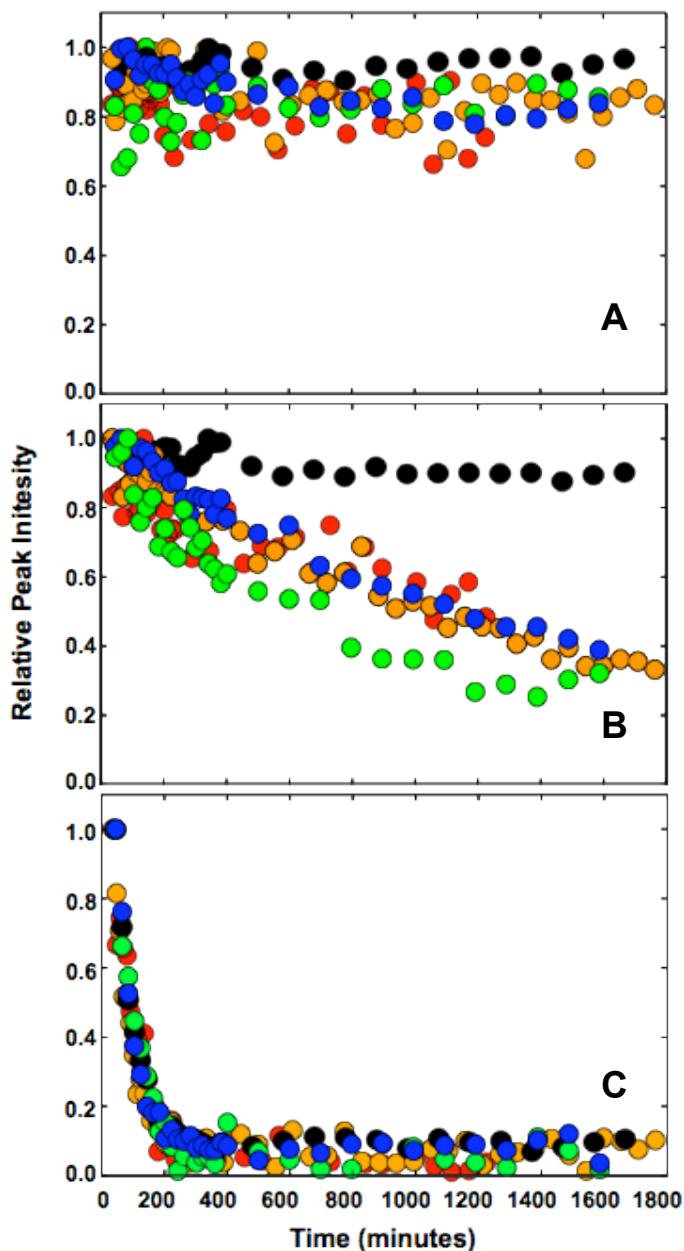


Figure 3-9: Representative comparisons of H^N solvent exchange rates between WT IL-1 β and permutant proteins.

The decay of amide signals over time is shown for WT IL-1 β (●), PM23 (●), PM65 (●), PM76 (●), and PM142 (●), illustrating the differences in the amide signal decay. (A) Residue I104 is an example of an amide proton that is protected from exchange. (B) I19 is an example amide proton that has an intermediate rate of exchange over time for the permutated proteins, which is different, from the slow rate of exchange seen in WT, and (C) L106 illustrates amide proton that is less protected from deuterium exchange.

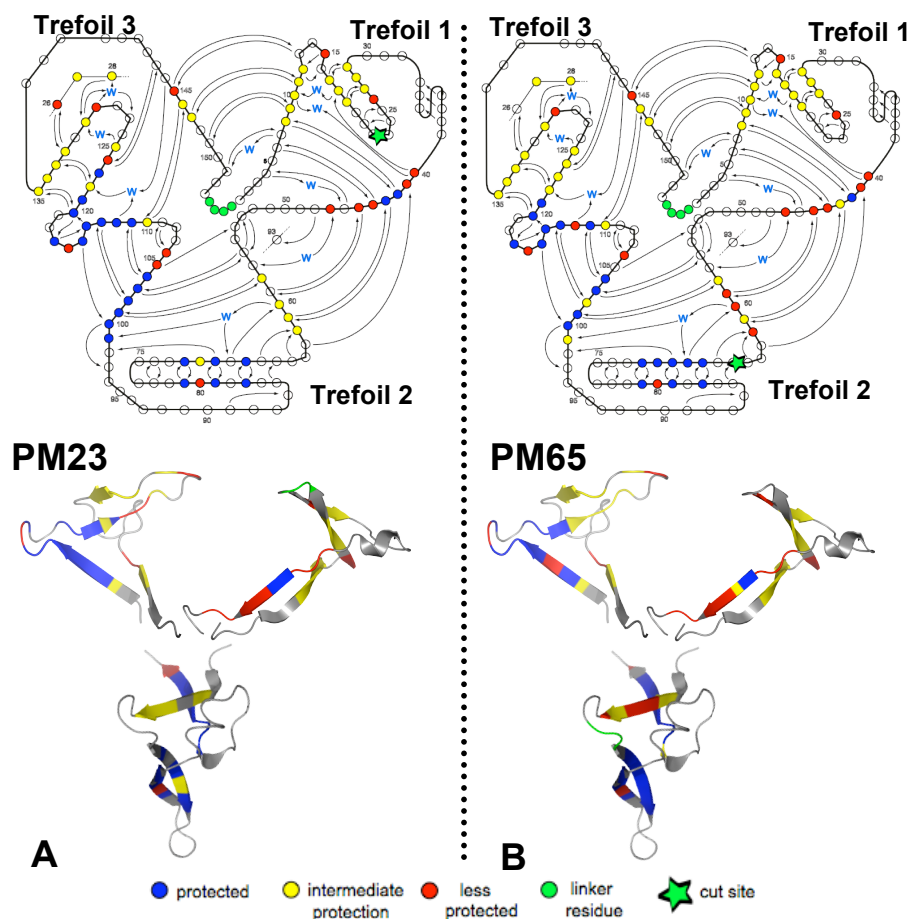


Figure 3-10: Illustrations depicting hydrogen/deuterium exchange (H/D) for the IL-1 β permutations, (A) PM23 and (B) PM65.

NMR detected H/D exchange studies on two permutants were conducted to determine local or global differences in the native state stability of secondary structure with respect to wild type. The upper figure is a 2D splay diagram of the H/D results for permutations of IL- β . Circles in the figure represent each amino acid in the polypeptide chain. **Blue** circles represent amide backbone residues that are stable, or protected, from deuterium exchange. **Yellow** circles represent residues that show some protection from exchange while **red** circles represent those that exchange away rapidly. The schematic of each permutation highlight regions of hydrogen bonding stabilization in proteins that are generally destabilized. Trefoil subunit 1 and the strand following the β -bulge are more dynamic than WT in the permuted variants, showing less protection. Stable residues in the second and third trefoil subunits for both permutations are similar to WT IL-1 β . The lower figure highlights the results on the molecule of IL-1 β , in the trefoil subunit layout. The trefoil subunit ribbon molecule was generated using MacPyMOL (90) and PDB ID 6I1B.

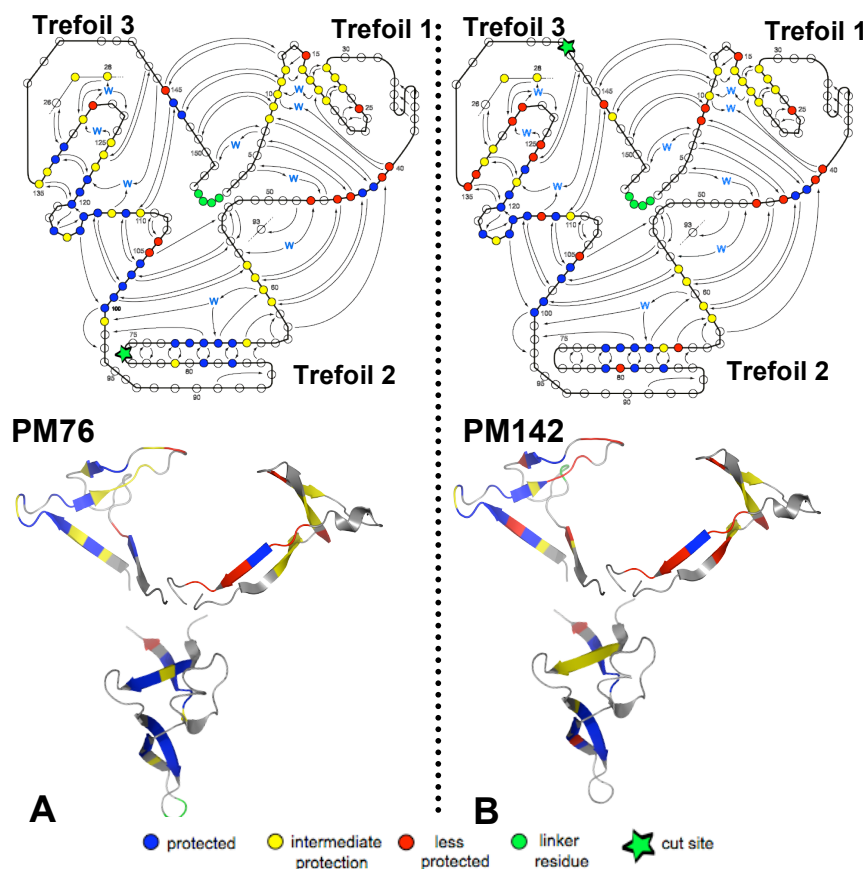


Figure 3-11: Illustrations depicting hydrogen/deuterium exchange (H/D) for the 1 β permutations, (A) PM76 and (B) PM142.

NMR detected H/D exchange studies on two permutants were conducted to determine local or global differences in the native state stability of secondary structure with respect to wild type. The upper figure is a 2D splay diagram of the H/D results for permutations of IL- β . Circles in the figure represent each amino acid in the polypeptide chain. **Blue** circles represent amide backbone residues that are stable, or protected, from deuterium exchange. **Yellow** circles represent residues that show some protection from exchange while **red** circles represent those that exchange away rapidly. The schematic of each permutation highlight regions of hydrogen bonding stabilization in proteins that are generally destabilized. Trefoil subunit 1 and the strand following the β -bulge are more dynamic than WT in the permuted variants, showing less protection. Stable residues in the second and third trefoil subunits for both permutations are similar to WT IL-1 β . The lower figure highlights the results on the molecule of IL-1 β , in the trefoil subunit layout. The trefoil subunit ribbon molecule was generated using MacPyMOL (90) and PDB ID 6I1B.

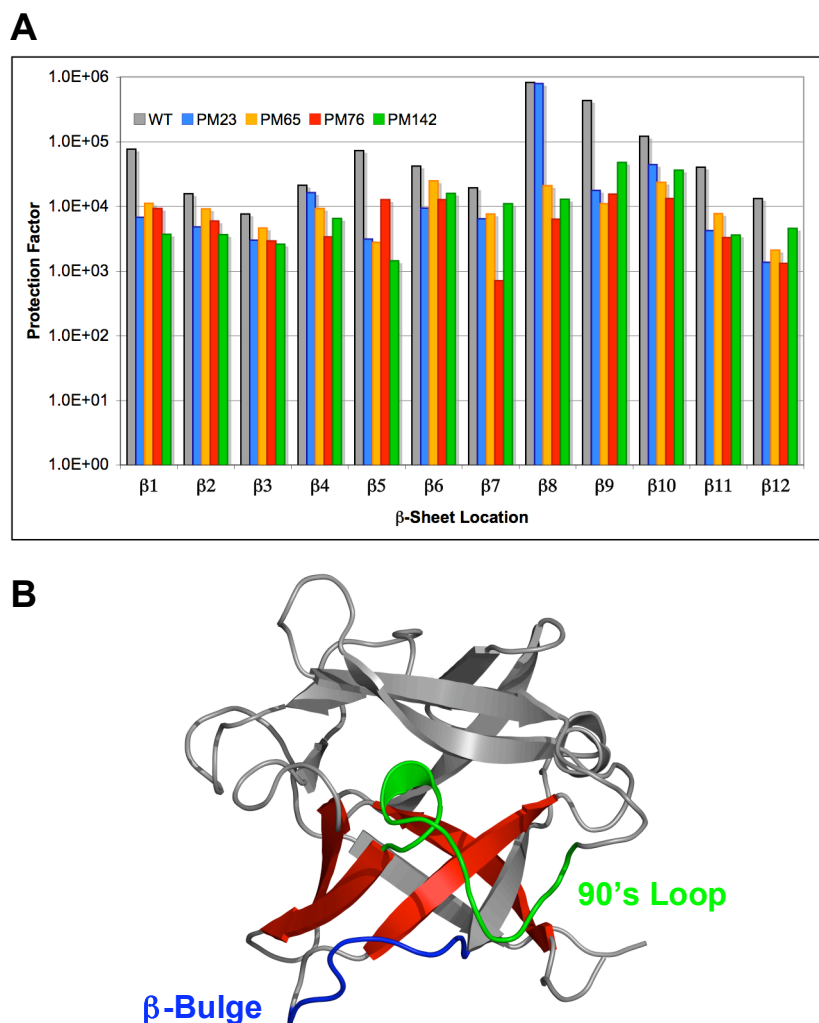


Figure 3-12: The estimated protection factors show similar pattern of protection for all proteins with four β -strands showing less protection in the region located near the functional loop.

(A) The graph represents the estimated average protection factor for each β -strand in all the proteins calculated from fitting the H/D exchange data. WT is in grey, permutants PM23 in blue, PM65 in orange, PM76 in red, and PM142 in green. The pattern of protection is similar for all the permutations with respect to WT, although the average protection factor is reduced for all permutants. Overall, β -strand 1, 5, 8 and 9 shows the greatest effect with decreased protection factors for all permutations with respect to WT. (B) The molecule of IL-1 β with the differences in protection factors mapped in red. These strands are located near the β -bulge functional loop (blue) and the 90's loop (green) in space. The ribbon molecule was generated using MacPyMOL (90) and PDB ID 6I1B.

by a majority of the stable probes in WT showing less protection from exchange, permutations exhibiting protection factors near an order of magnitude less than WT. The difference in protection factors for β -strand 1 may be due to the to the presence of the linker clashing with the β -bulge (**blue** in Figure 3-12B) that is located near the C-terminal end in space. The difference in protection factors for β -strands 5, 8 and 9 may be a result of the permutations having to pack the β -bulge, which is close to the 90's loop (**green** in Figure 3-11B) in space, in order to maintain the functionality of the proteins, therefore disrupting the local environment and altering the rate of H/D exchange.

Discussion

Circular permutations provide an excellent framework for studying the effects of chain connectivity on the global fold of proteins. Despite many successful studies of permutant proteins, work on circular permutants of DHFR indicate that some regions of a sequence may constitute essential folding elements, and permutation at these sites may inhibit folding or disturb the native fold (94). However, circular permutation of several different families of proteins still resulted in native-like structure(93). Most circular permutations result in minor structural changes and minimal loss of stability (98). However, certain regions of a protein may be more tolerant of disruptions than others (101). Circular permutations were tolerant at more than half of the 158 possible sites in DHFR (94).

Combined experimental/theoretical models of the folding of IL-1 β are in good

agreement (36, 63) and indicate that the folding of IL-1 β appears to be influenced primarily by topological effects. Therefore, it is of interest to characterize the global fold and global and local stability of circular permutations prior to determination of the folding mechanism. NMR experiments were completed in order to assess global and local structural features of IL-1 β permutant variants relative to WT, especially with the variation of the N- and C- termini. Initial expression and purification indicate that permutations or cut-sites within the β -bulge and the 90's loop prevent folding to a stable native state. Follow-up NMR spectral work showed no characteristic fingerprint but instead as demonstrated in Figure 3-3, degenerate chemical shifts for resonances are consistent with denatured protein. These two regions of IL-1 β are important functionally and apparently suggest that they are also important for the energetics and stability of the β -trefoil fold of IL-1 β .

Similar ^1H - ^{15}N HSQC spectra confirm the assessment that the overall fold for all other permutant variant studied remains intact compared to WT (Figure 3-4). The ^1H - ^{15}N signals of the IL-1 β amide proton resonances have a unique chemical shift dispersion and a pattern to the protein that are correlated to the secondary structure and tertiary interactions (35, 47). The ^1H - ^{15}N HSQC spectra of PM23 (**blue**), PM65 (**orange**), PM76 (**red**) and PM142 (**green**) were essentially identical to WT (**black**) except for perturbations attributed to the cut sites in each permutant as well as four additional cross-peaks in the four permutant spectra attributed to the TAQT linker. Unlike DHFR where permutations within the kinetically important folding element did not fold (94), cut sites within the area encompassing the intermediate structure formed

as a prerequisite to folding (strands 5-9 and residue 42) (i.e. PM65 and PM76) in IL- β did not alter the global fold. This suggests that although these turns are important in forming a folded protein, they are not essential. Or, the kinetic intermediate is so important that there are back-up plans in place.

Isotopically labeled protein was used for ^1H - ^{13}C - ^{15}N triple resonance NMR spectroscopy. NMR experiments were performed in order to confirm the sequence-specific assignments for each permutation. From the HNCA spectral data, residue-specific $^{13}\text{C}^\alpha$ chemical shifts were acquired and were used as empirically accurate barometers of secondary structure propensities (82, 102, 103). Figure 3-5 indicates that most of residue-specific deviations that have affected dihedral angles were seen at topologically equivalent sites at turns and hinge points, it appears there is a compensatory twisting of angles in order to preserve the native global fold. Turns are important in creating the topology and the arrangement of the β -strands for β -trefoil proteins (42, 44, 47, 81). Consistent with those studies, our data indicate destabilization in the turns in order to maintain the overall β -trefoil fold of the permutations. The residues, in which the dihedral angles twist in an opposite, and possibly compensatory fashion, occur mostly at the interface between the cap and the barrel core of the protein. Conservation of function is the driving force to preservation of domains (104). Therefore, the strain of the permutation causes backbone angles of certain residues close to the barrel shift to preserve the barrel. The stress introduced by the twist in the strand can then be dissipated by distributing compensatory ϕ, ψ angle shifts a few residues away, either within the cap or at the interface of the two.

In order to further analyze the results of the CSI of the permutant variants, Ramachandran plots were generated in order to compare how the ϕ and ψ values clustered for the different permutations relative to WT. Figures 3-7 and 3-8 both illustrate residue-specific changes within the Ramachandran plots overlaid on a plot of WT. Generally, most of the residue backbone dihedral angles cluster in the preferred α and β regions of the plots, indicating similar torsion angles and therefore secondary structure to WT protein. The variants shown in Figure 3-7A, PM23 in **blue** and 3-7B, PM142 in **green**) do not show significant differences as a result of the rearrangement. The two variants with the cut sites located within the structure of the kinetic intermediate (3-8A, PM65 in **orange** and 3-8B, PM76 in **red**) have more residues that are shifted. However, although the plots of PM65 and PM76 appear different compared to WT, the overall scatter of the torsion angles for both permutations sample the same core α and β regions with respect to WT and are shifted within error of the WT plot. This may indicate permutant population ensembles sampling more unstructured regions. Trefoil subunit 1 appears to be where the strain from the permuted structures is released, as most of the deviations from WT appear to be in the first trefoil subunit for all the permutations. This may be indicative of the “pinching” of the barrel in order to maintain the functionally important β -bulge (63). The geometrically frustrated β -bulge in IL-1 β occurs between the pairing of strands 4 and 5 where the proline residue in strand 5 interrupts the standard intrastrand β -sheet hydrogen-bonding pairing. Residues 47-53 in strand 4 loop out to accommodate the geometric twist of the imide peptide bond of the proline residue before resuming the normal hydrogen bonding pattern

between strands. (44) The disruption of the standard intra-strand hydrogen-bonding pattern in order to form the bulge at residues 47-53 adds to the strain to the native fold by “pinching” the side of the barrel (63).

To further assess the global stability and local stability at the level of the individual residue, H/D solvent exchange was followed. Predominantly, differences in protection factors were seen in trefoil subunit one and β -strands 5, 8, and 9. These differences may be attributed to increased sampling of unstructured states of the functional loop as the permutant variants macroscopically maintain the overall global fold and possibly conserve function. The similarity in thermodynamic stability for particular strands may be an indication that the permutations folds along a similar route as IL-1 β , thus conserving the initial contacts that form the kinetic intermediate. H/D solvent exchange on BPTI suggested that the important protein-folding contacts are within the slowest exchanging protons (105). Applying this analysis to the permutant variants of IL-1 β , backbone amides that were slow to exchange are located within the region of the proteins that have been shown to fold first in WT.

Taken together, circular permutation of IL-1 β result in variants that maintain the native tertiary structure, as well as variants that don't. Those variants with a global fold similar to WT demonstrate similar levels of protection from solvent exchange. While the β -sheet core of the protein is not entirely slow exchanging, residues within the core that are slow to exchange are consistent with residues determined experimentally to contribute to the kinetic intermediate(37, 38). Knowledge of the overall structure and

stability as well as local structure and stability of the permutant variants lays the groundwork for the interplay of chain connectivity and folding energetics.

Chapter 4

Circular Permutation of Interleukin-1 β Affects the Transition of the Folding Intermediate to the Native Ensemble

Abstract

Experiments were conducted in order to characterize the affects of circular permutations on the folding mechanism of interleukin-1 β (IL-1 β), a member of the β -trefoil family of proteins. Theoretical models indicate that the folding mechanism of IL-1 β has a strong topological dependence and has a more complex folding route and a well-populated folding intermediate both experimentally and theoretically. Circular permutations at various loops and turns throughout the protein were less stable than WT. Kinetic refolding and unfolding experiments were carried out in order to determine how different the folding mechanisms are for each permutation of IL-1 β as compared to WT. Folding rates indicates the formation of the intermediate remains the same while the slow phase of folding is significantly affected. These effects are the result of the change in connectivity and contact order and not the linker.

Introduction

The transition states and intermediates formed on the folding route and the rate of folding are largely driven by the topology of the folded state for well-designed proteins (15, 33, 48, 72, 95, 97, 106). For example, despite low primary sequence homology, phi analysis of the folding of proteins of similar tertiary folds which follow a two-state model where only the unfolded or native protein are detected in equilibrium and kinetic experiments are in good agreement with theoretical predictions and the energetic landscape is said to be funneled (24, 107-111). A classical example of topological constraints on folding is exemplified in the studies of the SH3 domains from

acylphosphatase and the protein kinase Src which revealed that these two-state folding proteins have similar transition states in folding (6, 15, 54, 112).

While it is largely accepted that the landscape for the folding of small two-state folding proteins is funneled (17-25). It is clear that more complex, larger proteins and enzymes are subject to the competing pressures of efficient folding, maintaining function and avoiding toxic gain of function during evolution (26-32). It is then essential to determine the limits of topologically driven models-Are they limited to small single-domain two-state folding proteins? No. Pioneering work from the Onuchic and Jennings laboratories demonstrated for the first time that such topology-based folding models also correctly simulated the experimental folding mechanisms of the large systems dihydrofolate reductase (DHFR) and IL-1 β (33-35). In addition, the same holds true for the members of the β -trefoil family of proteins, IL-1 β , FGF-1 and hisactophilin. These proteins share similar topologies, low sequence homology, and folding mechanisms that includes the population of discrete intermediates under certain conditions (6, 15, 37-41).

Experimentalists and theorists have shown that the folding rates for small two-state folding proteins correlate well with the topological parameter referred to as the relative contact order (*CO*) (7, 48-51). The parameter *CO* compares the difference in topology between proteins of different lengths. The parameter is small for proteins where local contacts are favored and large when residues in a protein interact with partners far away in the protein sequence.(7, 48). Relative contact order has been usefully captured the features of protein folding, where proteins with many local

contacts (e.g. α -helices) fold faster than those with predominately non-local contacts (β -sheet proteins) (7, 52). While this simple topological parameter is effective in predicting folding rates for small two-state folding proteins, it fails to predict the folding rates of larger, multi-state proteins (51). Therefore, changes in the contact order of larger proteins should have an affect on the rate of folding.

While changes in the contact order may affect the rate of folding for larger proteins, it does not affect the overall topology. The study of circular permuted proteins presents a particularly interesting way of testing this topology-based model. Application of this same topology-based model to the study of circular permuted proteins for two simple two-state folding proteins, SH3 and CI2 was also in very good agreement with the experimental observations (49, 54, 55). The differences between the folding mechanisms of the permuted and wild type protein are correlated to the change in native state. Based on simulated data, topology is an important determinant in the transition state and intermediate ensemble (15, 33, 48). In IL-1 β , experimental results indicate side-chain interactions also change the energetics of the folding funnel where the transition state has been altered for the rate-determining step in folding (34).

Circularly permutating the amino acid chain involves linking the N- and C-terminal ends together by a chemical bond or a peptide linker sequence. This works best when the N- and C-termini are close in space. The polypeptide chain is subsequently broken between residues i and $i + 1$, so that i and $i + 1$ becomes the new N- and C-termini of the circularly permuted protein. A circular permutation of bovine pancreatic trypsin inhibitor was first designed to investigate the role of chain

connectivity on protein folding (53). More recently, circular permutation studies have been useful in understanding key topological determinants in the folding and stability of a number of protein systems (49, 52, 92, 95, 96, 98, 113-115). The variety of structural motifs represented by these proteins demonstrates that the propensity to fold is not limited by the type of secondary structure nor the distribution of amino acids in the sequence (95). Thus, while the primary sequence is shifted, it is unchanged at the same time chain connectivity and contact order are modified. While the contact order for individual permutations will differ, the overall topology remains the same. Therefore, differences between WT and permutant proteins should be the result of topological modifications without regard to steric or charge-charge interactions. Simulations on the β -trefoil family of proteins demonstrated that the global fold determines the energy landscape, whereas the amino acid sequence determines the routes preferred within the landscape (36).

While extensive research, both experimental and theoretical, has contributed to understanding how the different parameters contribute to protein folding, experiments have been limited to well-characterized, smaller, two-state folding proteins. Understanding the affects of these same parameters on more complex, multi-state proteins has proved more challenging. IL-1 β has a β -trefoil global fold that contains 12 β -strands; six form the core β -barrel, and six strands the hairpin cap (44, 81). Experimental and theoretical studies agree that IL-1 β folds via early formation of a central core that is a well-populated kinetic intermediate that forms on the millisecond timescale followed by turnover to the native structured state that occurs on the seconds

to hours timescales (depending on experimental conditions) (33, 38, 45, 46). Real-time NMR kinetic experiments of the denaturant-induced *unfolding* of IL-1 β revealed a rugged unfolded landscape where, unexpectedly, the native-like turns were observed to be the most persistent structures within the topology. Indeed, turns were the last to unfold (47). In the present study, we utilized the fact that the N- and C-termini of IL-1 β are close to one another in the native structure and could easily be joined with molecular biological techniques to create a series of circularly permuted proteins (53, 92, 96, 116-119). The experimentally identified major folding intermediate and the persistent turns observed in real-time *unfolding* studies provide a natural starting places for designing new N-and C- termini into IL-1 β .

Here we present the effects of engineering new N- and C-termini into IL-1 β on the folding of the mutant protein. Initial studies focused on the permutants with “cut sites” within the observed early intermediate formed during the folding of the WT protein. Permutations between residues 65 and 66 (PM65), 75 and 76 (PM76), both located in the second trefoil subunit, were designed in the middle of the intermediate structure that includes residues 58 to 123 (Figure 3-2B). In addition, we constructed two permutations at turns and loops in the first (permutation at residues 22 and 23, PM23) and third (permutation at residues 141 and 142, PM142) trefoil subunits. The TAQT linker, used to fuse together the native N- and C- termini, was optimized for biological activity of IL-1 β and shows identical biological behavior to the WT protein (92). To test what affect the linker may have on the folding (if any), PM 76 was constructed with four different linkers **TAQT**, **GGGG**, **GGGGG**, and **GGGGGG**. We discovered that

cut sites within the functional regions of the protein did not fold. We also discovered that whether or not the cut site was within the sequence of the early core formation that the rate of intermediate formation of the central core was essentially unchanged. However, interconversion of the intermediate to the native state was clearly slowed. Equilibrium denaturation studies indicate that all permutants have destabilized native state and decreases cooperativity in folding where permutations within the area of the kinetic intermediate, PM65 and PM76, demonstrated the greatest loss in stability. All PM76 proteins had the same equilibrium and kinetic behavior despite the variation in size and composition of the linker used indicating that the changes observed in all the permutations were a result of the change in connectivity and not an affect of the linker.

Special Methods

To construct a permutation with varying linker lengths, we followed the same tandem-gene method (See Chapter 3, Special Methods), making modifications to two primers used to form the double-gene. Primers used for the construction of the IL-1 β permutants containing the poly-glycine linker (Figure 4-1):

Primer Cg: 5' GGC GGGGGTGGCGCACCTGTACGATCACTGAACTGC 3'

Primer B4mer: 5' GGTGCGCCA CCCCCGCCGG AAGACACAAATTGCATGGTGAA 3'

Primer B5mer: 5' GGTGCGCCA CCCCCCCCCGCCGG AAGACACAAATTGCATGGTGAA 3'

Primer B6mer: 5' GGTGCGCCA CCCCCCCCCCCCCGCCGG AAGACACAAATTGCATGGTGAA 3'

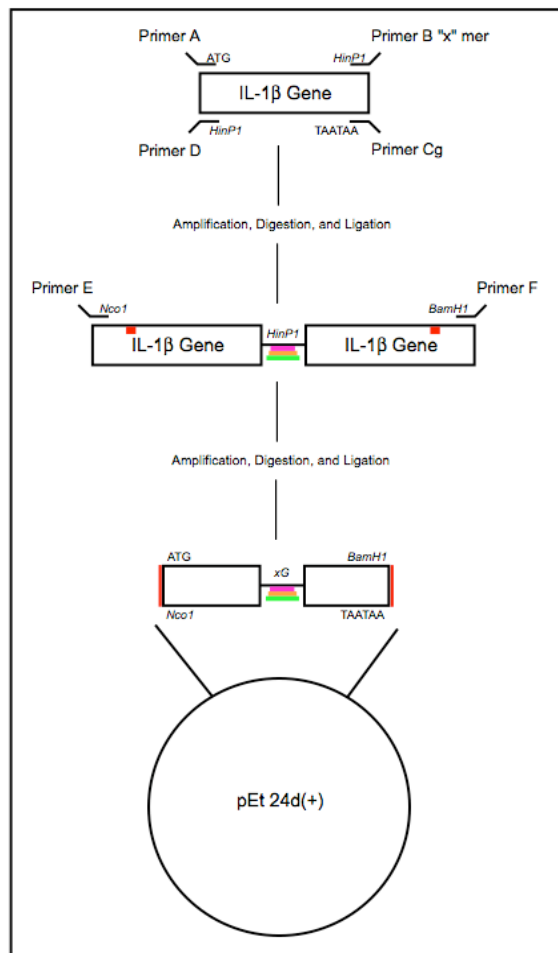


Figure 4-1: Schematic of tandem-gene design for the construction of the IL-1 β permutant linker variants.

Representation of the design of the glycine linker variants. The linkers are designated by color, 4G (**magenta**), 5G (**orange**), and 6G (**green**) and are represented by the colored linker in the figure. This color scheme will be used throughout the thesis.

Glycine linker constructs were created using the same principle as above with Primer A remaining the same and Primer B changing for fragment 1 to include the multiple glycine linker in place of the TAQT linker and a *HinPI* restriction site, rather than the *SfiI* restriction site. Primer D remained the same and Primer C was changed to include the multiple glycine linkers in place of the TAQT linker and the *HinPI* restriction site for fragment 2 in place of the *SfiI* restriction site. The same primers were used in a PCR reaction for the formation of the permutants from the ligated fragments as a template.

Results

β -Trefoil Superfold Remains Intact in all IL-1 β Permutants Proteins

Similar ^1H - ^{15}N HSQC spectra presented in Chapter 3 confirm the assessment that the overall fold for each permutation remains intact compared to WT (Figure 4-2). The ^1H - ^{15}N signals of the IL-1 β amide proton resonances have a unique chemical shift dispersion and a pattern to the protein that are correlated to the secondary structure and tertiary interactions (35, 47). ^1H - ^{15}N HSQC spectra of PM23 (**blue**), PM65 (**orange**), PM76 (**red**) and PM142 (**green**) were essentially identical to WT (**black**) except for perturbations attributed to the cut sites in each permutant as well as four additional cross-peaks in the four permutant spectra attributed to the TAQT linker.

All Permutants are Destabilized Relative to WT and have Decreased Cooperativity in Folding

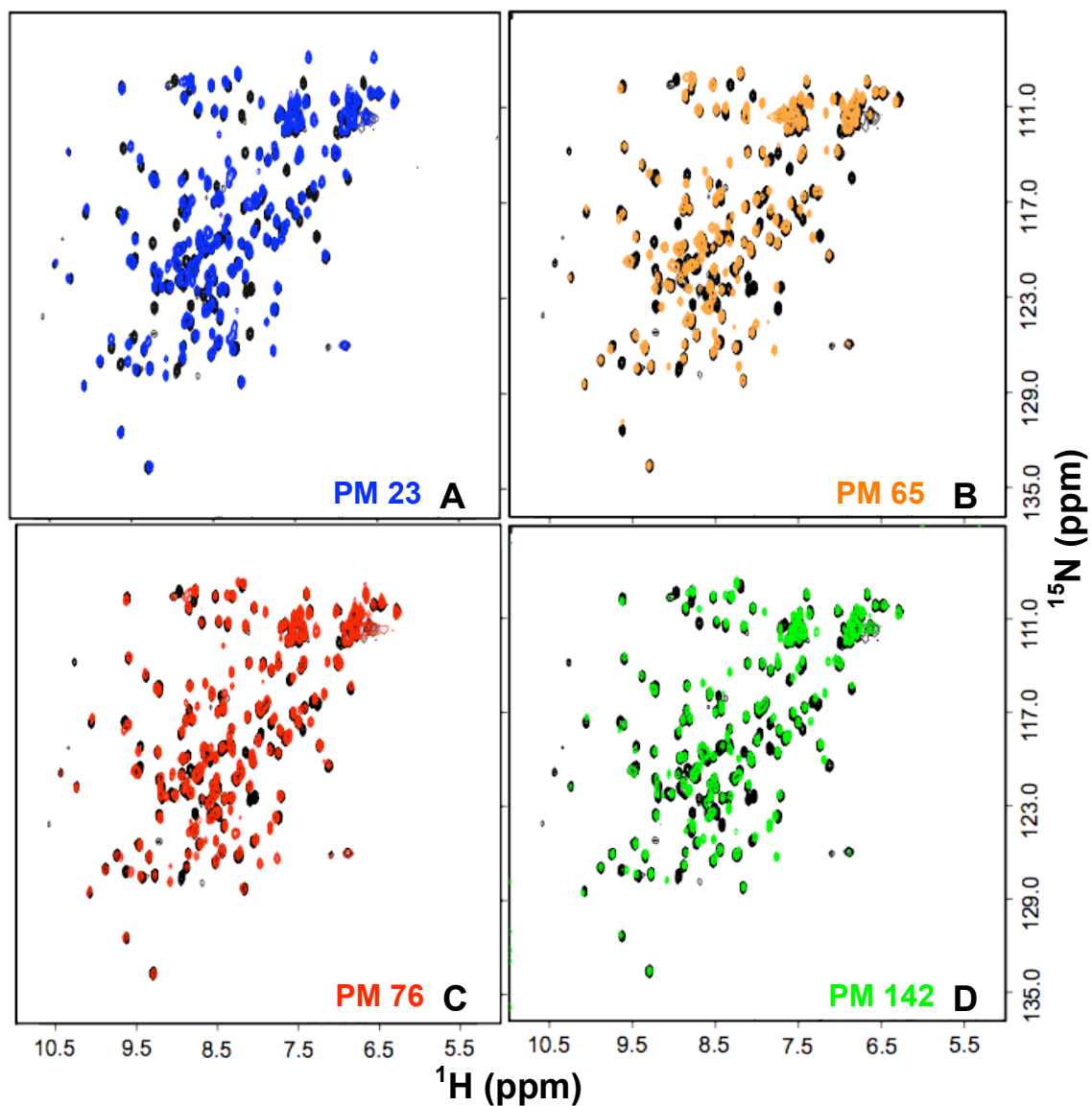


Figure 4-2: Analysis of the fingerprint pattern of ^1H - ^{15}N -HSQC spectra of wild type and permutant IL-1 β strongly indicate similar tertiary structure and an intact β -trefoil fold.

These representative spectra demonstrate similarities in the global fold of the proteins. Each permutant spectrum is overlaid with a spectrum of WT IL-1 β (in **black**). (A) PM 23 overlaid in **blue**. (B) PM 65 overlaid in **orange**. (C) PM 76 overlaid in **red**. (D) PM 142 overlaid in **green**.

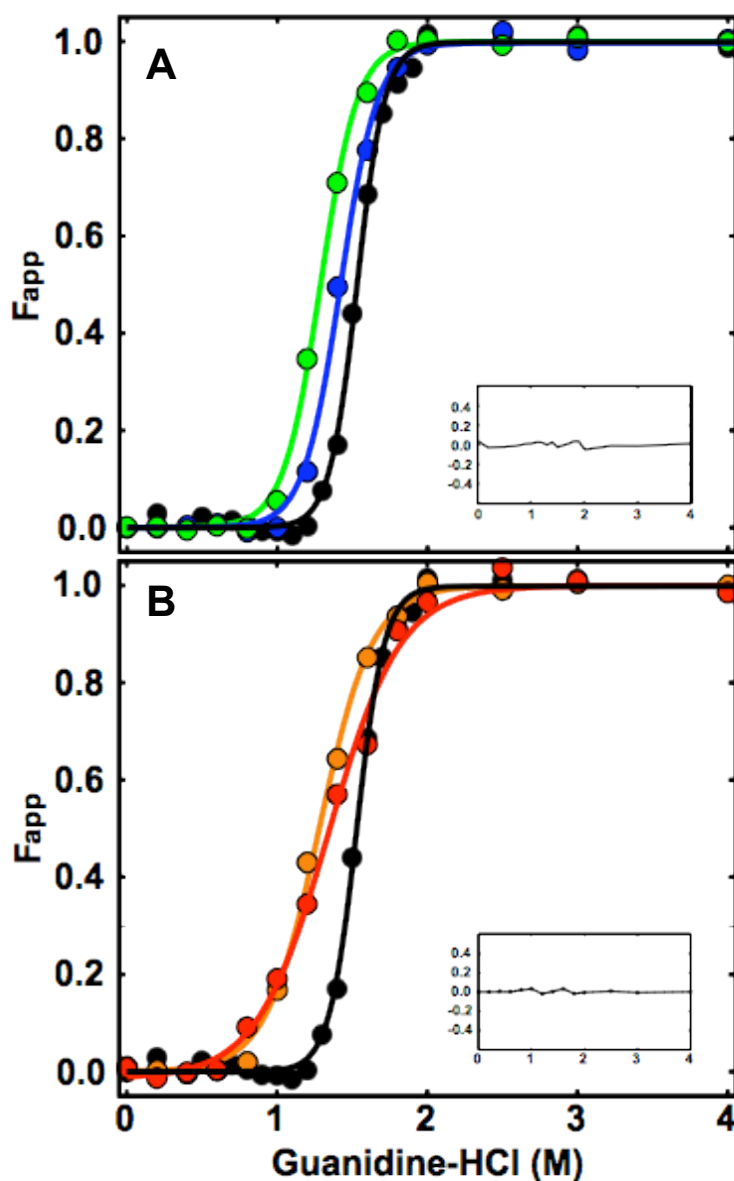


Figure 4-3: Plots of F apparent (F_{app}) as a function of denaturant concentration for the equilibrium unfolding of wild type and permutant proteins at pH 6.5 and 25°C indicate destabilized protein variants.

(A) Equilibrium denaturation curves for IL-1 β WT (●), PM23 (●), and PM 142 (●) plotted as F_{app} versus denaturation concentration. Continuous lines representing best-fit curves are fit to a two-state model are shown in the same color scheme. The residuals of the fit are shown as the inset. (B) An overlay of IL-1 β WT (●) with permutations PM 65 (●), and PM 76 (●). The inset is the residuals for the two-state fit. Both data sets indicate decreased stability as a result of the permutations. Thermodynamic parameters from the two-state best-fit model for each construct are given in Table 4-1.

Table 4-1: Thermodynamic Parameters for WT and permutant IL-1 β

IL-1β	$\Delta G_{N-U}^{a,b}$ (kcalmol ⁻¹)	$\Delta\Delta G_{N-U}^{a,b}$ (kcalmol ⁻¹)	$m\text{-value}_{N-U}^{a,b}$ (kcalmol ⁻¹ M ⁻¹)	C_m^c (M)
WT	7.7 \pm 0.2	0	6.2 \pm 0.3	1.5 \pm 0.1
pm 23	6.8 \pm 0.4	-0.9 \pm 0.4	4.8 \pm 0.2	1.4 \pm 0.1
pm 65	4.3 \pm 0.3	-3.4 \pm 0.4	3.4 \pm 0.5	1.3 \pm 0.2
pm 76	4.0 \pm 0.1	-3.7 \pm 0.2	2.9 \pm 0.3	1.3 \pm 0.1
pm 142	6.2 \pm 0.5	-1.5 \pm 0.5	4.8 \pm 0.4	1.4 \pm 0.2

Changes in folding parameters upon circular permutating IL-1 β at various turns and loops. The equilibrium data were fit using MATLAB in order to obtain equilibrium parameters for folding, ΔG_{N-U} . Changes in ΔG_{N-U} ($\Delta\Delta G_{N-U}$) were obtained using WT as a reference. m -value indicates changes in the accessible surface area upon folding and indicate cooperativity of folding.

^a Equilibrium transition data were evaluated using a two-state folding model.

^b Data were obtained by calculating the average wavelength and calculating the relative average wavelength in terms of F_{app} as a function of [Gnd-HCl].

^c C_m values were taken from dividing the ΔG_{N-U} by the m -value.

To compare the differences between the thermodynamic stability of wild-type and permuted IL-1 β , equilibrium chemical denaturation experiments were performed to determine the extent to which topological modification had on the thermodynamic stability and cooperativity of the native state. The wild type and permuted proteins were titrated over a range of guanidine hydrochloride concentrations from 0 to 4M, at pH 6.5 and 25°C. The folding transition was monitored by the changes in the Trp120 fluorescence intensity as a function of denaturant. Figure 4-3 shows the apparent fraction, F_{app} , of unfolded protein at increasing concentrations of Gnd-HCl, as determined by average fluorescence wavelength and the calculated ΔG and m -values are listed in Table 1. The continuous lines representing best-fit curves in figure 4-3 are all fit to a two-state model. All permutants of IL-1 β are destabilized relative to WT ranging 1.8 to 3.7 kcal/mol (see Table 4-1). Cut sites in the first (PM23) and third (PM142) trefoil of IL-1 β (figure 4-3A) slightly decreases the stability of the protein, whereas cuts in the second trefoil (PM65, PM76), show greater destabilization of the proteins (Figure 4-3B). The cooperativity (m -value) of the permutants (Table 4-1) is decreased relative to wild type.

Fluorescence-Detected Kinetics of Permutations Indicate Changes in Interconversion Rates from Intermediate to Native State

The folding of the circular permutations was followed by fluorescence-detected stopped flow and manual mixing to determine if folding kinetics changed with respect to the native state. The rapid increase in signal, which is described by two exponential

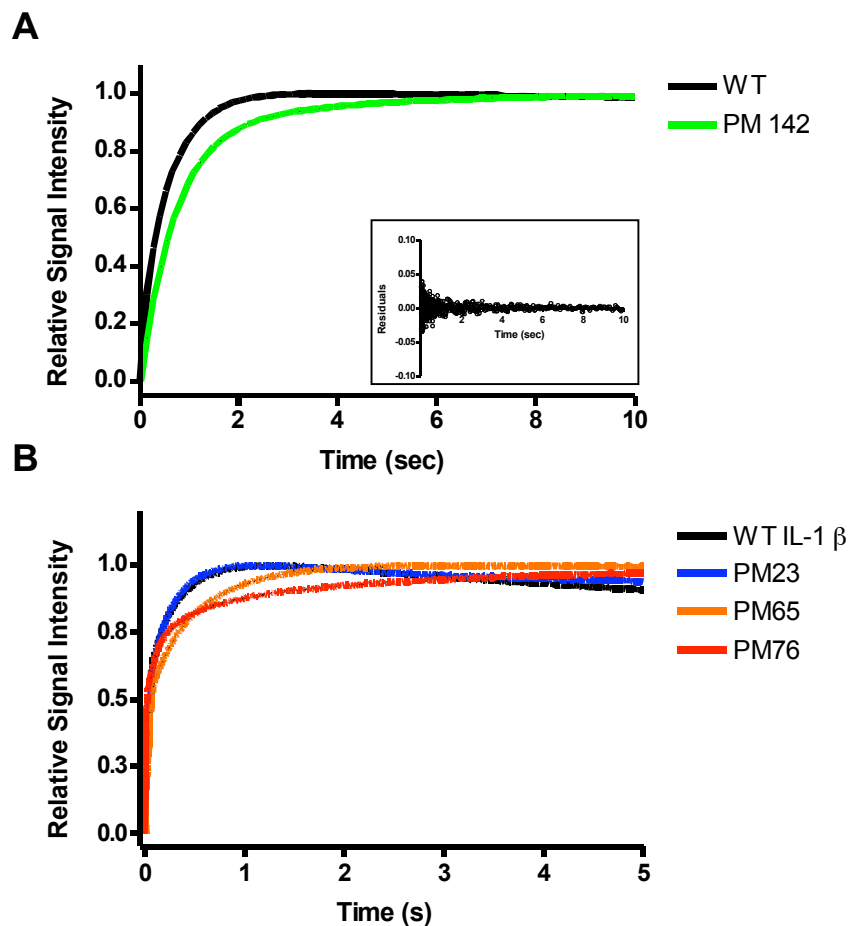


Figure 4-4: Representative traces of the fast phase (τ_2) of folding collected by stopped-flow fluorescence indicating the similarities in the observed rates of folding.

(A) Wild type IL-1 β is in **black** while PM142 is in **green**. The traces are of stopped-flow kinetic refolding jumps from 2.2M Gnd-HCl to 0.4M Gnd-HCl. The tryptophan side chain was excited at 293nm wavelength while the emission was collected for wavelengths >320 nm. (Inset) Representative plot of the residuals for the stopped-flow linear least squared fits. WT and permutant proteins were fit to a three-exponential model. (B) ANS stopped-flow fluorescence-detected refolding of WT and permutant IL-1 β . WT, in **black**, and permutant IL-1 β protein (PM23 in **blue**, PM65 in **orange**, and PM76 in **red**) was refolding from an unfolded state in the presence of ANS. The traces are representative of refolding jumps from 2.2M to 0.3M Gnd-HCl. Data was collected for 250 seconds at 25°C in logarithmic mode with an excitation wavelength of 365nm, and the emission was collected using a cutoff filter >420 nm. The first 5 seconds is shown for clarity.

time constants, τ_3 , that occurs on the millisecond timescale, and τ_2 , that occurs on the millisecond to second timescale, measures the population of a highly fluorescent intermediate from the unfolded state. Measurements of the values of τ_3 have the most experimental error due to the fast rate and the small amplitude of the kinetic trace (45, 71) therefore; elucidation of the effects of the permutations on τ_3 is difficult to interpret (data omitted). In addition, Finke, 2003, indicates the phase results from transient aggregation of the unfolded state and is not folding. Figure 4-4A shows the first 10 seconds of a refolding reaction upon dilution from 2.2M to 0.4M Gnd-HCl for wild type (in **black**) and permutant (PM142, in **green**) as monitored by stopped-flow fluorescence. The inset is a plot of the residual errors for the fit of the data to a three exponential. All the permutations show experimentally negligible changes in the refolding reaction (data not shown). Therefore, the transition of the unfolded to intermediate is unaffected.

We can monitor the formation and disappearance of such intermediate species by following the observed fluorescence signal change that occurs as 8-anilino-1-naphthalenesulphonic acid (ANS) binds and dissociates from these intermediates (120). ANS is a popular hydrophobic dye used to probe early folding events in proteins (121). ANS does not bind to the unfolded state of IL-1 β , but it binds to hydrophobic clusters, associated with the intermediate, that are solvent exposed giving a large change in fluorescence intensity during detection. We used this knowledge of ANS binding experiments to further probe the folding mechanism of permutants of IL-1 β to give clearer insight into the τ_2 process. Figure 4-4 is a representative graph of the stopped-

flow refolding jump for WT IL- β and various permutants in the presence of ANS. The traces confirm that the rate value of formation of the intermediate from the unfolded is the same and within experimental error of WT IL-1 β .

Fluorescence-detected manual mixing monitors monophasic decay of fluorescence intensity. The slow decay of fluorescence is designated τ_1 , which measures the population of the native state from the intermediate, which is on the tens of seconds' timescale and fits to one exponential. A trace of each permutation is overlaid individually with WT IL-1 β as relative intensity of the manual mixing fluorescence signal over time in Figure 4-5. Striking effects as a result of circularly permutating IL-1 β are obvious when comparing the manual mixing kinetic refolding data between the wild type and permutant proteins. Under strong denaturing conditions, we observe single-exponential kinetics for the manual mixing unfolding of wild-type IL-1 β and the permutations, τ_{unf} . The data for all the proteins were collected at pH 6.5 and 25°C and were fit by a single exponential phase. All permutations unfold faster than WT IL-1 β . Figure 4-6 shows the chevron plots of the log of the observed rate values τ_1 and τ_{unf} , determined in manual mixing fluorescence experiments, and rate value τ_2 , determined in stopped-flow fluorescence. The behavior of the rate values of τ_1 , τ_2 , and τ_{unf} of each permutant (colored data points) as a function of denaturant, Gnd-HCl, is compared to WT IL-1 β (**black** lines). The observed rate for the intermediate phase, τ_2 , shows similarities in the relaxation times with respect to WT. The relaxation times for

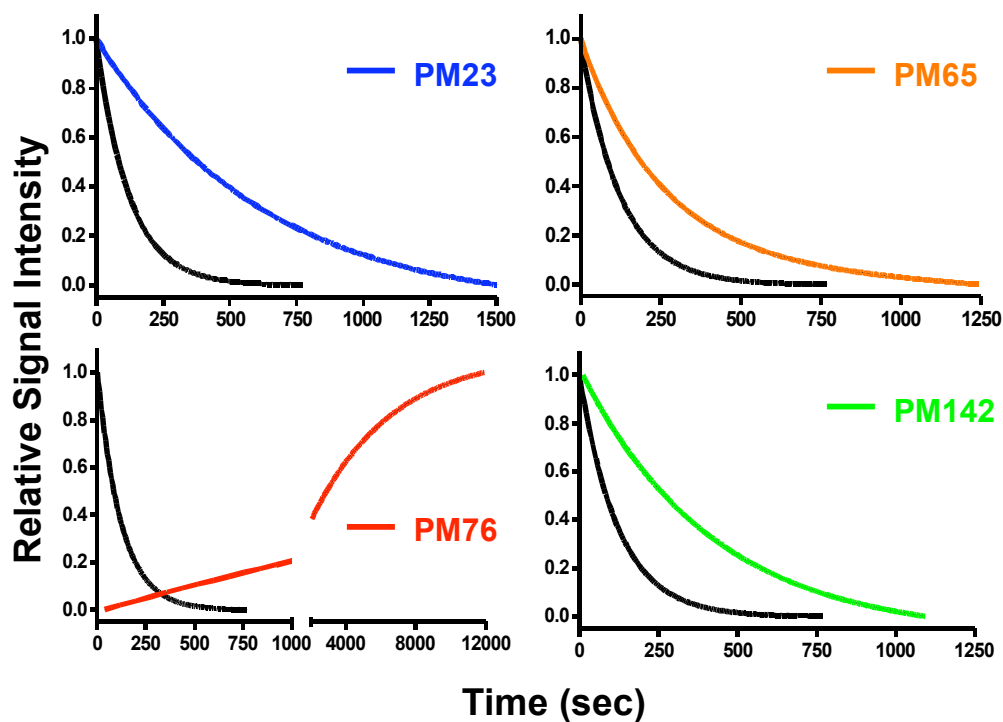


Figure 4-5: Representative traces of manual mixing fluorescence kinetics for wild type and circularly permuted IL-1 β showing the differences in the observed refolding kinetics.

Wild type IL-1 β is shown in **black** while permutants are indicated in each panel in their representative color scheme. The traces demonstrate the difference in the determined rate of refolding for all permutant variants. The traces represent the refolding jump from 2.2M Gnd-HCl to 0.4M. The tryptophan side chain was excited at 293nm wavelength while the emission intensity was monitored at 343nm. The data was collected at pH 6.5 at 25°C. Wild type and permutant proteins were fit to a two-exponential model.

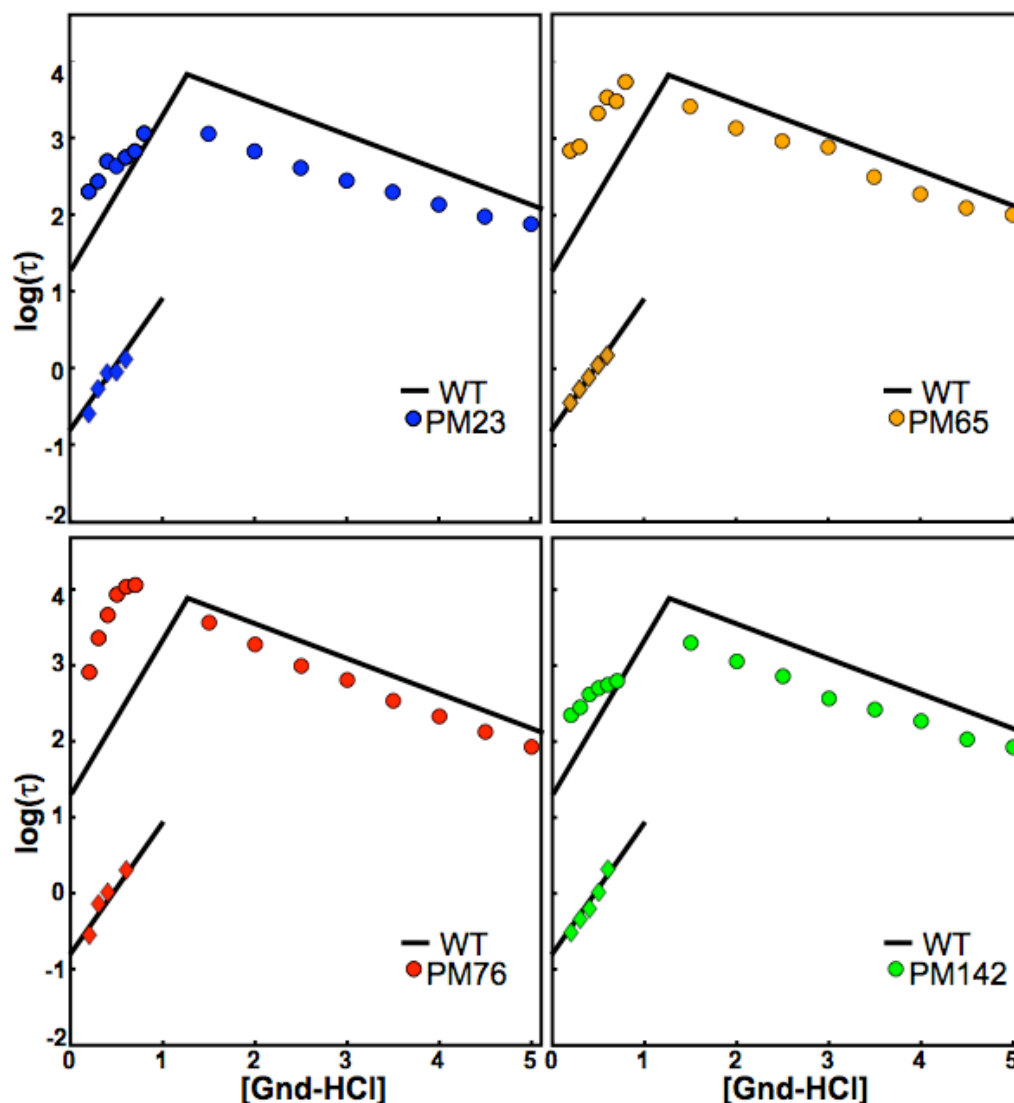


Figure 4-6: Chevron plots of the log of the relaxation rates for the permutations of IL-1 β indicating the similarities and differences in determined folding rates.

A comparison of the relaxation rates obtained by both stopped-flow and manual mixing refolding and unfolding experiments for WT IL-1 β (—) indicating the differences between (A) PM 23 (●), (B) PM 65 (●), (C) PM 76 (●), and (D) PM 142 (●). The relaxation times were determined by a global analysis of both stopped-flow and manual mixing kinetic data. The circles (●) and diamonds (◆) on the left of each plot represent the τ_1 and τ_2 phases of refolding, respectively. Significant differences are seen in the τ_1 phase of refolding. The circular data points (●), on the right represent the relaxation rates for unfolding (τ_{unf}). All permutations unfold faster than WT. The refolding data points are shown for Gnd-HCl jumps to concentrations less than 1.0M plotted from 0.2 to 0.6M Gnd-HCl, while unfolding data points are for jumps to concentrations greater than 1.5M from 1.5M to 5.0M Gnd-HCl.

refolding to 0.3M Gnd-HCl for τ_2 are 326 ms, 358 ms, 494 ms, 677 ms, and 548 ms, for wild type, PM23, PM65, PM76 and PM142, respectively. The slow phase, τ_1 , exhibits the most significant changes. The rate values of τ_1 for PM65 (Figure 4-6B) and PM76 (Figure 4-6C) show the largest changes, with increases of an order of magnitude. The decreasing fluorescent phase, τ_1 , occurs with a relaxation time of 95 seconds, 4.5 minutes, 13.1 minutes, and 4.7 minutes for wild type, PM23, PM65, PM76 and PM142 respectively, at 0.3M Gnd-HCl at pH 6.5 and 25°C. The right side of the chevron plot represents the unfolding region. From these plots it is apparent that all the permutations cause a decrease in the relaxation times for unfolding. Upon unfolding to 1.5M Gnd-HCl the relaxation times for wild type, PM23, PM65, PM76 and PM142 were 93.1 minutes, 18.8 minutes, 43.7 minutes, 60.5 minutes and 33 minutes, respectively. At 5M Gnd-HCl, the relaxation times obtained were 134 seconds, 76 seconds, 102 seconds, 85 seconds, and 84 seconds, for wild type, PM23, PM65, PM76, PM142, respectively. This is consistent with the equilibrium denaturation data showing a destabilized native state.

Variation in Linker Size and Composition does not affect PM76 β -Trefoil Stability, Cooperativity or Folding Rates

In order to determine if the observed thermodynamic and kinetic effects of the circular permutations are mediated by the presence of the biologically active linker, we systematically altered the artificial linker length between the native N- and C- termini of PM76 to assess the role of the linker on the folding kinetics and stability of permutant

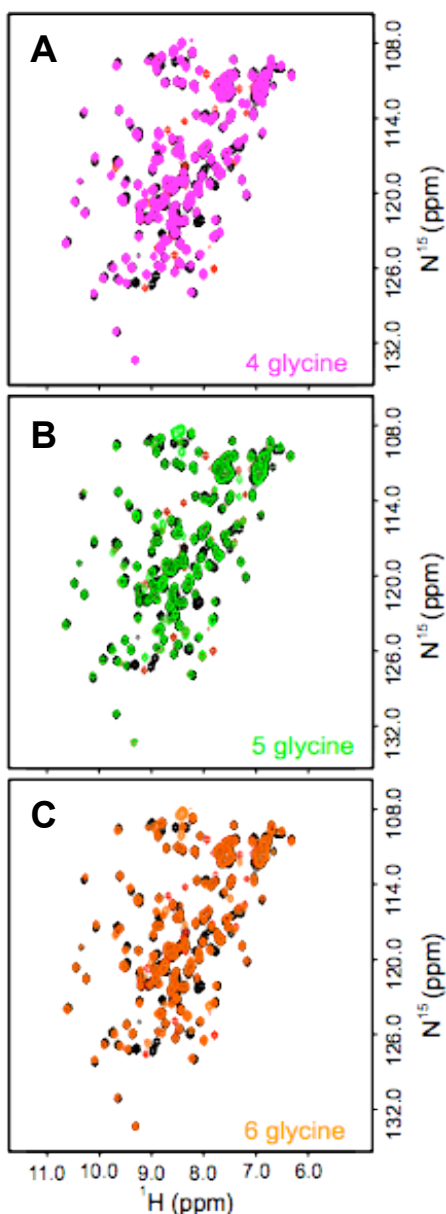


Figure 4-7: Analysis of the fingerprint pattern of ^1H - ^{15}N -HSQC spectra of wild type IL-1 β and the respective linker variants strongly indicate similar tertiary structure to the parent permutant, PM76, and an intact β -trefoil fold.

These representative spectra were to determine the affects of linker length and composition on the global fold of the protein. Each linker variant spectra are overlaid with a spectrum of WT IL-1 β (●) and pm76-TAQT (●). (A) The spectra of the linker variant of pm76 with 4-glycine (4G) replacing TAQT overlaid in **magenta**. (B) The spectra of the 5-glycine linker variant (5G) overlaid in **green**. (C) The spectra of the 6-glycine linker variant (6G) overlaid in **orange**. The overall pattern remains unaffected by the linker variations.

proteins. Using the same technique to engineer the permutations, glycine linker variants were created (Figure 4-1). A four-glycine linker (**GGGG**) was created for more flexibility and two length variants, a five-glycine (**GGGGG**) and a six-glycine (**GGGGGG**) were constructed.

As the purification and isolation of the linker variants indicated a similar global fold to WT protein, analysis of ^1H - ^{15}N NMR HSQC spectra was used to confirm this assessment. Figure 4-7 contain the HSQC spectra of WT IL-1 β and PM76 with four different linkers. WT spectrum is in black. Figure 4-5A is the spectrum of PM76 with the four-glycine linker (4G) (**magenta**) overlaid on both WT IL-1 β (**black**) and PM76 with the TAQT linker (**red**) spectra. Figure 4-7B and 4-7C are the spectra of the five-glycine PM76 (5G) (**green**) and six-glycine linkers PM76 (6G) (**orange**), respectively, overlaid with WT and PM76, TAQT spectra. Variations in the linker size and the composition has not affected the HSQC spectrum. The four cross-peaks are attributed to the addition of the TAQT linker (in the **red** HSQC spectrum) and the multiple overlapping resonances in the glycine region of each HSQC, around 8.5ppm, 108ppm for the glycine linkers in **magenta**, **green** and **orange** spectra (Figure 4-7A-C).

Equilibrium denaturation studies show that varying linker size and composition has no affect on thermodynamic stability relative to PM76-TAQT (Figure 4-8A). The free energy of folding of PM76 with each linker construct was within error (Table 4-2) of PM76-TAQT and the *m*-value unchanged. The kinetic behavior of folding of the linker variants of PM 76 was followed by fluorescence-detected stopped-flow and manual mixing described in Figures 4-4 to 4-6 and accompanying text. Figure 4-8B

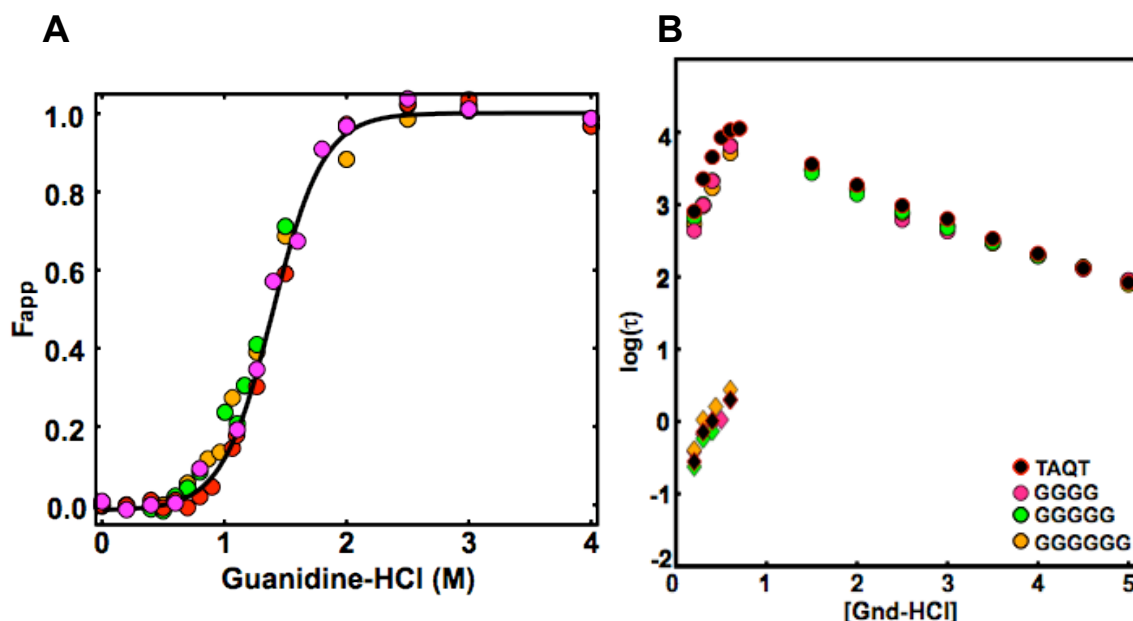


Figure 4-8: Plots of the equilibrium titration showing no difference in equilibrium stability or cooperativity and chevron plot showing no variation in folding kinetics due to linker size.

(A) An overlay of linker variants equilibrium denaturation curves pm 76 with the TAQT linker (●), 4G (●), 5G (●) and 6G (●) plotted as F_{app} versus denaturation concentration. The continuous line representing the best-fit curve is fit to a two-state model is shown in **black**. Equilibrium unfolding was monitored by fluorescence at pH 6.5 and 25°C. (B) A comparison of the relaxation rates obtained by both stopped-flow and manual mixing refolding and unfolding experiments indicating the similarities in data points are shown for denaturant jumps from 2.2M Gnd-HCl to concentrations less than 1.5M, plotted from 0.2M to 0.6M Gnd-HCl. Unfolding data points are for jumps to concentrations greater than 1.5M Gnd-HCl plotted from 1.5M to 5.0M Gnd-HCl. All reactions were determined at pH 6.5 and 25°C. The observed rates of PM76 with the biologically active TAQT linker (**black** data points) and the 4-glycine (4G) (**magenta** data points), the 5-glycine (5G) (**green** data points) and 6-glycine (6G) (**orange** data points) linker variants are plotted together.

Table 4-2: Thermodynamic Parameters for PM76 and Permutant Linker Variants

IL-1β Variant	$\Delta G_{N-U}^{a,b}$ (kcalmol⁻¹)	$\Delta\Delta G_{N-U}^{a,b}$ (kcalmol⁻¹)	m-value_{N-U}^{a,b} (kcalmol⁻¹M⁻¹)	C_m^c (M)
pm 76	4.0±0.1	-3.7±0.1	2.9±0.3	1.3
4G	3.3±0.5	-4.4±0.2	2.5±0.1	1.3
5G	3.2±0.3	-4.5±0.1	2.4±0.4	1.3
6G	3.2±0.4	-4.5±0.1	2.5±0.2	1.3

Changes in folding parameters upon incorporation of longer linker variants for the circularly permuted IL- β . The equilibrium data were fit using MATLAB in order to obtain equilibrium parameters for folding, ΔG_{N-U} . Changes in ΔG_{N-U} ($\Delta\Delta G_{N-U}$) were obtained using WT as a reference. m -value indicates changes in the accessible surface area upon folding and indicate cooperativity of folding.

^aEquilibrium transition data were evaluated using a two-state folding model.

^bData were obtained by calculating the average wavelength and calculating the relative average wavelength in terms of F_{app} as a function of [Gnd-HCl].

^c C_m values were taken from dividing the ΔG_{N-U} by the m -value.

show the chevron plot of the log of the relaxation rates for the refolding and unfolding kinetics of each linker variant (4G, 5G, 6G) and the parent permutant PM76-TAQT as a function of denaturant, Gnd-HCl. The values of the τ_1 , τ_2 and τ_{unf} rates of PM76 with the four different linkers are essentially unchanged despite the change in size and composition.

Discussion

Simulated data has shown with small, two-state folding proteins, that the differences between the folding mechanisms of the permuted and wild-type protein are related to the change in the native state topology (54). Permuted proteins have been used in experimental studies for establishing stability and global fold determinants. Experimental data on circular permutations of IL-1 β allow us to explore the suggested topological effects of altering the chain connectivity and the contact order between WT and permutations with little contribution from sterics, charge differences, side-chain interactions, etc., associated with point mutations (54). Despite many successful studies of permutant proteins, work on circular permutants of DHFR indicate that some regions of a sequence may constitute essential folding elements, and permutation at these sites may inhibit folding or disturb the native fold (95). Based on our current study (Chapter 3), the β -trefoil global fold remains the same in all four permutations of IL-1 β despite the shift in the primary sequence and the resulting change in connectivity and contact order. **Circularly Permutating IL-1 β Alters Stability**

It is common for sequence variants of IL-1 β to have altered thermodynamic

stability of the native state with little effect on the m -value (71). However, surface exposed T9 mutants (71) and H30 variants (35) do have changes in the cooperativity of the equilibrium unfolding transitions. The m -value of the transition is an indication of the degree of cooperativity of the transition as the protein unfolds. Shifting of the N- and C- termini and altering the chain connectivity decreased the thermodynamic stability and cooperativity (Figure 4-3 and Table 4-1). We see that the stability of the permutations has decreased as compared to WT IL-1 β with PM 65 and PM76, located in region of WT IL-1 β associated with the kinetic intermediate, showing the greatest drop in stability, approximately 3.4-3.7 kcal/mol (Figure 4-3B and Table 4-1). The permutations with the greatest decrease in stability also show the largest changes in the cooperativity of the folding transition (Figure 4-3B and Table 4-1). The decrease in stability appears to be correlated with the trefoil location of the cut sites with alterations in the second trefoil contributing more significantly to the decreased stability and cooperativity (PM65 and PM76) versus trefoil one (PM23) and trefoil three (PM 142) where the changes are less significant. These differences may be attributed to a more dynamic native state for the permutations, where native fluctuations are greater than WT IL-1 β . This may be related to a globally diffuse transition state where cooperativity is optimized and native fluctuations of WT protein are reduced for biological function (98). The increased dynamics of the permutations may be a result of maintaining the proteins' function as the native fold is maintained despite the changes.

Circularly Permutating IL-1 β Alters Folding Kinetics

While it is interesting to characterize essential folding sites, it is important to

identify changes in folding mechanism that are a result of a change in the final fold versus changes in folding mechanism. For β -trefoil proteins, this will give insight into the folding mechanism. Since IL-1 β is a member of the β -trefoil family and theoretical models indicate that the folding mechanism of IL-1 β has a strong topological dependence and has a more complex folding route and a well-populated folding intermediate both experimentally (38) and theoretically (33). Kinetic refolding and unfolding experiments were carried out in order to determine how different the folding mechanisms are for each permutation of IL-1 β as compared to WT. Figure 4-6 A-D indicate that the phase of refolding associated with formation of a structured kinetic intermediate, τ_2 , has not been affected by the changes in connectivity. The detection of the folding intermediate with ANS further confirms the similarity in τ_2 (Figure 4-4B). This may be a result of a locally condensed nucleus (98) where the similarities in the kinetics for intermediate phase of folding are related to the shorter, local contacts of the core barrel structure still being formed. Simulations on the folding pathways of IL-1 β suggest that chain connectivity affect the protein by only making the shorter loop length contacts more probable than longer ones (63). The more obvious effects of the permutations are seen in the slow phase, τ_1 , of folding associated with the turnover from the intermediate to the native. The most notable changes are exhibited by PM 65 and PM 76 where the relaxation rates for the formation of the native ensemble differs by almost an order of magnitude. The slower relaxation rates in the final phase of folding for the permutations may be an affect of changes in the proteins ability to access the longer-range contacts.

It has been shown that both contact order and stability play important roles in determining the folding rates of proteins. As indicated in this study, the changes in the contact order and the decreased stability have slowed folding for all permutations. The affect of these parameters alter the longer-range contacts that are critical determinants for the folding routes that IL-1 β accesses when it is refolding (36). As the formation of the intermediate is necessary en route to the native state, the “pinching” of the barrel to form the local contacts forms first, excluding some of the long-range contacts needed to form the nascent barrel. This occurs to kinetically safeguard the native structure and to compensate for the overall low thermodynamic stability of the native state where rate is traded for structural specificity (98, 109). The linking the N- and C- termini and rearrangement of the protein sequence, causes the refolding of the permutations to sample folding routes on the same energy landscape that were previously less likely to occur (36). Overall, the formation of the native state was affected by the linking of the native terminal ends and rearrangement of the contact order of the permutations rather than by the addition of the linker as determined by these studies.

Recently, theoretical studies identified the multiple folding routes that may be sampled by IL-1 β (36). The changes to the connectivity and the linking of the native terminal ends may give insight into the effects on the route distribution for this slow folding protein. IL-1 β appears to fold by a direct route where the central region folds early, contacts involving the functionally important β -bulge are made and lead to the “pinching” of the barrel. Simulations have also shown that WT IL-1 β protein samples a route that “backtracks,” unfolding the contacts in the terminal ends that form first and

re-attempts to fold (36). Upon linking the native terminal ends, it appears that the permutations fold via a less favored route further slowing the folding process. Since the overall topology of the permutations is the same as WT, the slowed turnover from intermediate to the native may be explained by an increased population of the ensemble sampling the route where the N- and C- terminal regions form first and then associate too close to the β -barrel, not allowing the proper packing of the β -bulge, inhibiting further folding to the native protein. The local contacts that are involved in the formation of the kinetic intermediate come together similar to WT while the packing of the functional loop and the long-range contacts are effected by the permutations indicating that backtracking occurs during the transition from the intermediate to the native state.

Chapter 5

The Removal of the β -Bulge Functional Loop in IL-1 β Alters Folding While Maintaining a Similar Global Fold

Abstract

Recent simplified theoretical models have determined that the folding of the cytokine, IL-1 β is slowed by the presence of the β -bulge, a functional loop located between strands 4 and 5 of the molecule. Additional simulations on the removal of the functional loop and introduction of a swapped turn from the receptor antagonist, IL-1ra, resulted in faster folding of the hybrid, β -sheet protein. In this experimental study, we remove the β -bulge of IL-1 β and replace it with a tight turn from IL-1ra., in order to probe the effects on the geometrically frustrated structure and the effects on folding. Data indicate that the deletion construct has a similar overall fold and thermodynamic stability compared to WT, while the conversion of the intermediate ensemble from the unfolded state is faster.

Introduction

The principle of minimal frustration states that trapping is minimal and the energetic depth of the folded state is much larger than the depth of any other local minima (6, 14, 15, 107, 122-126). As local energetic trapping or frustration is sufficiently small, most of the heterogeneity in folding routes observed in the folding landscape becomes a consequence of the chain connectivity and overall folding motif. Therefore, topology appears to be the dominant driving force when energetic frustration is reduced. Previous work in this thesis described the role of chain connectivity on the native state topology of IL-1 β and what affects rearrangement of the polypeptide chain had on the folding mechanism of this β -trefoil protein. Experiments revealed the effects

on the interconversion of the intermediate to the native state, where folding was further slowed by the rearrangement..

An emerging hypothesis is that a rough energy landscape and slow folding are often related to the functional necessity of conserving protein-protein or protein-ligand interaction sites (57-60). Combined experimental and theoretical studies demonstrate that topology effects are dominant factors in the folding of IL-1 β and that changes within the native ensemble are governed by specific topological constraints on the fold (76) and that specific surface residues modulate long-range crosstalk between separate docking sites for the IL-1 receptor (35). Recent theoretical studies have led to the suggestion that formation of contacts involving the functionally important β -bulge in IL-1 β is a major factor in the slow folding of the protein (63).

Recent theoretical studies revealed that IL-1 β appears to have two competing ‘modes’ of folding. One mode shows folding initiating at the N- and C- terminal regions and associate to close to the β -barrel, where further folding to native appears inhibited. (127). The protein “backtracks” by unfolding these contacts, and tries again. The second mode has the central region folding first, contacts involving the functionally important β -bulge are made, and lead to the “pinching” of the barrel. The protein fold from this state, closing the β -barrel by forming the N- and C- terminal contacts(128).

Regions which are geometrically-frustrated can be identified by a combination of experimental and theoretical kinetic studies. Recently, simulations indicate that efficient folding of IL-1 β requires that the β -bulge form *before* the contacts between the N- and C- terminal strands are stabilized, otherwise the formation of contacts between

the N- and C- termini inhibit formation of this functional loop (128). Additionally, MD simulations on an IL-1 β hybrid swapping out the β -bulge for a structurally homologous loop from IL-1ra showed faster folding rates compared to WT and less occurrences of backtracking, suggesting that the slow folding and the backtracking are a result of the necessary packing of this functional loop (127).). It also suggests interplay between folding and function. In an effort to determine if the formation of the β -bulge, slows the observed folding reaction we constructed an IL-1 β sequence variant in which the β -bulge is removed and replaced with a tight turn from the structural homolog, the natural antagonist and competitive inhibitor, IL-1ra. Experimental data indicate that the IL-1 β variant with the deletion of the bulge construct has a native fold similar to WT IL-1 β , but with areas of increased amide proton solvent-exchange. Protein folding experiments indicate changes in the population and formation of the intermediate ensemble and in the unfolding of the bulge-less protein.

Special Methods

Construction of the bulge deletion in IL-1 β

The construct of IL-1 β with the β -bulge deletion was constructed by incorporating point mutations by PCR using the following primers:

5'-TCCTTGTACAAGGAAGGGCAGTGGCCTTGGGC-3'

5'-GGCCACAGGCCTTTTGTTCATTACTAGGCCTTCCTTGTAC-3'

The mutations incorporated the *StuI* restriction enzyme cut site in two locations, between residue 51, glutamate, and 52, glutamate, and between residue 57, proline, and 58, valine. Following PCR, the amplified product was digested with *DpnI* to remove

the parent DNA, and then transformed into DH5 α competent cells. Colonies were picked and grown in LB with kanamycin antibiotic overnight at 37°C. Plasmid DNA was purified using the Eppendorff Miniprep Kit. The purified DNA was sequenced to confirm the point mutations. The DNA was then digested with restriction enzyme *StuI*. The digested product was run on a 1% agarose gel to separate the digested fragment from the larger cut vector. The gel was purified using the Qiagen Gel Purification Kit. The isolated cut expression vector was then ligated overnight using T4 DNA ligase. The resulting ligation was transformed into DH5 α and plated on LB/kanamycin plates. Colonies were picked and screened for the bulge deletion. After confirmation of the bulge deletion, point mutations were incorporated to change the resulting turn, K54, I55, and P56, in the bulge deletion to resemble a turn in IL-1ra (Figure 5-1). The following primers were designed for PCR:

5'-TCCTTGTACAAGGAAGGGCAGTGGCCTTGGGC-3'

5'GCCCAAGGCCACTGCCCTTCCTTGTACAAAGGA-3'

The primers yielded point mutations from KIP at position 54-56 to LHS, that is a turn found in the equivalent region of murine IL-1ra. The resulting PCR amplified product was transformed into DH5a competent cells following *DpnI* digest. Colonies were picked and grown in LB with kanamycin antibiotic overnight at 37°C. Plasmid DNA was purified as before and the DNA sequenced to confirm the point mutations.

IL-1 β Deletion Variant Expression and Protein Purification

The bulge deletion with the LHS turn was created in the bacterial expression vector pET24d(+) (New England Biolabs). This construct was transformed into *E. coli*

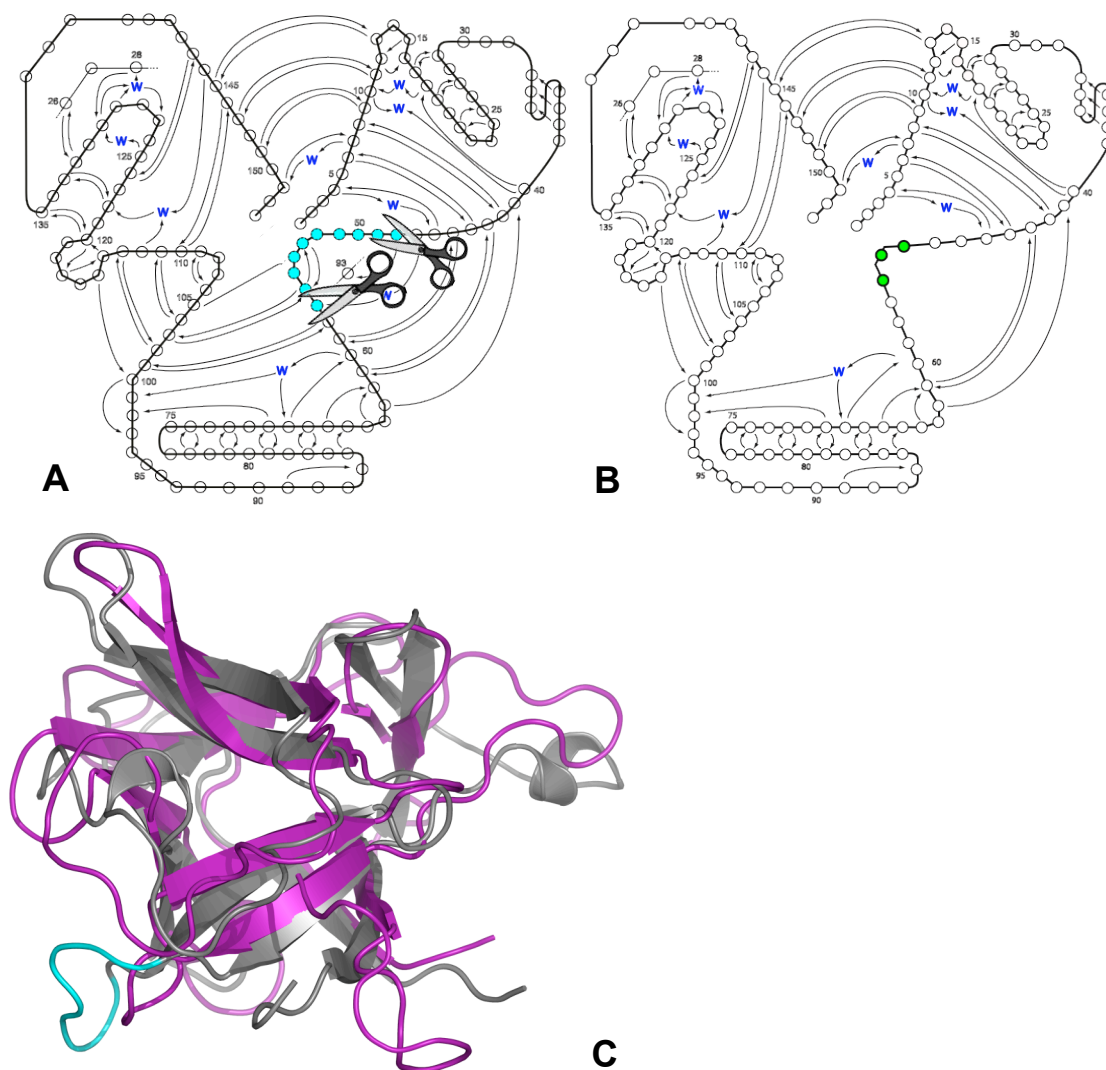


Figure 5-1: 2D splay diagrams of the secondary structure of (A) IL-1 β and (B) IL-1 β with the β -bulge removed and replaced with a loop to mimic IL-1ra.

(A) The splay diagram of IL-1 β with the location of the β -bulge colored cyan and the location of the cut sites indicated by scissors. (B) The splay diagram of IL-1 β with the bulge deleted and a loop form IL-1ra inserted, in green. Throughout the chapter, this splay will be used to represent the bulge deletion construct, although the amino acid numbering will remain the same as WT IL-1 β . (C) Representation of the molecule of IL-1 β (grey) and IL-1ra (purple) overlaid to show the similarities in structure. The β -bulge is indicated in cyan.

host strain BL-21 (DE3). Expression and purification of the protein followed the protocol outline in **GENERAL METHODS** with some modifications. The protein pellet was dissolved in ca. 20 ml of 24 mM NH₄OAc, 2mM EDTA and 1mM β ME at pH 6.5 (buffer A) after fractionation and dialyzed overnight with three changes of buffer with at least three hours between change in the same buffer. The dialysis was centrifuged as previously mentioned, filtered and applied to a cation exchange column (Pharmacia) equilibrated in buffer A. The protein was eluted in a 40 column volume linear gradient of buffer B (750 mM NH₄OAc, pH 6.5). Uniformly labeled protein was isolated following the same protocols.

Residue-specific ¹³C chemical shifts

The relative deviation in ¹³C α ppm for each specific amino acid residue for the deletion construct was calculated as described in **GENERAL METHODS** with changes to the equation as the follows:

$$\text{Relative } \Delta\delta_{13\text{C}} = (\delta_{13\text{C}} \text{ WT IL-1}\beta - \delta_{13\text{C}} \text{ bulge-less IL-1}\beta) / (\delta_{13\text{C}} \text{ WT IL-1}\beta - \delta_{13\text{C}})$$

where $\delta_{13\text{C}}$ refers to the chemical shift of the ¹³C α of the individual amino acid in a random coil, $\delta_{13\text{C}}$ bulge-less IL-1 β is the chemical shift of the specific amino acid residue in the bulge deletion, and $\delta_{13\text{C}}$ WT IL-1 β is the chemical shift of the specific amino acid residue in wild-type IL-1 β . Random coil ¹³C chemical shifts for C α atoms were taken from the literature (82, 83). Changes greater than ± 5 were deemed significant.

NMR Processing and Analysis

All NMR experiments were processed using NMRPipe (129). The resulting processed spectra were analyzed using Sparky (130).

Results

¹H-¹⁵N HSQC spectrum of the bulge deletion of IL-1 β

The deletion of the β -bulge between strand 4 and strand 5 of IL-1 β was constructed to determine the structural effects of removal of this functional loop on the formation of the protein. The location of the bulge and the resulting deletion are illustrated in the 2D splay in Figure 5-1A,B. The β -bulge was removed and replaced with the tight turn between strand 4 and strand 5 that is in IL-1ra. The native global folds of IL-1 β and IL-1ra are structurally homologous, but differ in the presence of a hairpin turn connecting strands 4 and 5 in IL-1ra as opposed to the β -bulge in IL-1 β (Figure 5-1C). Figure 5-2 is a ¹H-¹⁵N HSQC spectrum of the bulge-less variant (**cyan**) overlaid with WT IL-1 β (**black**). The overall global fold of the bulge deletion remains similar to WT based on NMR spectral evidence as well as protein biochemistry during bacterial expression and protein purification. The ¹H-¹⁵N spectrum acquired for the chimera protein shown in Figure 5-2 is similar in chemical shift pattern and dispersion indicating an intact β -trefoil. Backbone amide resonances seen in the ¹H-¹⁵N spectrum have a unique chemical shift dispersion and pattern that is correlated to the secondary structure and tertiary interactions of the β -trefoil global fold(35, 47). The ¹H-¹⁵N HSQC spectrum of the bulge-less variant is essentially identical to WT (**black**), except for perturbations attributed to the deletion of the bulge and the introduction of the three-residue turn. Triple resonance ¹H-¹³C-¹⁵N spectroscopy was performed to confirm

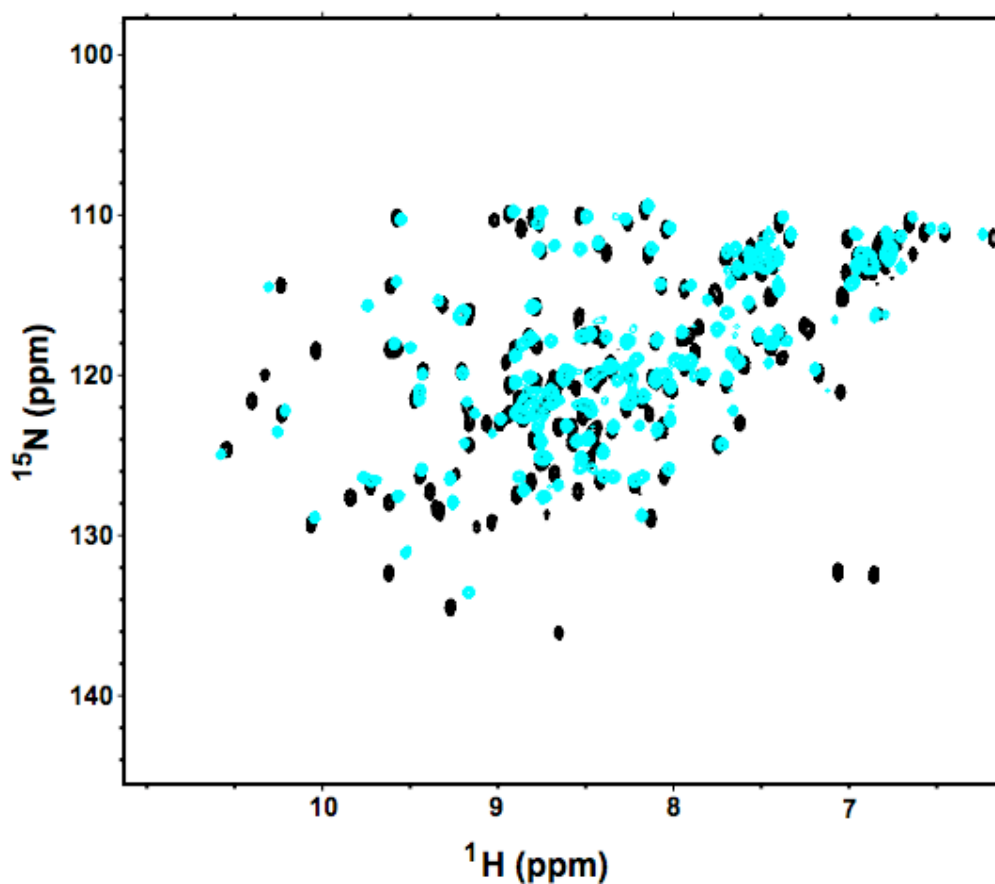


Figure 5-2: Comparison Spectra of the fingerprint pattern of ^1H - ^{15}N -HSQC spectra of the bulge-deletion construct (cyan) and wild type IL-1 β (black) indicate similar tertiary structure and an intact β -trefoil fold.

The representative spectra demonstrate the similarities in the pattern of chemical shift dispersion in the two native proteins.

resonance assignments for the bulge-less construct (Figure 5-3).

$^{13}\text{C}^\alpha$ chemical shifts

The deviations of the $^{13}\text{C}^\alpha$ chemical shifts from random coil are empirically correlated to the ϕ , ψ backbone dihedral angles of the peptide bonds. Chemical shifts of the α -carbons in proteins have been empirically correlated to the secondary structure of the folded and unfolded proteins at the level of individual residues (102). Variations in $^{13}\text{C}^\alpha$ chemical shifts are more dependent on the ϕ , ψ backbone dihedral are less influenced by salt, pH, ionic strength and other solvent parameters. An observed $^{13}\text{C}^\alpha$ chemical shift indicates a preferential population of either the α - or β - region of ϕ , ψ space for a given residue. Deviations from the native state α -carbon chemical shift upon destabilization can be interpreted as a change in the average conformation of that dihedral (76). Following the same primary sequence numbering for the amino acids in the polypeptide chain or WT, relative $^{13}\text{C}^\alpha$ chemical shift deviations for the bulge-less variant of IL-1 β were derived from HNCA spectra. Variations between backbone $^{13}\text{C}^\alpha$ chemical shifts of the WT and the deletion IL-1 β proteins were analyzed. The relative $\Delta\delta_{13\text{C}}$ shift was calculated using equation 1 (See **SPECIAL METHODS**). Figure 5-4 is a plot of the average relative $\Delta\delta_{13\text{C}}$ for each amino acid in the bulge-less construct. Changes greater than ± 5 ppm were deemed significant. Most of the changes in chemical shift between the chimera and the WT IL-1 β proteins are seen at turns and hinge points (Figure 5-4B and C) throughout the native fold. A majority of residue-specific deviations are seen in the first and third trefoil subunits. The residues that exhibit stabilization in β -structure, G22, E25, F42, S57, N85, K103, E111, W120, G136

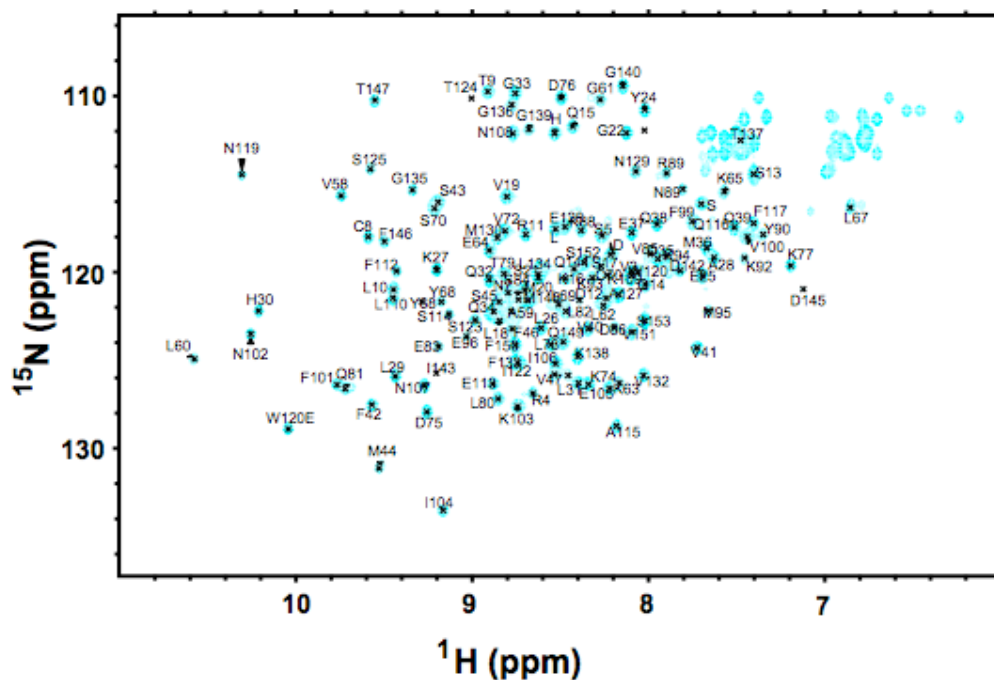


Figure 5-3: Representative ^1H - ^{15}N HSQC spectra of bulge-deletion construct indicating assigned resonance peaks.

The sequence-specific assignments are depicted on the ^1H - ^{15}N spectrum of the bulge-less IL-1 β variant. Assignments were determined by completing ^1H - ^{13}C - ^{15}N triple resonance experiments: HNCA, HNCAB, CBCACO(NH

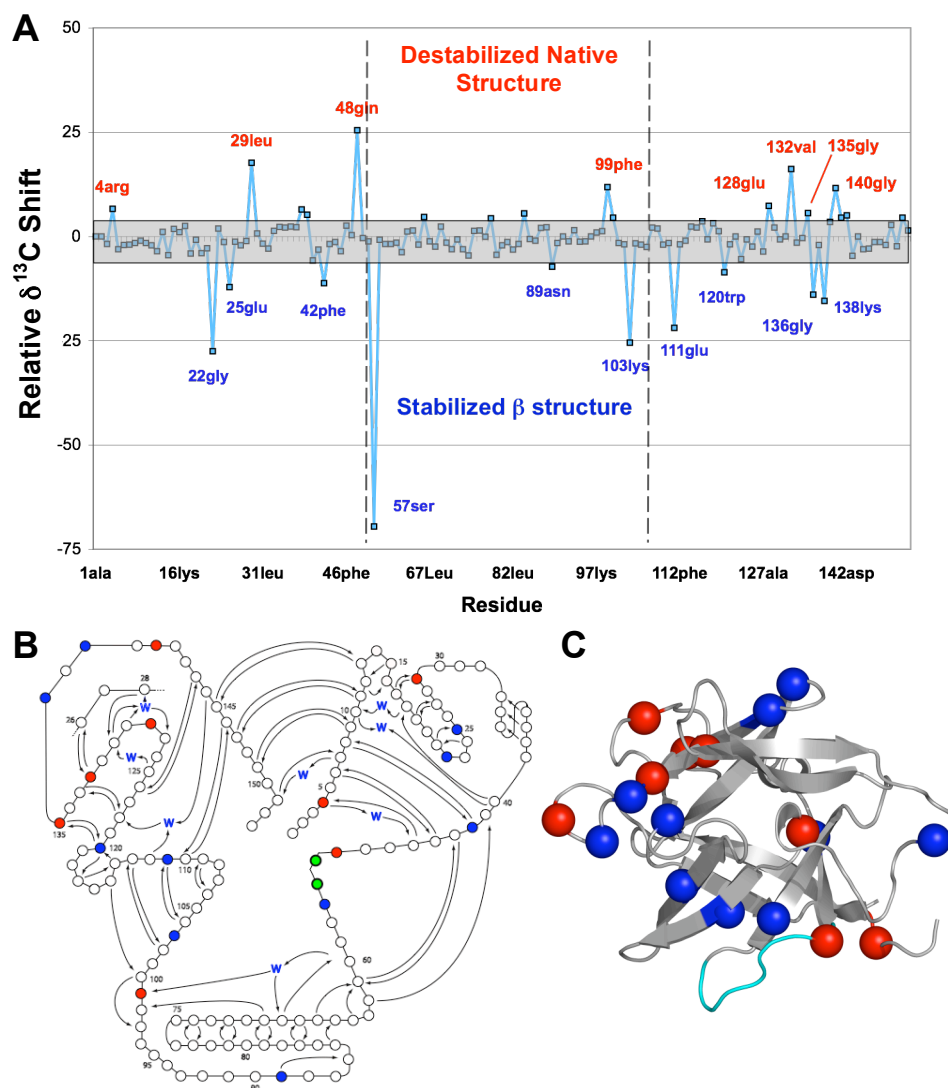


Figure 5-4: Effects of the bulge-deletion on $^{13}\text{C}^\alpha$ chemical shifts of the chimeric IL-1 β residues indicate differences at turns and hinge-points of the molecule.

(A) Graphical representation of the relative $\Delta \delta_{^{13}\text{C}}$ for $^{13}\text{C}^\alpha$ chemical shifts of deletion variant residues. The **cyan** line represents the average deviation for the permutations at each amino acid. The vertical dashed lines indicate the location of the 2nd and 3rd trefoil subunits. The grey area indicates shifts that are considered similar to WT protein. Residues with the most significant shifts are indicated. (B) The residues with the most significant differences found in common with each permutation mapped onto the 2D splay of the bulge-less IL-1 β . **Red** circles (●) represent C^α shifts that are destabilized β -structure while the **blue** circles (●) represent stabilized β -structure. (C) C^α shift differences indicated in the 2D splay mapped onto the molecule following the same **red** and **blue** color scheme. This figure was made with MacPyMOL(90) using PDB ID 6I1B.

and K138, are predominately located in the β -strands that contribute to the barrel core of the protein and the hairpin cap and are colored **blue**. Destabilization in native structure is seen in residues R4, L29, Q48, F99, E128, V132, G135 and G140 that are located in loops leading into turns and are colored **red** (Figure 5-4C). It is important to note that the largest apparent deviation, S57, is one of the amino acids in the turn replacing the β -bulge.

Ramachandran Plots

To further investigate the structural differences in the bulge-less construct variants, dihedral Ramachandran plots were generated using the PREDITOR web server (84). and the backbone α -carbon, β -carbon, nitrogen and proton chemical shifts determined from HNCA and the CBCA(CO)NH NMR experiments. Dihedral angle distributions demonstrate a strong preference for the low energy core α - and β - regions of the Ramachandran plot as defined by Morris *et al.*, 1992. Figure 5-5A presents the Ramachandran plot for the bulge-less protein overlaid on that of WT IL-1 β . Overall, the torsion angle distribution of the bulge-less IL-1 β is similar to WT as indicated by the overlapping points. Differences are identified as residue torsion angles that shifted the sampling into another quadrant. For example, a residue sampling β -core in WT now samples α -core in the deletion construct. Differences seen are in the first turn in the first trefoil subunit of the protein, connecting β -strand 1 and 2, as indicated by the **red** spheres on the protein molecule (Figure 5-5B). Residues in the bulge less variant predominately sampled the same plot region as WT. Those that changed are indicated, and switched from the β -core region to the α -core.

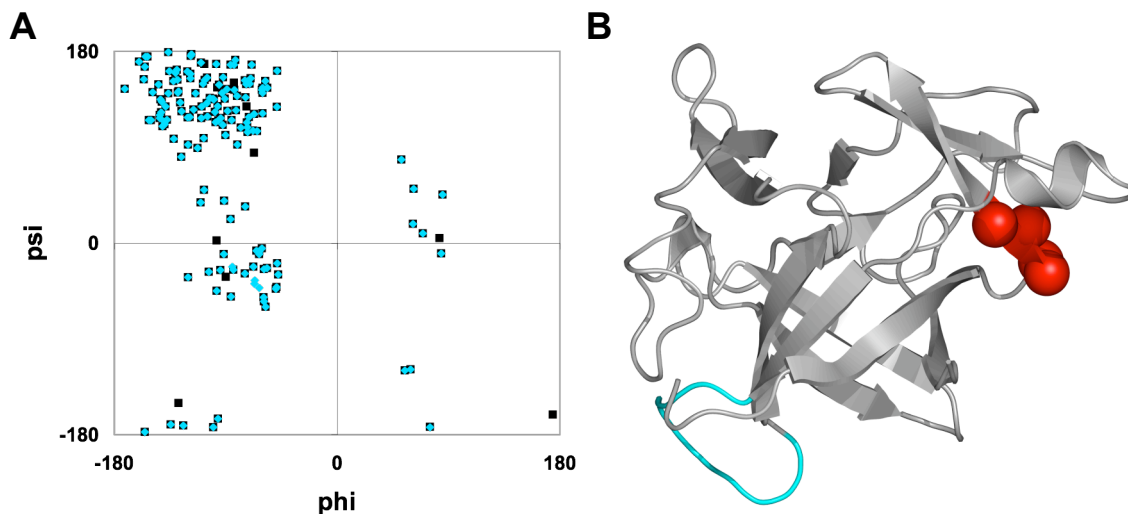


Figure 5-5: Representation of (A) the Ramachandran plot of the bulge-less construct of IL-1 β overlaid with (B) the differences mapped onto the molecule indicating changes in the first turn of the first trefoil subunit, where differences moved into different regions of phi/psi space.

(A) The Ramachandran plot of the chimeric protein (◆) overlaid with WT (■) show the similarity in the overall distribution of the dihedral angles. Differences were found in the first trefoil subunit with residues Q14, Q15, K16 and S17 having torsion angles that still sample core regions. (B) The molecule of IL-1 β with the differences mapped as red spheres. The location of the β -bulge is indicated in cyan.

Native-State Hydrogen-Deuterium Solvent Exchange (HDX)

The ^1H - ^{15}N HSQC spectrum of the bulge-less variant is well dispersed and the cross-peaks in each respective spectrum have been assigned (Figure 5-3). Native-state hydrogen-deuterium solvent exchange (HDX) measures the rate of exchange of backbone amide hydrogens with deuterium. The rate of exchange is strongly correlated the level of protection, which in IL-1 β results from secondary structural hydrogen bonding. The H/D exchange rates of backbone amide protons of individual amino acid residues can be determined from acquiring a series of ^1H - ^{15}N HSQC spectra over time. The time-dependent changes in signal intensity or volume can then be fit to an exponential equation to determine the individual rates of exchange (see **General Methods**). The H/D exchange rate for ~70 of 153 amide protons in WT and bulge-less proteins was measured at pD 5.4 at 36°C. Figure 6 shows the ^1H - ^{15}N HSQC spectra of the time-course of H/D exchange for the bulge-less variant of IL-1 β . Residues that were slow to exchange are similar to those slow exchanging residues in WT (Figure1-2).

In Figure 5-7, residues from various areas of the molecule with non-overlapping ^1H - ^{15}N resonances were chosen as examples of differing rates of exchange. Figure 5-7A is a representative plot of slow amide proton exchange for all proteins. Figure 5-7B and 5-7C indicate amide protons that have intermediate (5-7B) and fast (5-7C) exchange, respectively.. Figure 5-8A and 5-8B are illustrations depicting the individual rates of H/D exchange of the bulge-less variant as a 2D splay (5-8A), and mapped back onto the molecule (5-8B). The measured exchange rates were plotted as protected (**blue** data points) for slow exchange rates, intermediate protection (**yellow** data points) for

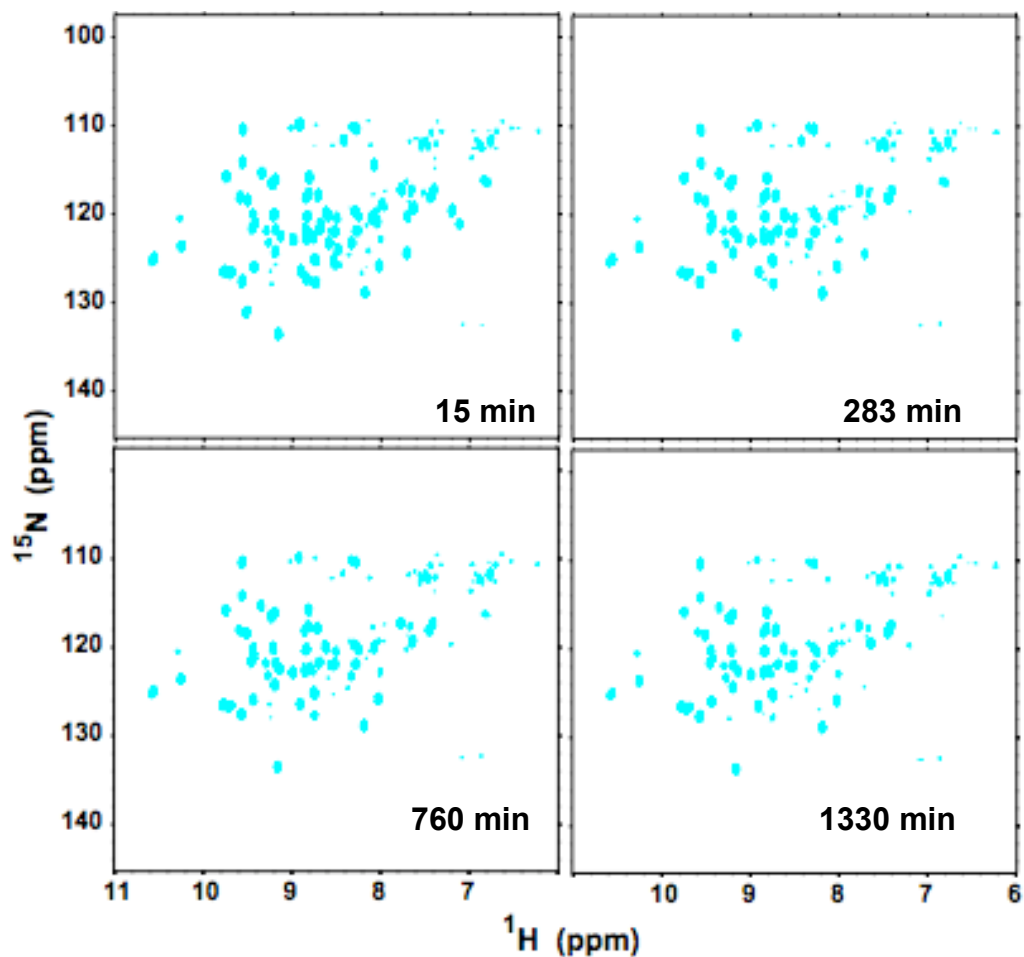


Figure 5-6: A series of ^1H - ^{15}N -HSQC spectra demonstrating the time course of hydrogen-deuterium (HDX) exchange monitored by NMR for the bulge-less $\text{Il-1}\beta$ variant.

The ^1H - ^{15}N HSQC spectra indicate the change in peak intensity over time for the bulge-less variant. The time course highlights peaks that are stable to exchange. The remaining probes used to determine the effects of H/D exchange as a result of deleting the functional loop are similar to those remaining in WT protein.

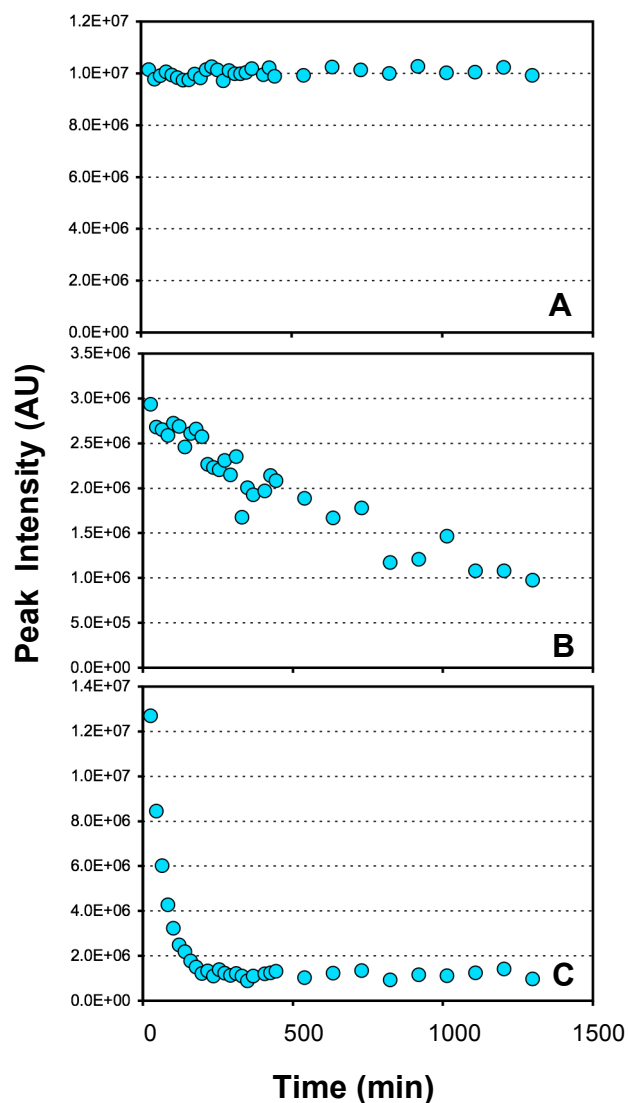


Figure 5-7: Representative comparisons of H^N solvent exchange rates for bulge-less variant of IL-1 β .

The decay of amide signals over time is shown for the bulge-less protein (●) illustrating the differences in the amide signal decay. (A) Residue E111 is an example of an amide proton that is highly protected from solvent exchange. (B) E67 indicates amide protons that have an intermediate rate of protection from solvent exchange over time for the bulge-less IL-1 β and (C) E25 illustrates amide protons that are less protected from deuterium exchange. Quantitative assessments follow.

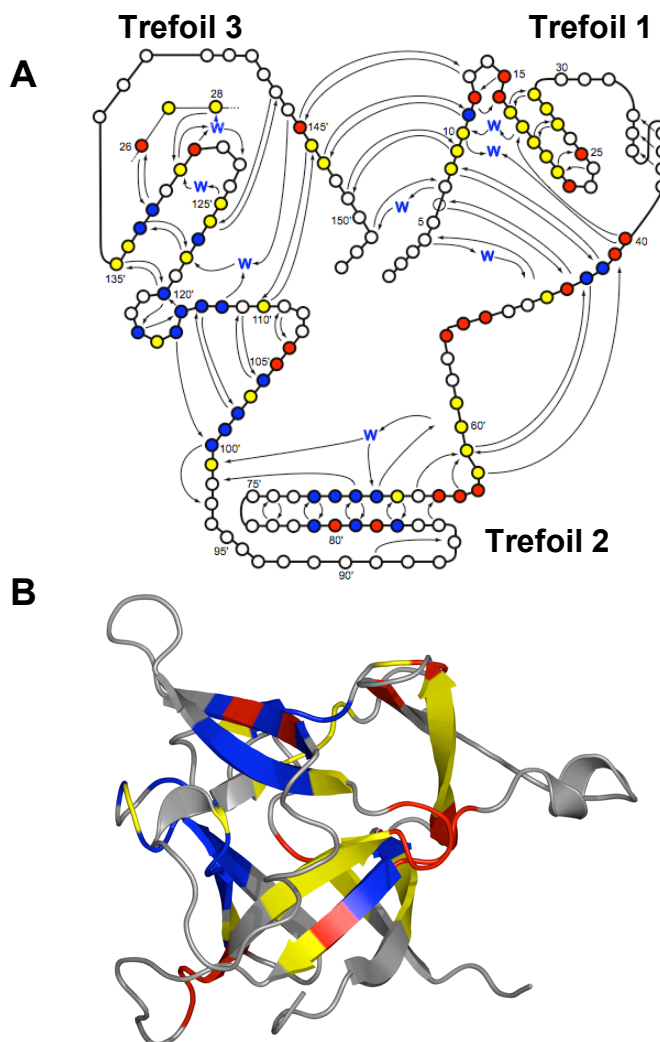


Figure 5-8: Representation of the results from H/D exchange indicates a more dynamic protein with less sites of protection upon removal of the β -bulge.

NMR detected H/D exchange studies on the bulge-deletion of IL-1 β were conducted to determine local or global differences in the native state stability of secondary structure with respect to wild type. (A) The 2D splay diagram of the H/D results for the bulge-less construct of IL-1 β . Circles in the figure represent each amino acid in the polypeptide chain. **Blue** circles represent amide backbone residues that are stable, or protected, from deuterium exchange. **Yellow** circles represent residues that show some protection from exchange while **red** circles represent those that exchange away rapidly. The schematic highlights regions of hydrogen bonding stabilization. Stable residues in the second and third trefoil subunits for both permutations are similar to WT IL-1 β . (B) The H/D results represented on the molecule of IL-1 β , following the same color scheme.

rates of intermediate exchange, and less protected to WT, indicating changes in the protein dynamics. The majority of the changes in protected (**red** data points) for fast exchange. The schematic of the bulge-less variant highlights local hydrogen bonding destabilization in a protein that is equal in global thermodynamic stability to WT. The majority of the changes in protection are in the first and third trefoil subunits involved in the cap formation and β -strand 5, which is the location of the loop swap. The bulge-less variant appears more open to solvent exchange than WT IL-1 β as demonstrated by a majority of the stable probes in WT showing less protection in their hydrogen bonding as a result of the deletion..

A direct comparison of the changes as a result of deleting the β -bulge is represented in Figure 5-9. The 2D splay indicates most of the changes occurring at the topologically equivalent areas in trefoil subunits 1 and 3, related to the formation of the hairpin cap. The majority of the changes in specific amino acid exchange rates appear away from the deletion site.

The Bulge-Deletion is Similar in Global and Thermodynamic Stability to WT and has Similar Cooperativity in Equilibrium Folding

The thermodynamic stability of WT and chimeric IL-1 β , equilibrium chemical denaturation experiments were performed to determine the extent to which removal of the geometrically frustrated β -bulge had altered the thermodynamic stability and cooperativity of the native state. The wild type and bulge-less proteins were titrated over a range of guanidine hydrochloride concentrations from 0 to 4M, at pH 6.5 and 25°C. The folding transition was monitored by the changes in the Trp120 fluorescence

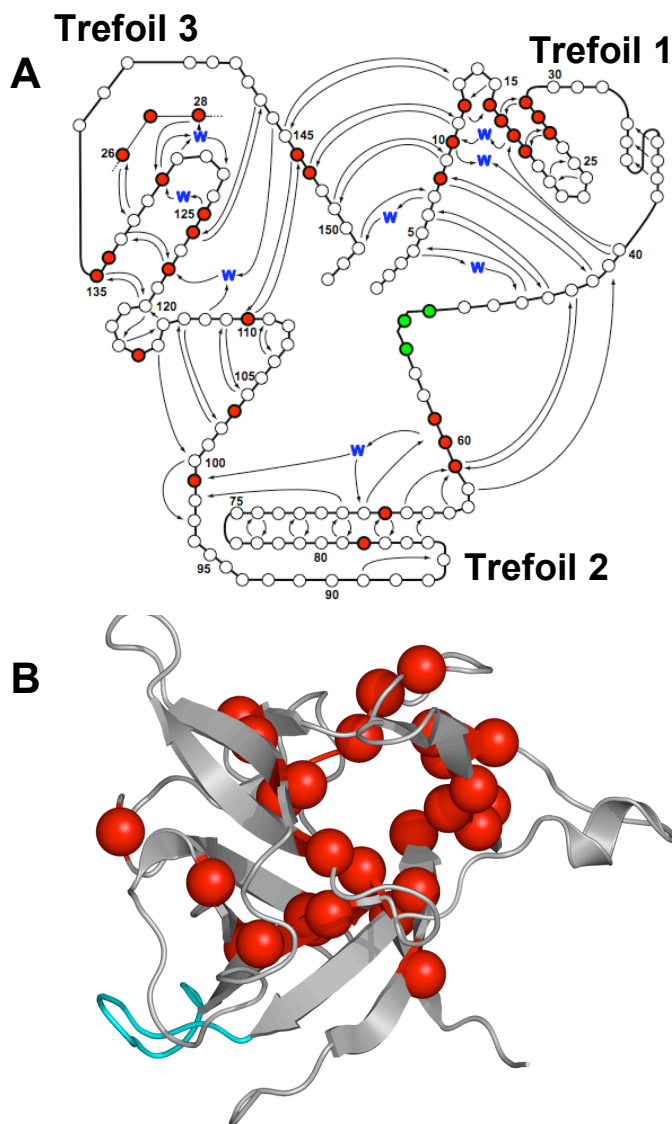


Figure 5-9: Representation of the results from comparing the H/D solvent exchange data of the bulge-less construct with WT IL-1β. Differences appear away from the site of the loop deletion.

(A) The 2D splay diagram indicates residues with different rates (**red**) of solvent exchange when compared to WT IL-1β. (B) All differences were mapped back onto the protein molecule of WT IL-1β. The **cyan** indicates the location of the β-bulge. Differences appear away from the location of the loop swap. All differences that are represented are of residues with increased solvent exchange as a result of the loop swap.

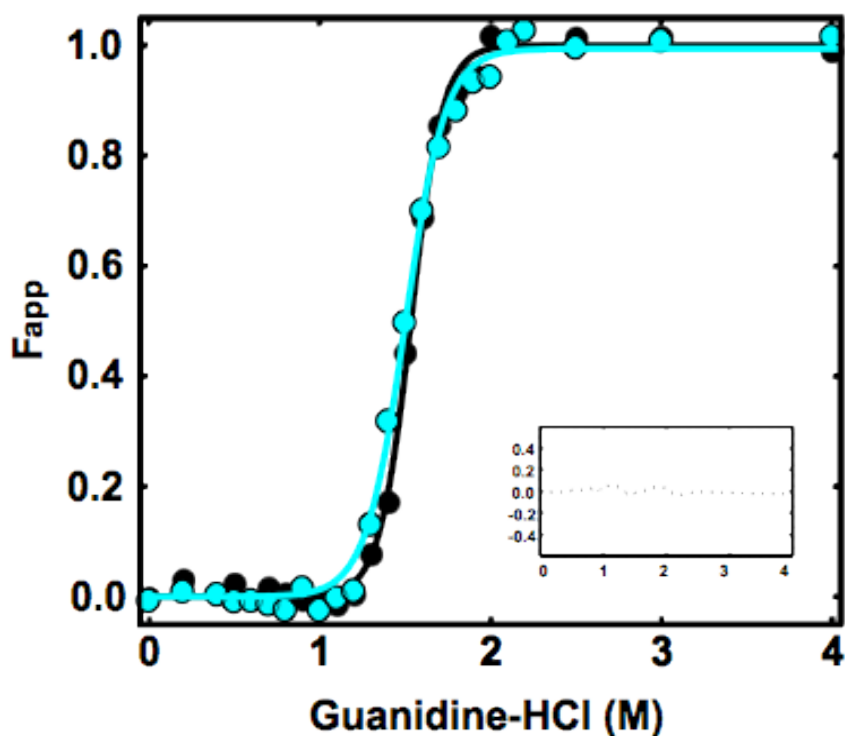


Figure 5-10 Plots of F_{app} as a function of denaturant concentration for the equilibrium unfolding of IL-1 β and the β -bulge deletion construct showing similar stability.

Equilibrium denaturation curves for IL-1 β WT (●) and deletion construct (●) plotted as F_{app} versus denaturation concentration. Continuous lines representing best-fit curves are fit to a two-state model are shown in the same color scheme. The residuals of the fit are shown as the inset. Thermodynamic parameters from the two-state best-fit model for the construct are given in Table 5-1. The inset represents the residuals from the fit.

Table 5-1: Thermodynamic Parameter Comparison for IL-1 β and the Deletion Construct

IL-1β	$\Delta G_{N-U}^{a,b}$ (kcalmol ⁻¹)	$\Delta\Delta G_{N-U}^{a,b}$ (kcalmol ⁻¹)	$m\text{-value}_{N-U}^{a,b}$ (kcalmol ⁻¹ M ⁻¹)	C_m^c (M)
WT	7.7 \pm 0.2	0	6.2 \pm 0.3	1.5
Bulge Deletion	7.6 \pm 0.3	-0.1 \pm 0.2	5.1 \pm 0.2	1.5

Changes in folding parameters upon deletion of the β -bulge in IL-1 β . The equilibrium data were fit using MATLAB in order to obtain equilibrium parameters for folding, ΔG_{N-U} . Changes in ΔG_{N-U} ($\Delta\Delta G_{N-U}$) were obtained using WT as a reference. m -value indicates changes in the accessible surface area upon folding and indicate cooperativity of folding.

^aEquilibrium transition data were evaluated using a two-state folding model.

^bData were obtained by calculating the average wavelength and calculating the relative average wavelength in terms of F_{app} as a function of [Gnd-HCl].

^c C_m values were taken from dividing the ΔG_{N-U} by the m -value.

intensity as a function of denaturant. Figure 10 shows the apparent fraction, F_{app} , of unfolded protein at increasing concentrations of Gnd-HCl determined by average fluorescence wavelength and the calculated ΔG and m -values are listed in Table 5-1. The continuous lines representing best-fit curves in Figure 5-10 were fit to a two-state model. The bulge-less variant exhibits similar thermodynamic stability and cooperativity (m -value) as WT (see Table 5-1) indicating that deleting the β -bulge from WT and replacing it with a tight turn had no effect on the overall stability of the protein and its ability to fold.

Fluorescence-Detected Kinetics of the Bulge-Deletion Variant Indicates Faster Formation of the Intermediate and Similar Transition to the Native State

The folding of the bulge-less construct was followed by fluorescence-detected stopped flow and manual mixing to determine if folding kinetics changed with respect to wild type as a result of swapping the bulge for a turn. The proteins were refolded at pH 6.5 and 25°C and the signal intensity monitored over a series of denaturant concentrations from 0.2M to 0.6M.Gnd-HCl. The kinetic behavior of folding for WT IL-1 β is characterized by an increase in fluorescence on the hundreds of millisecond timescale, followed by a slow decay of the fluorescence intensity to the native state. The rapid increase in signal, which is described by two exponential time constants, τ_3 , that occurs on the millisecond timescale, and τ_2 , that occurs on the millisecond to second timescale, measures the population of a highly fluorescent intermediate from the unfolded state. Measurements of the values of τ_3 have the most experimental error due to the fast rate and the small amplitude of the kinetic trace (45, 71). Therefore,

elucidation of the effects of the bulge-deletion on τ_3 is difficult (data omitted). Figure 5-11 shows the first 5 seconds of a refolding reaction upon dilution from 2.2M to 0.3M Gnd-HCl for wild type IL-1 β (in **black**) and the bulge-deletion variant (in **cyan**) as monitored by stopped-flow fluorescence. The kinetic trace for the variant shows a noticeable difference in the refolding reaction as the formation of the intermediate from the unfolded state is faster than WT.

ANS is a popular hydrophobic dye used to probe early folding events in proteins (121). The formation and disappearance of an intermediate folding ensemble can be monitored by following the observed fluorescence signal change that occurs as ANS binds to the intermediate state and then dissociates from the folded native state. (120). ANS does not bind to the unfolded state of IL-1 β or the bulge-less construct, but does transiently bind the native state, with a nominal fluorescence signal. The advantage of ANS is that it binds to hydrophobic clusters exposed while the protein is unfolded. Upon initiation of refolding, those areas that have ANS bound and are solvent exposed give a large change in fluorescence intensity during detection as ANS is released. These hydrophobic, solvent-exposed areas are associated with the intermediate. ANS binding experiments were performed to give clearer insight into the τ_2 process, i.e. the turnover of intermediate to native state, and also confirm the faster rate of formation determined above. Figure 5-11 is a representative graph of the stopped flow refolding jump for WT IL-1 β and the bulge-less variant in the presence of ANS. The traces confirm that the rate value of formation of the intermediate from the unfolded differs for the bulge-less

protein compared to WT IL-1 β , as seen in the noticeably different traces where ANS appears to be released much faster in the bulge-less variant than WT.

Fluorescence-detected manual mixing monitors monophasic decay of fluorescence intensity. The slow decay of fluorescence is designated τ_1 , which is the rate that the population of the intermediate turns over to the native, τ_1 is on the tens of seconds' timescale and fits to one exponential. The inset in Figure 5-11 represents the bulge-less variant overlaid with WT IL-1 β as relative intensity of the manual mixing fluorescence signal over time. Comparison of the manual mixing kinetic refolding data between the wild type and bulge-less proteins show little difference and were deemed similar in rate values. Under strong denaturing conditions, we observe single-exponential kinetics for the manual mixing unfolding of wild type IL-1 β and the bulge-less construct, τ_{unf} . The data for all the proteins were collected at pH 6.5 and 25°C and were fit by a single exponential phase. The bulge-less construct unfolds faster than WT IL-1 β .

Figure 5-12 shows the chevron plots of the log of the observed rate values τ_1 and τ_{unf} , determined in manual mixing fluorescence experiments, and rate value τ_2 , determined in stopped-flow fluorescence. The behavior of the rate values of τ_1 , τ_2 , and τ_{unf} for the bulge-less construct (colored data points) as a function of denaturant, Gnd-HCl, is compared to WT IL-1 β (**black** lines). The observed rate for the intermediate phase, τ_2 , has faster relaxation times than WT. The relaxation times for refolding to 0.3M Gnd-HCl for τ_2 are 326 ms and 179ms for wild type and bulge-deletion, respectively. The slow phase, τ_1 , exhibits similar relaxation rates. The decreasing

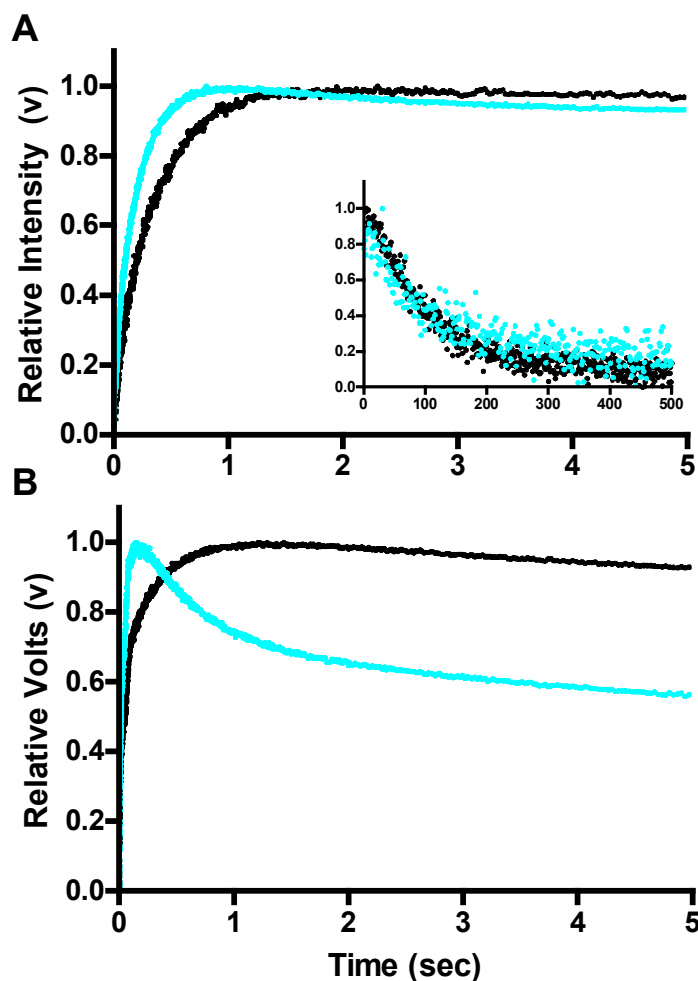


Figure 5-11: Representative traces of the fast phase (t_2) of folding collected by stopped-flow fluorescence indicating the differences in the observed rates of folding.

(A) Wild type IL-1 β is in **black** while the bulge-less construct is in **cyan**. The traces are of stopped-flow kinetic refolding jumps from 2.2M Gnd-HCl to 0.3M Gnd-HCl. The tryptophan side chain was excited at 293nm wavelength while the emission was collected for wavelengths >320nm. (Inset) Representative plot of the manual mixing refolding for both WT and the bulge-less construct, following the same color scheme, indicating the similarities in the slow phase, τ_3 , of folding. (B) ANS stopped-flow fluorescence-detected refolding of WT and mutant IL-1 β . WT, in **black**, and bulge-deletion in **cyan**, was refolding from an unfolded state in the presence of ANS. Traces confirm differences in τ_3 of folding. The traces are representative of refolding jumps from 2.2M to 0.3M Gnd-HCl. Data was collected for 250 seconds at 25°C in logarithmic mode with an excitation wavelength of 365nm, and the emission was collected using a cutoff filter >420 nm. The first 5 seconds is shown for clarity.

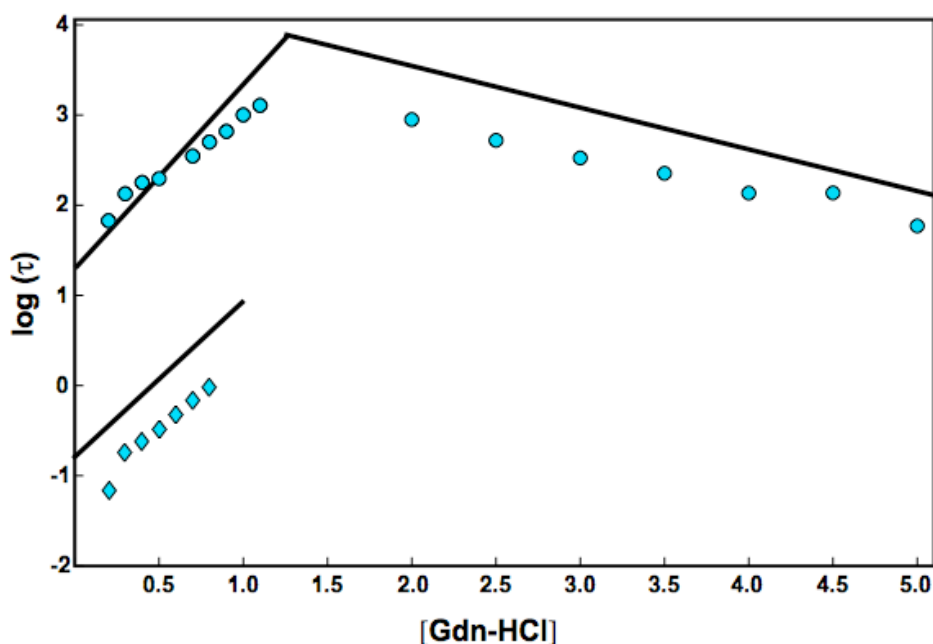


Figure 5-12: Chevron Plot of the log of the relaxation rates for the construct of IL-1 β containing the bulge deletion showing effects in intermediate formation and in unfolding.

A comparison of the relaxation rates obtained by both stopped-flow and manual mixing refolding and unfolding experiments for WT IL-1 β (—) indicating the differences of the bulge-deletion. The circles (●) and diamonds (◆) on the left of the plot represent the τ_1 and τ_2 phases of refolding, respectively. The circular data points (●), on the right represent the relaxation rates for unfolding (τ_{unf}). Both τ_2 and τ_{unf} show effects as a result of deleting the β -bulge. The relaxation times were determined by a global analysis of both stopped-flow and manual mixing kinetic data. All reactions were acquired at pH 6.5 and 25°C. The refolding data points are shown for Gdn-HCl jumps to concentrations less than 1.0M plotted from 0.2 to 1.0 M Gdn-HCl, while unfolding data points are for jumps to concentrations greater than 1.5M from 2.0M to 5.0M Gdn-HCl.

fluorescent phase, τ_1 , occurs with a relaxation time of 95 seconds and 138 seconds, for WT and bulge-less IL-1 β respectively, at 0.3M Gnd-HCl at pH 6.5 and 25°C. The right side of the chevron plot represents the unfolding region. From these plots it is apparent that removal of the β -bulge and insertion of the tight turn cause a decrease in the relaxation times for unfolding. Upon unfolding to 1.5M Gnd-HCl the relaxation times for wild type and bulge-less IL-1 β were 48.6 minutes and 14.9 minutes respectively. At 5M Gnd-HCl, the relaxation times obtained were 134 seconds and 59 seconds for wild type and bulge-less IL-1 β , respectively.

Discussion

In order to determine if the topological frustration in the folding of the trefoil family is associated with functionally important interaction sites, an IL-1 β construct was engineered with the functional loop swapped out for a turn. The β -bulge, found between strands 4 and 5 of IL-1 β , was replaced with a turn from IL-1ra. Theoretical models of the folding of IL-1 β suggested that the slow folding of the trefoil structure of IL-1 β is related to the formation of the β -bulge, which is functionally important and not conserved across the trefoil family. Although it is possible that the insertion of the IL-1ra tight turn into IL-1 β could induce strain into the fold and destabilize the protein or cause problems with the efficient folding of the protein by promoting aggregation and/or inhibiting folding, it has been shown in previous protein engineering experiments directed toward identifying receptor binding sites that the trefoil fold of IL-1 β is robust and can tolerate insertion/deletions and mutations in the β -bulge (131-134). In this

study, the deletion of the bulge resulted in a protein with a native global fold similar to WT IL-1 β , as demonstrated in the HSQC spectrum (Figure 5-2).

Triple resonance experiments were performed in order to confirm sequence-specific residue assignments for the bulge-deletion NMR spectra. From the HNCA spectra, residue-specific $^{13}\text{C}^{\alpha}$ chemical shifts were obtained and used as a barometer of secondary structure propensities (82, 103). Figure 5- demonstrates that most of the residue-specific deviations that indicate destabilized β -structure were seen at topologically equivalent sites at turns and hinge points. Residues that were determined to have stabilized β -structure occur mostly with those that participate in β -strand formation. This is particularly interesting as similar deviations were seen in all permutations (Chapter 3) and as well as in experiments detailing the modulation of the native basin of IL-1 β (76). These residues may represent critical points in the formation of the barrel or in maintaining the overall trefoil fold of the protein to salvage the proteins' functional purpose of receptor binding and signaling.

While the overall global fold and stability of the bulge-less variant appears similar to WT protein and the structural propensities for topologically important residues remains consistent, the pattern of hydrogen-deuterium native solvent exchange for the bulge-less protein shows local areas of lesser stability. . Areas that show these effects are located in β -strand 5, which follows the area associated with the functional loop, and topologically equivalent locations in trefoil subunit 1 and 3. The protein appears to “breathe” more, compared to WT, which may be a result of the robust β -trefoil topology maintaining the proteins' ability to bind to the receptor. The majority of

the differences appear away from the deletion site. This long-range transmission of effects of IL-1 β has been seen before in experiments investigating the role of H30. H30 is located on the surface of the molecule at one of the two distinct binding sites on IL-1 β (35). Mutants at position 30 substantially decreased the affinity of IL-1 β for the receptor, while maintaining the same global fold and the same folding mechanism. Comparison of the residue-specific hydrogen/deuterium solvent exchange between WT and H30 mutants showed transmission of local destabilization along the hydrogen bond network of the β -sheet (35). It has been hypothesized that the β -bulge in IL-1 β acts as “trigger” to induce the conformational change in the receptor and facilitate signaling (62).

The structural analysis of this chimera IL-1 β /IL-1ra shows similarities in global fold. Regions of the chimera “breathe” more than WT as a result swapping the β -bulge for a turn. The loop-swap results in faster formation of the intermediate and faster unfolding. These observed changes in rates of formation of the intermediate might be the result of less backtracking, and therefore a faster turnover of the intermediate species to the native. While the τ_3 phase is similar to WT, the accumulation of the intermediate is faster because less backtracking is occurring, resulting in a less complex folding mechanism. This is consistent with the theoretical hypothesis that multiple routes are traversed by IL-1 β on its energy landscape and are the result of a necessarily more complicated folding to conserve an important functional fold ((63, 127).

Taken together, the removal of the β -bulge demonstrates the robustness of the β -trefoil fold and the link of folding to function. While changes seen here correlate well

with theoretical simulations, further folding and biological experiments probing the loop swap in the 90's region, with and without the β -bulge, may further give further insight into the frustration that occurs during folding of IL-1 β .

Chapter 6

Capturing the Folding Moment: Folding/Backtracking and Refolding of Interleukin-1 β using Real-time NMR

Abstract

IL-1 β is a cytokine within the β -trefoil family. Data from our laboratories indicate that the folding/unfolding routes are rough. Follow-up theoretical studies predicted backtracking events that could contribute to the broad transition barrier and the experimentally observed long-lived intermediate. The backtracking route is attributed to the frustration introduced by the packing of the functional loop (the β -bulge, residues 47 to 53) to the nascent barrel. We employed real-time refolding NMR experiments to test for the presence of backtracking events predicted from our theoretical studies. Structural variants of IL-1 β , a β -bulge deletion and a circular permutation that opens the protein in the middle of the experimentally-observed kinetic intermediate, were also refolded and studied in order to determine the affects on the observed folding reactions. The functional loop deletion variant demonstrated less backtracking than in WT protein while the permutation still maintains backtracking in agreement with theoretical predictions. Taken together, these findings indicate that the backtracking results from geometric frustration introduced into the fold for functional purposes.

Introduction

The β -trefoil family of proteins has similar native conformations, fold slowly, and have been the subject of numerous experimental and theoretical folding studies (36#36, 41, 63, 135-139). IL-1 β is a cytokine within the b-trefoil family that has a global fold composed of a repeating trefoil unit ($\beta\beta\beta$ loop β -motif), forming a 6-stranded β -barrel pinned by three 2-stranded hairpin turns to form a “cap” closing one

end of the barrel (42)(Figure 6-1A and 6-1B). The functional loop, the β -bulge, is located between strands 4 and 5, as depicted. Experimental and theoretical data show that IL-1 β folds through an on-route intermediate ensemble characterized by the protection of β -strands 6 through 10 from hydrogen-deuterium exchange (33, 38, 46) (Figure 6-1A). Real-time NMR kinetic experiments of the denaturant-induced *unfolding* of interleukin-1 β revealed a rugged landscape where native-like turns were unexpectedly persistent and outlasted all other observed structural features (47).

Interestingly, theoretical *refolding* studies also indicate the presence of a rugged, broad barrier for the folding kinetics of β -trefoil proteins (36). Three major routes are populated during the refolding of the b-trefoil family, two of which are mostly observed with other members, e.g. FGF-1 and hisactophilin, the direct route and the ends-together route (Figure 6-2, see figure caption for details). While IL-1 β has not been observed experimentally to fold through the N- and C- termini ends-together route, we explored whether we could facilitate folding by the ends-together route by linking the N- and C-termini of WT IL-1 β and introducing new terminal ends, forming a circular permutation. Full denaturant dependent studies and comparisons of the observed perturbations in the folding and unfolding kinetics showed that circularly permutating IL-1 β affected the transition of the folding intermediate to the native ensemble. Variations in linker lengths of the circular permutation did not affect the intermediate and native state formation of the protein (see Chapter 4). In addition, simulations

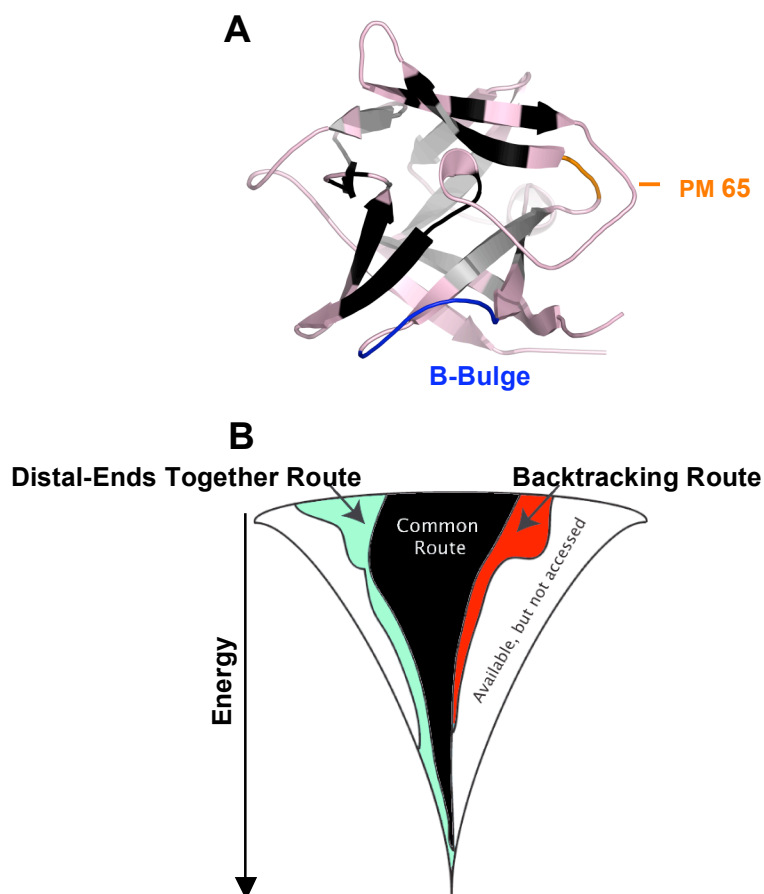


Figure 6-1: Representations of the IL-1 β and the theoretical folding routes of interleukin-1 β based on simulation data by Chavez et al., 2006.

(A) Ribbon diagram of IL-1 β demonstrating the areas of that are protected from hydrogen-deuterium exchange and are associated with the on-pathway intermediate. **Black** indicates areas of early protection while **grey** represents areas of late protection. **Blue** highlights the region in the protein referred to as the β -bulge while **orange** demonstrates the location of the cut-site for the circular permutation, PM65. (B) The energy landscape of the β -trefoils family. The proteins accesses one main route, initiating in the middle and one flanking trefoil. Nuances of topology or energetics may cause the early packing of the core to be problematic, which causes the main route to be less favorable and causes two routes, previously unnecessary, to be accessed. One of these routes bridges the distal ends of the protein together first and one backtracks.

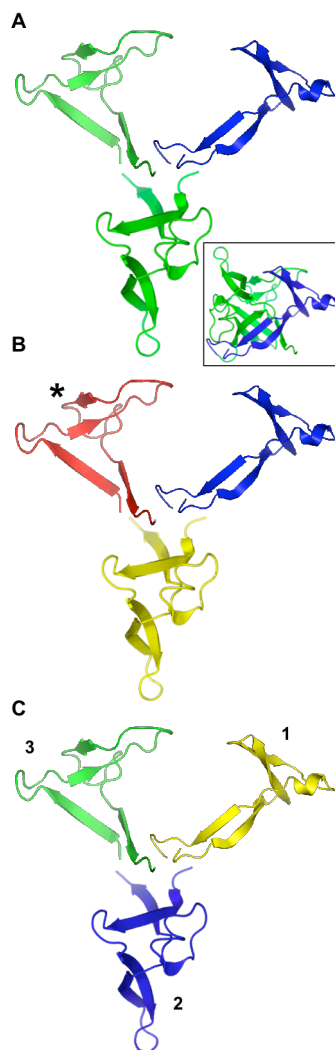


Figure 6-2: A visual representation of the multiple folding routes of interleukin-1 β based on simulation data by Chavez et al., 2006.

The proposed folding routes are depicted with colors to indicate the order by which the individual trefoil subunits fold to form the stable, 6-stranded barrel structure. **Green** indicates the area in which folding is initiated and folds earliest that initiates folding while **blue** indicates the area that folds last. (A) The direct route of folding where trefoil subunits 2 and 3 come in forming the barrel followed by trefoil 1, initiating the packing of the barrel and the cap into the native structure. Statistically, it is the least populated route. (Inset) The native structure of IL-1 β colored to demonstrate the folding sequence. (B) The backtracking route where subunit 3 (**red**) forms first, followed by local unfolding in that region and formation of trefoil 2. The folding then progresses where trefoil subunits 2 (**yellow**) and 3 (**blue**) come in forming the barrel followed by trefoil 1, initiating the packing of the barrel and the cap into the native structure. For clarity, an asterisk also indicates the red trefoil. (C) The ends-together route where trefoil subunit 3 initiates folding, followed by subunit 1, allowing the ends to form a stabilized barrel structure. Statistically, this is the most populated route. The folding route in B is unique to IL-1 β in the β -trefoil structural family. For clarity, the numbering of each subunit is indicated in Figure C.

suggest that IL-1 β folds by a unique backtracking route not seen in other members of the family. It has been suggested that the backtracking route occurs as a result of the topological frustration the functional β -bulge (residues 47 to 53) causes during folding (63). To test this hypothesis, we removed the β -bulge and compared the results of folding studies for this protein to those observed for WT and circular permutant proteins.

While not routine, real-time NMR spectroscopy has been used to follow the *unfolding* (47, 140-143) and the *refolding* (144, 145) of a few proteins which fold on an appropriate timescale. Given proper conditions, rapid mixing methods to initiate folding coupled with procedures to reduce the rate of protein folding have made it possible to follow protein folding by NMR on a timescale of seconds to hours, under conditions closely similar to those used for optical techniques (146).

We used real-time NMR methods to track the refolding of WT and mutant IL-1 β proteins. In agreement with theoretical predictions (36, 63), we show for the first time that IL-1 β , a topologically frustrated protein, undergoes backtracking during refolding. In contrast, the mutant protein (the bulge-less), designed to remove the predicted major functional loop responsible for the topological frustration (63), which leads to backtracking, does not show evidence for this behavior in our studies. Taken together, our experimental results support the hypothesis that topological frustration in folding may be introduced by necessary functional moieties and comes at the cost of highly efficient folding.

Special Methods

Cloning, Expression and Protein Purification

Cloning, expression, purification and purity of ^{15}N -enriched WT IL-1 β and IL-1 β variants followed protocols outlined in **GENERAL METHODS**.

Real-Time Refolding via NMR

^{15}N -enriched protein samples were unfolded in 100 mM sodium acetate- d_3 (Aldrich), 3M Gnd-HCl, pH 5.4 overnight. Refolding was initiated by dilution of the unfolded protein solution with 100mM sodium acetate- d_3 , 5% D_2O to a final concentration of 0.8M Gnd-HCl for WT IL- β and the bulge-deletion, and 0.6M Gnd-HCl for the circular permutation, and a final protein concentration of $\sim 11\text{mg/ml}$. Experiments were run at 22°C .

All NMR spectroscopy on ^{15}N -enriched IL-1 β , the bulge-less and circular permutant proteins were obtained on a Bruker DMX 500 NMR spectrometer, equipped with a triple-resonance gradient probe. Two-dimensional ^1H - ^{15}N heteronuclear single quantum coherence (HSQC) spectra were acquired as before (35, 47).

In order to acquire more data points during refolding, 1D ^1H spectra were serially acquired instead of 2D HSQC as in ref 14. To simplify the crowded protein spectrum, we used the 1D homonuclear equivalent of a refocused INEPT ^1H - ^{15}N experiment, which results in a spectrally-edited (147) INEPT transfers the magnetization from the ^1H nuclei to the ^{15}N and back again to ^1H , resulting in a proton spectrum of only the amide protons resonances and those of the side chain NH_2 . NH_2 resonance signals originating from residual denaturant, Gnd-HCl, were reduced by a selective 180° shifted Laminar pulse. The offset was set at -978 Hz and a Sinc1.1000

shape was used for the pulse. Pulse amplitude or power was selected to achieve the lowest intensity for the guanidine peak and to maximize amide proton signal intensities.

Sixty 1D INEPT spectra were collected after initiation of protein refolding with a dead time of 2 minutes. Individual spectrum acquisition time was 3 minutes and total run time was 182 minutes. Sequence-specific assignments for amide proton resonances were based on published work (47) and three-dimensional CBCA(CO)NH and HNCA spectra (148). Two-dimensional ^1H - ^{15}N HSQC spectra were processed using Felix 2004 software (MSI, San Diego, CA) while 1D INEPT spectra were processed using MetReC-Lite (Mestrelab Research SL, Spain).

Results and Discussion

NMR spectroscopy is useful tool for uncovering the presence of heterogeneous populations representing different folding ensembles of species during folding/unfolding of IL-1 β (38, 46, 47). While monitoring folding events using pulse-labeling hydrogen-deuterium exchange and NMR is an effective method for determining folding events at atomic resolution, the number of proteins that can be probed is limited by protein resonance assignments as well as whether the protein can tolerate the necessary sudden changes in pH for pulse-labeling. Oftentimes, aggregation is a problem, even for proteins who are well-behaved at neutral pH. To circumvent this problem, we chose to monitor *refolding* in chaotropic conditions where minimal aggregation occurs and the native fold remains intact. Figure 6-3 is an HSQC spectrum of WT IL-1 β at the completion of the refolding experiment in our final conditions for

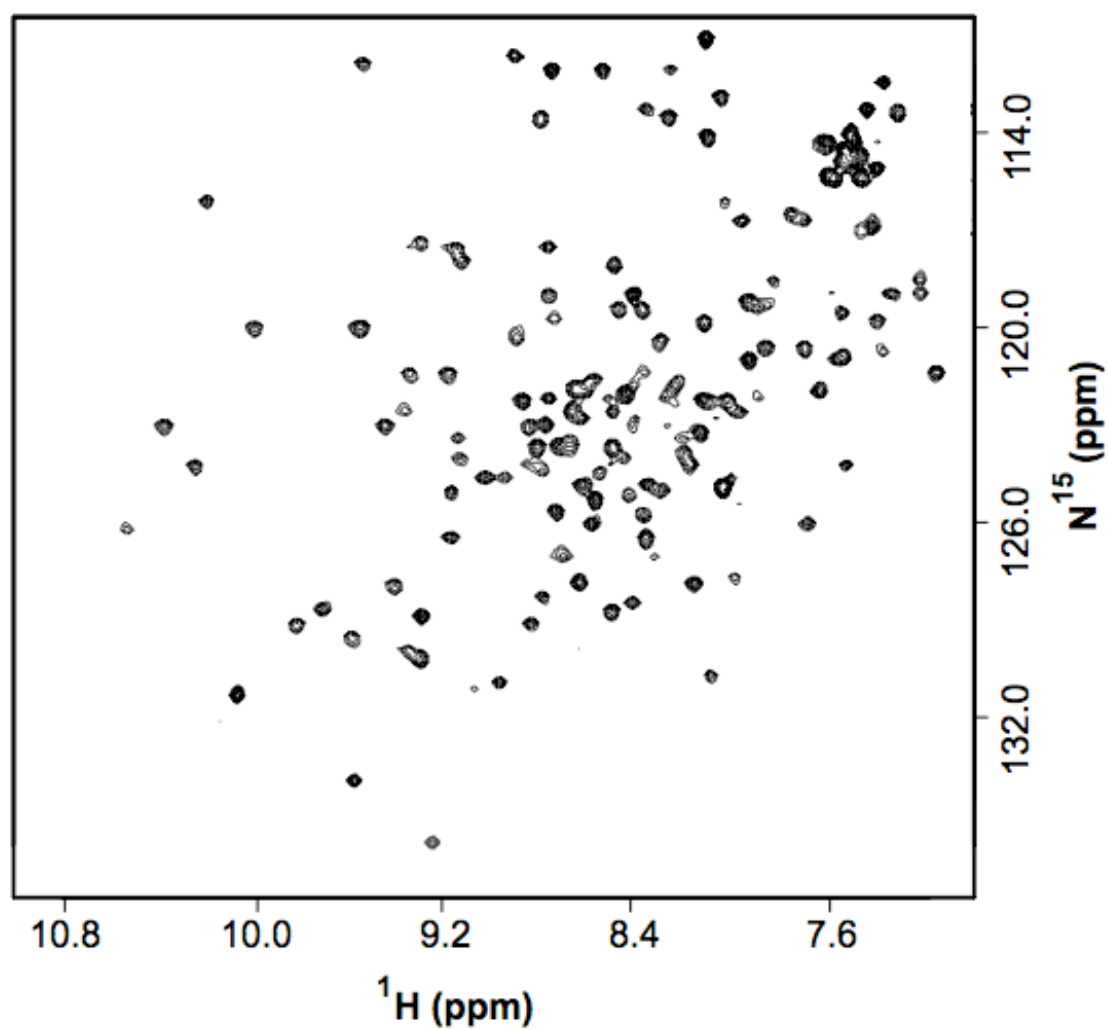


Figure 6-3: 2D representation of the final fold of WT IL-1 β in 0.8M Gnd-HCl.

A ^1H - ^{15}N HSQC of refolded IL-1 β in 0.8M Gnd-HCl at the completion of the refolding reaction. IL-1 β was unfolded in 3M Gnd-HCl, pH 5.4 overnight at 4°C. The refolding reaction was initiated by dilution to a final protein concentration of ~11mg/ml and 0.8M Gnd-HCl.

WT and mutant proteins. The overall chemical shift dispersion in the final refolded conditions of 0.8M Gnd-HCl is indicative of β -sheet tertiary structure and is very similar to the pattern exhibited by the native β -trefoil fold in the absence of denaturant (47) demonstrating a fully formed, natively folded protein. While fast 2D HSQC were sufficiently “quick” to follow real-time *unfolding*, more time resolution was needed for tracking the folding reaction, in particular, for detecting the presence of backtracking. Hence, we used 1D “versions” to gather more time points on a given time scale. Using ^{15}N -enriched proteins, we could use inept transfer to select for amide protons and increase sensitivity.

Unfolded protein was rapidly introduced in conditions that strongly favor the formation of the native protein and reduces the rate of protein folding to a timescale of tens of minutes, in order to follow refolding by NMR. Once refolding was initiated, backbone amide proton resonances were monitored by 1D homonuclear equivalent of a refocused INEPT ^1H - ^{15}N experiment (see **Special Methods**). The spectral data resulting from serial acquisition of 1D INEPT spectra during refolding is characterized by the formation of resonance peaks coming in and increasing over time (Figure 6-4) for all IL-1 β variants. The specific backbone amide proton resonances for residues N119, N102, and H30 of WT IL-1 β are highlighted in Figure 6-5A. These signals are well resolved and easy to follow over time. The signals appear early during the refolding reaction, followed by a fluctuation in intensities over time, until the peak intensities stabilize to that observed for the native protein under the final conditions. This behavior is consistent with the predicted backtracking route from theoretical studies (Figure 6-2B) where there is a rearrangement within the protein of some of the native contacts

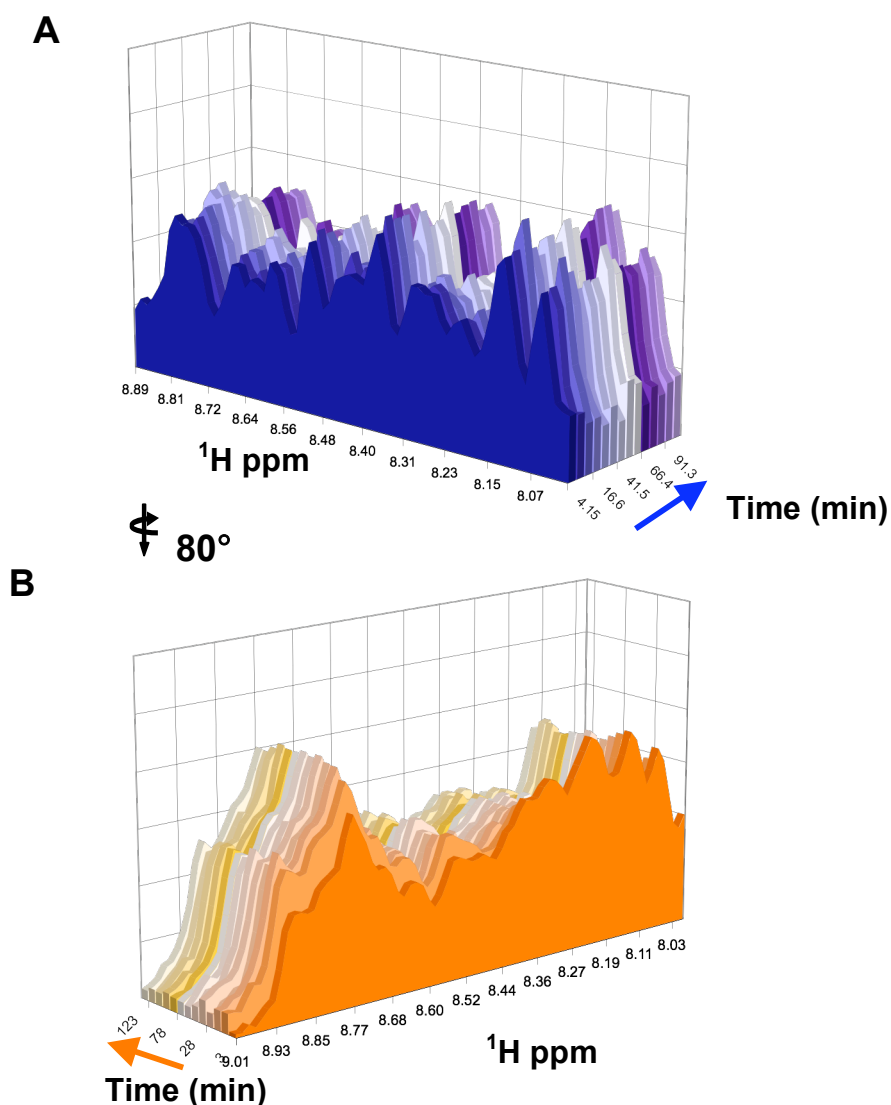


Figure 6-4: Schematic of serial 1D spectra representing the core resonances of the molecule during the refolding reaction for (A) WT IL-1 β and (B) the functional loop deletion construct of IL-1 β .

A series of 1D plots representing the refolding progression for (A) WT IL-1 β and (B) the bulge-deletion construct, rotated 80° about the y-axis to better illustrate the differences from WT. The series of traces illustrate peak intensities filling in as refolding progresses to completion. The **blue** and **orange** arrows indicate the direction of refolding from initiation to the completion of the refolding reaction.

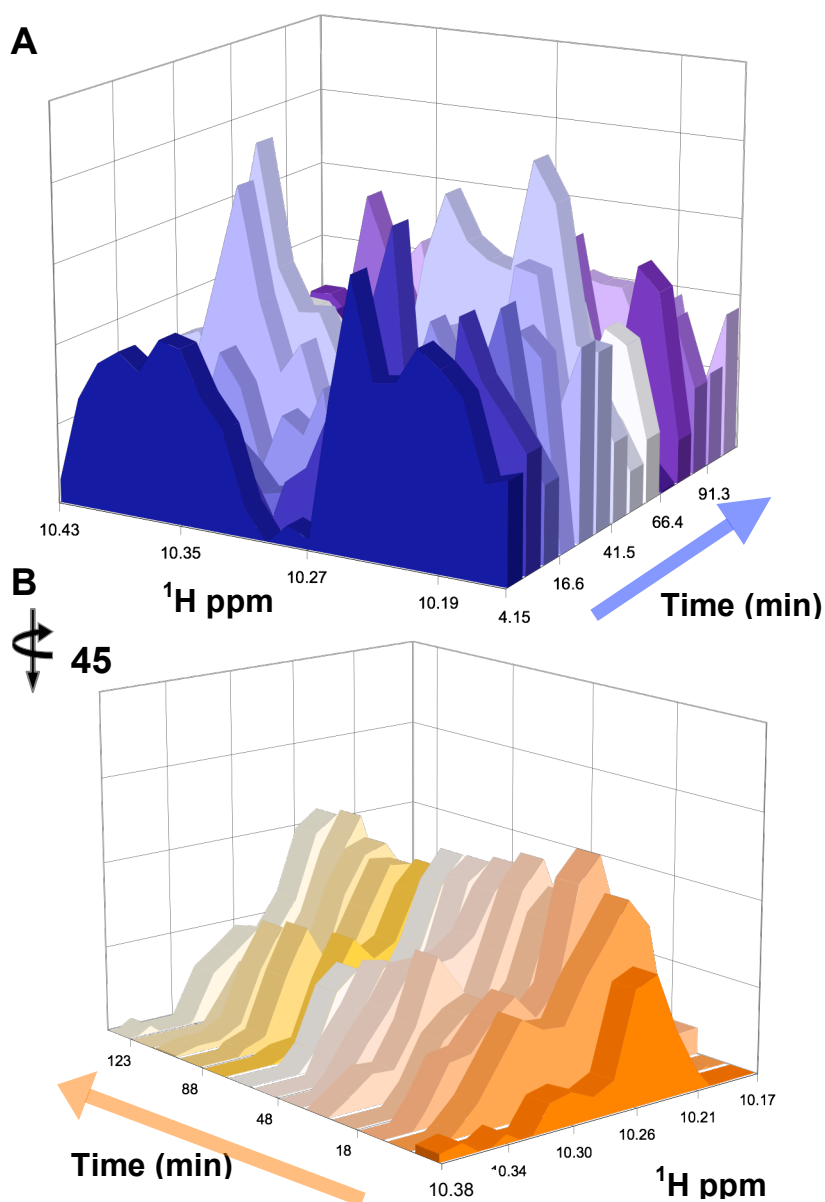


Figure 6-5: Time-dependent ^1H - ^{15}N spectral changes of representative regions in WT (blue) and in the bulge-less construct (orange) during the refolding.

(A) The 1D spectra of resonance peaks for WT IL-1 β for residues N119 at 10.18ppm, H30 at 10.23ppm, and N102 at 10.35ppm. The blue arrow indicates increasing time from the initiation of refolding to the completion of the refolding. (B) 1D spectra representing the same three amino resonances for the bulge deletion construct for residues H30 at 10.24ppm and the overlapping peak of N102 and N119 at 10.30ppm. The orange arrow indicates increasing time from the initiation of refolding to the completion of the refolding. For clarity, the orientation is rotated 45° from that of Figure A.

along the folding trajectory, causing specific contacts to unfold and refold before completing the refolding process (63). This rearrangement has a noticeable affect on the signal intensity of the peaks and is thought to occur in the vicinity of the functionally important b-bulge of IL-1 β that is not present in the other family members, even the highly conserved IL-1 β receptor antagonist protein.

A similar region of the spectra is given for the β -bulge-less variant in Figure 6-5B, rotated 45° from the orientation used for WT protein for clarity, as depicted. The series of 1D ^{15}N -HSQC spectra with resonances for N119, N102 and H30 gradually appear and peak intensities increase and then plateau over time, with significantly reduced fluctuations in intensities as compared to that observed for the WT protein (Figures 6-5A and 6-5B). We attribute these noticeable differences to the backtracking route, where unfolding and refolding of local contacts alter the intensities of the peaks, generating visible differences in the spectra. Taken together with theoretical predictions (36, 63), these results are consistent with the relationship between the geometrical frustration introduced by the β -bulge and the backtracking route (Figure 6-2).

While family members may prefer a certain route, small changes in energetics (coming from changes in pH, mutations, ionic strength, pressure *etc.*) may alter the road taken. This feature of the energy landscape leads to a certain robustness that still facilitates folding under diverse situations. However, introduction of specific functional units that lead to geometric frustration during folding can alter the energy landscape and impede fast folding. Figure 6-1B is a cartoon representation of the energy landscape observed for the folding of the b-trefoil family of proteins from simulated data (36, 63). Interestingly, hisactophilin, the simplest of the β -trefoil

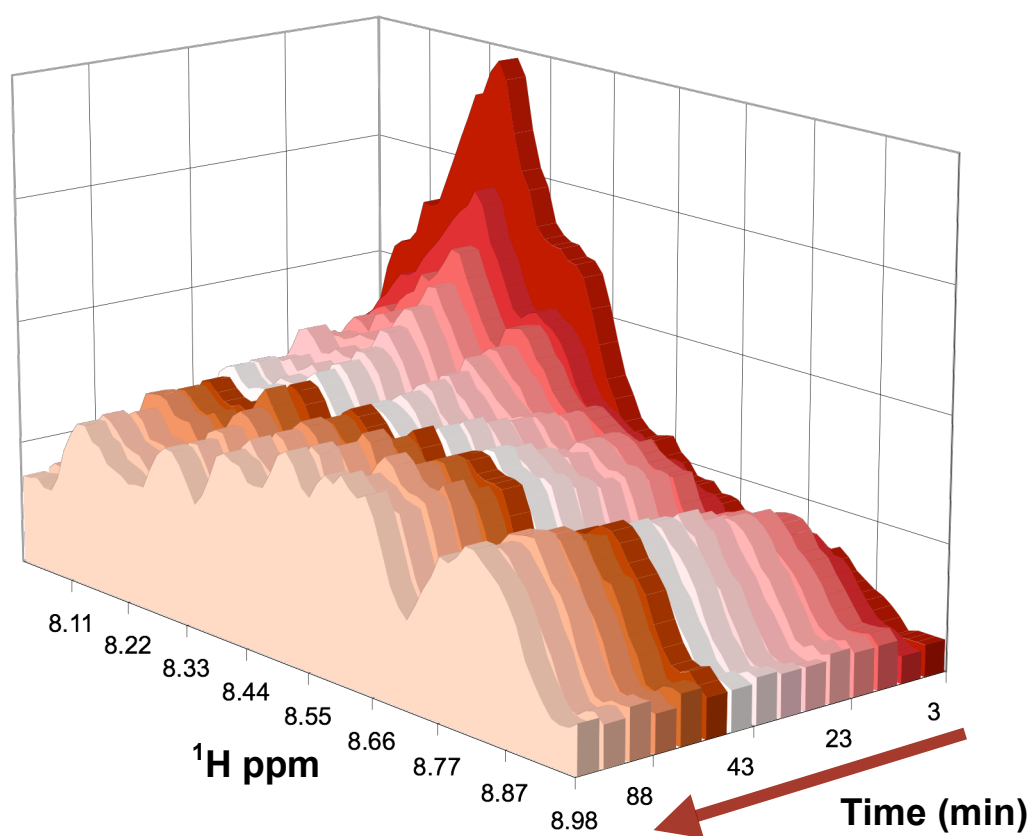


Figure 6-6: Schematic of serial 1D spectra representing the core resonances of the molecule during the refolding reaction for a permutation of the IL-1 β protein.

A series of 1D plots representing the refolding progression for a permutant variant of IL-1 β . The **dark red** arrow indicates the direction of refolding from initiation to the completion of the refolding reaction. The series of traces illustrate peak intensities filling in as refolding progresses to completion.

family proteins studied to date, folds the most efficiently and by the direct route, where the trefoil subunits fold in progression of one another (3-2-1 or 1-2-3). However, introduction of specific contacts in the simulations can lead to frustration in folding, not unlike that seen for the IL-1 β protein. Since topology determines which order of contact formations leads to the native state most efficiently, the chain connectivity and the distribution of contact lengths can make part of the energy landscape inaccessible and lead to a rerouting beyond a certain point (7, 14, 48, 55, 63, 112). As a result of linking the terminal ends of WT IL-1 β and introducing a new N- and C- termini, forming a circular permutation, the refolding NMR data indicates a noticeably slower progression to a fully refolded protein, while still sampling the backtracking route (data not shown). This is consistent with simulations showing that perturbations in the energetics of IL-1 β altered the dominant folding route where the overall landscape remained the same but the dominant route shifted to those routes previously less sampled (36).

While the permutant shows backtracking, similar to WT protein, and the bulge-less variant shows very little backtracking, it is important to note that this is a local, not global, phenomenon. Figure 6-6 shows representative spectra of a different part of the spectrum as a function of time highlighting the progressive formation of the native structure of the permutant IL-1 β . This progression to natively folded protein is consistent throughout the spectra of WT and bulge-less proteins as well (Figure 6-4). This is significant as it correlates with theoretical data indicating that particular regions of WT IL-1 β exhibit backtracking and not the entire protein.

Chapter 7

Conclusion

The question of how an unfolded polypeptide chain folds to a biologically active, three-dimensional structure has been the driving force of scientists interested in the protein-folding problem. A variety of techniques, both experimental and theoretical, have been used to address this complicated question. Techniques used to address the protein folding problem in this thesis, involved using circular permutations to probe native state topology. A major question addressed by this approach is the role that topology plays determining the kinetics and mechanism of folding for IL-1 β , a slow folding protein known to populate an intermediate during folding.

First, what, if any, changes would occur, topologically, upon circularly permutating IL-1 β ? Four permutant variants (PM23, PM65, PM76, PM142) with cut sites at loops and turns, folded into a native state similar to WT, while two variants (PM52, PM100) located in loops important for biological functioning, did not fold. Although the global fold was the same as WT, there were local structural changes regionally as well with individual residues at topological stress points throughout the native structure. Alterations occurred in regions scattered between the cap and β -barrel, but not within the β -barrel itself. Differences were also seen within the first trefoil subunit, proximal to the biologically relevant β -bulge loop, and within the 90's loop. This may be a result of conserving the β -barrel of the protein for bioactivity. Therefore, changing the connectivity did not affect the topology of IL-1 β .

Although the global fold of IL-1 β was unaffected by circular permutations, were there changes in the kinetic behavior or the in the mechanism of folding? Results demonstrate that altering the chain connectivity to a protein with a more complex fold has little effect on the overall fold, despite the overall thermodynamic stability of the

protein being reduced. The kinetic behavior of the folding of IL-1 β was altered as a result of the permutations. The slow phase, i.e. the transition from intermediate to the native state, exhibited the most change as a result of the primary structural frame shift rearrangement. This is in good agreement with theoretical simulations that indicate potential multiple folding routes in IL- β and thus the increased sampling of alternative folding routes on the same energy landscape as a result of the energy perturbations introduced (36), in this case, by changing the contact order.

Topological constraints on folding led to the question of possible biological functional constraints to folding. Comparison of the structures of the IL-1 β /receptor and IL-1ra/receptor complexes led to the proposal that binding to IL-1 β induces a conformational change in the receptor, which may help to trigger the signal cascade (61, 62) Simulations and experimental work combined show that slow folding of the IL-1 β trefoil structure is related to the formation of the biologically crucial β -bulge. Not only is the β -bulge of IL-1 β functionally important, it is not conserved across the β -trefoil family of proteins. In order to investigate the effects on mechanism and kinetics of folding of IL-1 β , the β -bulge was swapped out for a tight turn. While the global fold and stability in the bulge-less variant remained similar to WT, structural and stability differences were seen at residue-specific topological stress points throughout the protein. The folding of the bulge-less protein also indicated, in good agreement with the theoretical model (63), that the functional β -bulge may indeed be a source of the topological frustration in the folding landscape, and therefore frustrating the folding of IL-1 β .

Interestingly, these experiments revealed an intrinsic property within IL-1 β

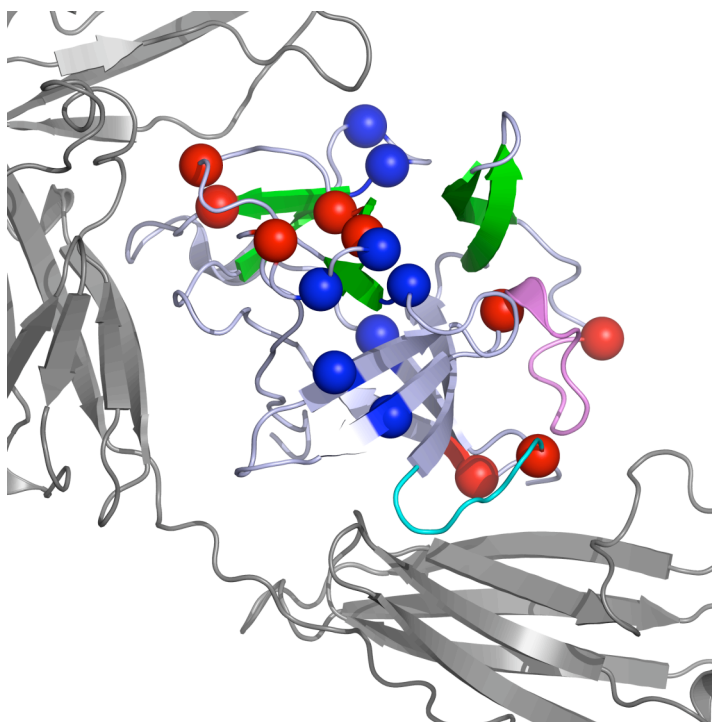


Figure 7-1: Representation of IL-1 β bond to the IL-1R1 receptor with ^{13}C chemical shift deviations highlighted, showing the potential biological relevance for these changes in IL-1 β constructs.

The depiction illustrates the orientation of the relative $^{13}\text{C}^\alpha$ chemical shifts with respect to IL-1 β 's interaction with the receptor. Red spheres indicate backbone residues that tended toward a destabilized native structure, while the blue indicate residues that are stabilized in the β -structure. Green depicts the location of the cap, while cyan and magenta indicate the location of both the functionally relevant loops

where similar residues within turns and loops act as topological stress points (Figure 7-1). Both with the circular permutations and the bulge-less variant, these turn residues appear to be responsible for dissipating the stress of the introduced change (i.e. linking the terminal ends and removing the functional loop). Similar compensatory structural effects at turns in very similar regions appear as a result of energetic perturbations under slightly destabilizing conditions to WT IL-1 β (76). The good agreement in that study between theoretical models and experimental solution results(76), along with the results within this thesis (Chapter 3 and Chapter 5), suggest that the distribution of structural heterogeneity induced by destabilizing conditions is largely determined by native-state topology(76) and function. Figure 7-1 highlights the importance of these stress points in maintaining the proper fit for the IL-1 β molecule within the binding pocket of the receptor.

Similarities were also found in the HDX data for all IL-1 β constructs, where local unfolding or more conformational sampling of the unfolded was isolated to the first trefoil subunit of IL-1 β . These similarities appear to also have biological relevance as trefoil subunit 1 is responsible for the interactions with the A binding site of the receptor and appears to be disordered upon binding to the receptor. Again, locally determined structural changes have biological relevance.

As a result of theoretical studies modeling backtracking in IL-1 β folding and hypothesizing that the cause is frustration introduced by the β -bulge, an NMR experiment was designed to probe for the backtracking effect(36, 63) along the folding pathway of IL-1 β , both in WT and bulge-less IL-1 β . This experimental study demonstrated the presence of backtracking in WT IL-1 β and the negligible presence of

it in the bulge-less construct. Again, theoretical (36, 63) and experimental studies were in good agreement.

Because of the continued success in coupling theoretical simulations with experimental results in order to better understand folding and function, further directions in research may focus on the other members of the IL-1 family of proteins, IL-1 α and the naturally occurring antagonist protein, IL-receptor antagonist, IL-1ra (149), as they are structurally related.

References

1. J. Juneja, J. B. Udgaonkar, *Curr. Sci* (Jan 1, 2003).
2. C. Levinthal, *J. Chim. Phys* (Jan 1, 1968).
3. A. Matouschek, A. R. Fersht, *Proc Natl Acad Sci U S A* **90**, 7814 (Aug 15, 1993).
4. J. N. Onuchic, N. D. Socci, Z. LutheySchulten, P. G. Wolynes, *Folding & Design* **1**, 441 (1996).
5. D. Baker, *Nature* **405**, 39 (May 4, 2000).
6. D. S. Riddle *et al.*, *Nature Structural Biology* **6**, 1016 (NOV, 1999).
7. A. R. Fersht, *Proceedings of the National Academy of Sciences of the United States of America* **97**, 1525 (Feb 15, 2000).
8. A. R. Fersht, *Curr Opin Struct Biol* **7**, 3 (Feb, 1997).
9. W. A. Eaton, V. Munoz, P. A. Thompson, C. K. Chan, J. Hofrichter, *Curr Opin Struct Biol* **7**, 10 (Feb, 1997).
10. G. A. Papoian, J. Ulander, P. G. Wolynes, *Journal of the American Chemical Society* **125**, 9170 (Jul 30, 2003).
11. H. Nymeyer, A. E. Garcia, J. N. Onuchic, *Proc Natl Acad Sci U S A* **95**, 5921 (May 26, 1998).
12. Y. Levy, P. G. Wolynes, J. N. Onuchic, *Proc Natl Acad Sci U S A* **101**, 511 (Jan 13, 2004).

13. N. Go, *Annu Rev Biophys Bioeng* **12**, 183 (1983).
14. N. Koga, S. Takada, *J Mol Biol* **313**, 171 (Oct 12, 2001).
15. C. Clementi, H. Nymeyer, J. N. Onuchic, *J Mol Biol* **298**, 937 (May 19, 2000).
16. M. S. Cheung, A. E. Garcia, J. N. Onuchic, *Proc Natl Acad Sci U S A* **99**, 685 (Jan 22, 2002).
17. R. E. Burton, G. S. Huang, M. A. Daugherty, T. L. Calderone, T. G. Oas, *Nature Structural Biology* **4**, 305 (Apr, 1997).
18. B. R. Simler, Y. Levy, J. N. Onuchic, C. R. Matthews, *Journal of Molecular Biology* **363**, 262 (Oct 13, 2006).
19. S. B. Ozkan, K. A. Dill, I. Bahar, *Protein Science* **11**, 1958 (Aug, 2002).
20. M. Panda, M. G. Benavides-Garcia, M. M. Pierce, B. T. Nall, *Protein Science* **9**, 536 (Mar, 2000).
21. M. Oliveberg, Y. J. Tan, M. Silow, A. R. Fersht, *Journal of Molecular Biology* **277**, 933 (Apr 10, 1998).
22. G. Srinivas, B. Bagchi, *Journal of Chemical Physics* **116**, 8579 (May 15, 2002).
23. G. Srinivas, B. Bagchi, *Current Science* **82**, 179 (Jan 25, 2002).
24. N. D. Socci, H. Nymeyer, J. N. Onuchic, *Physica D* **107**, 366 (Sep 1, 1997).

25. Y. Fukunishi, *Proteins-Structure Function and Genetics* **33**, 408 (Nov 15, 1998).
26. J. N. Onuchic, *Biophysical Journal* **88**, 186A (Jan, 2005).
27. P. G. Wolynes, *Quarterly Reviews of Biophysics* **38**, 405 (Nov, 2005).
28. R. Alsallaq, H. X. Zhou, *Biophysical Journal* **92**, 1486 (Mar 1, 2007).
29. A. Barzilai, S. Kumar, H. Wolfson, R. Nussinov, *Proteins-Structure Function and Genetics* **56**, 635 (Sep 1, 2004).
30. X. Yang, M. Wang, M. C. Fitzgerald, *Bioorg Chem* **32**, 438 (Oct, 2004).
31. N. Cremades, J. Sancho, E. Freire, *Trends Biochem Sci* **31**, 494 (Sep, 2006).
32. B. T. Andrews, A. R. Schoenfish, M. Roy, G. Waldo, P. A. Jennings, *J Mol Biol* **373**, 476 (Oct 19, 2007).
33. C. Clementi, P. A. Jennings, J. N. Onuchic, *Proc Natl Acad Sci U S A* **97**, 5871 (May 23, 2000).
34. D. K. Heidary, J. C. O'Neill, Jr., M. Roy, P. A. Jennings, *Proc Natl Acad Sci U S A* **97**, 5866 (May 23, 2000).
35. D. K. Heidary, M. Roy, G. O. Daumy, Y. Cong, P. A. Jennings, *Journal of Molecular Biology* **353**, 1187 (Nov 11, 2005).

36. L. L. Chavez, S. Gosavi, P. A. Jennings, J. N. Onuchic, *Proceedings of the National Academy of Sciences of the United States of America* **103**, 10254 (Jul 5, 2006).
37. C. L. Varley, B. L. Brown, N. Groome, P. R. M. Dobson, *Cytokine* **9**, 577 (AUG, 1997).
38. D. K. Heidary, L. A. Gross, M. Roy, P. A. Jennings, *Nature Structural Biology* **4**, 725 (Sep, 1997).
39. D. Samuel *et al.*, *Journal of Biological Chemistry* **276**, 4134 (FEB 9, 2001).
40. M. Blaber, J. DiSalvo, K. A. Thomas, *Biochemistry* **35**, 2086 (FEB 20, 1996).
41. C. S. Liu *et al.*, *Biochemistry* **40**, 3817 (APR 3, 2001).
42. A. G. Murzin, A. M. Lesk, C. Chothia, *J Mol Biol* **223**, 531 (Jan 20, 1992).
43. C. P. Ponting, R. B. Russell, *J Mol Biol* **302**, 1041 (Oct 6, 2000).
44. B. C. Finzel *et al.*, *Journal of Molecular Biology* **209**, 779 (Oct 20, 1989).
45. J. M. Finke, Thesis Ph D --University of California San Diego 2001 (2001).
46. P. Varley *et al.*, *Science* **260**, 1110 (May 21, 1993).
47. M. Roy, P. A. Jennings, *Journal of Molecular Biology* **328**, 693 (MAY 2, 2003).
48. K. W. Plaxco, K. T. Simons, D. Baker, *Journal of Molecular Biology* **277**, 985 (APR 10, 1998).

49. A. R. Viguera, L. Serrano, M. Wilmanns, *Nature Structural Biology* **3**, 874 (Oct, 1996).
50. A. R. Fersht, *Abstracts of Papers of the American Chemical Society* **219**, U283 (Mar 26, 2000).
51. D. N. Ivankov *et al.*, *Protein Science* **12**, 2057 (Sep, 2003).
52. T. R. Weikl, K. A. Dill, *Journal of Molecular Biology* **332**, 953 (SEP 26, 2003).
53. D. P. Goldenberg, T. E. Creighton, *J Mol Biol* **165**, 407 (Apr 5, 1983).
54. C. Clementi, P. A. Jennings, J. N. Onuchic, *J Mol Biol* **311**, 879 (Aug 24, 2001).
55. D. E. Otzen, A. R. Fersht, *Biochemistry* **37**, 8139 (Jun 2, 1998).
56. Y. Levy, J. N. Onuchic, *Acc Chem Res* **39**, 135 (Feb, 2006).
57. W. Y. Yang, M. Gruebele, *Nature* **423**, 193 (May 8, 2003).
58. B. K. Shoichet, W. A. Baase, R. Kuroki, B. W. Matthews, *Proc Natl Acad Sci U S A* **92**, 452 (Jan 17, 1995).
59. G. Schreiber, A. M. Buckle, A. R. Fersht, *Structure* **2**, 945 (Oct 15, 1994).
60. J. Kubelka, J. Hofrichter, W. A. Eaton, *Curr Opin Struct Biol* **14**, 76 (Feb, 2004).
61. G. P. Vigers, L. J. Anderson, P. Caffes, B. J. Brandhuber, *Nature* **386**, 190 (Mar 13, 1997).

62. H. Schreuder *et al.*, *Nature* **386**, 194 (Mar 13, 1997).
63. S. Gosavi, L. L. Chavez, P. A. Jennings, J. N. Onuchic, *Journal of Molecular Biology* **357**, 986 (Mar 31, 2006).
64. G. Venkataraman, R. Raman, V. Sasisekharan, R. Sasisekharan, *Proc Natl Acad Sci U S A* **96**, 3658 (Mar 30, 1999).
65. T. D. Pollard, S. Almo, S. Quirk, V. Vinson, E. E. Lattman, *Annu Rev Cell Biol* **10**, 207 (1994).
66. S. Jayaraman, S. Eswaramoorthy, D. Kumaran, S. Swaminathan, *Proteins-Structure Function and Genetics* **61**, 288 (Nov 1, 2005).
67. J. M. Finke, M. Roy, B. H. Zimm, P. A. Jennings, *Biochemistry* **39**, 575 (Jan 25, 2000).
68. J. C. Covalt, Jr., T. B. Cao, J. R. Magdaroag, L. A. Gross, P. A. Jennings, *Protein Expr Purif* **41**, 45 (May, 2005).
69. S. C. Gill, P. H. Vonhippel, *Analytical Biochemistry* **182**, 319 (Nov 1, 1989).
70. A. R. Rees, M. J. E. Sternberg, R. Wetzel, *Protein engineering : a practical approach*, The Practical approach series (IRL Press at Oxford University Press, Oxford ; New York, 1992), pp. xxv, 397.
71. J. C. Covalt, Jr., M. Roy, P. A. Jennings, *J Mol Biol* **307**, 657 (Mar 23, 2001).

- 72. D. K. Heidary, P. A. Jennings, *Journal of Molecular Biology* **316**, 789 (FEB 22, 2002).
- 73. J. M. Finke, P. A. Jennings, *Journal of Biological Physics* **27**, 119 (2001).
- 74. G. Bodenhausen, D. J. Ruben, *Chemical Physics Letters* **69**, 185 (1980).
- 75. S. Mori, C. Abeygunawardana, M. O. Johnson, P. C. M. Vanzijl, *Journal of Magnetic Resonance Series B* **108**, 94 (JUL, 1995).
- 76. M. Roy *et al.*, *Journal of Molecular Biology* **348**, 335 (Apr 29, 2005).
- 77. S. Grzesiek, A. Bax, *Journal of Biomolecular Nmr* **3**, 185 (Mar, 1993).
- 78. D. R. Muhandiram, L. E. Kay, *Journal of Magnetic Resonance Series B* **103**, 203 (Mar, 1994).
- 79. S. Grzesiek, M. Ikura, G. M. Clore, A. M. Gronenborn, A. Bax, *Journal of Magnetic Resonance* **96**, 215 (JAN, 1992).
- 80. P. C. Driscoll, G. M. Clore, D. Marion, P. T. Wingfield, A. M. Gronenborn, *Biochemistry* **29**, 3542 (APR 10, 1990).
- 81. G. M. Clore, A. Bax, P. C. Driscoll, P. T. Wingfield, A. M. Gronenborn, *Biochemistry* **29**, 8172 (SEP 4, 1990).
- 82. D. S. Wishart, B. D. Sykes, *Journal of Biomolecular Nmr* **4**, 171 (Mar, 1994).
- 83. D. S. Wishart *et al.*, *Journal of Biomolecular Nmr* **6**, 135 (SEP, 1995).

84. M. V. Berjanskii, S. Neal, D. S. Wishart, *Nucleic Acids Res* **34**, W63 (Jul 1, 2006).
85. B. A. Chrnyk, J. Evans, J. Lillquist, P. Young, R. Wetzel, *Journal of Biological Chemistry* **268**, 18053 (Aug 25, 1993).
86. D. W. Marquardt, *Journal of the Society for Industrial and Applied Mathematics* **11**, 431 (1963).
87. J. R. Knutson, J. M. Beechem, L. Brand, *Chemical Physics Letters* **102**, 501 (1983).
88. C. F. Bernasconi, *Relaxation kinetics* (Academic Press, New York, 1976), pp. xi, 288.
89. P. A. Jennings, S. M. Saalabethell, B. E. Finn, X. W. Chen, C. R. Matthews, *Methods in Enzymology* **202**, 113 (1991).
90. W. L. DeLano. (2002).
91. Y.-Z. Zhang, Thesis (Ph D in Biology), University of Pennsylvania, 1995. (1995).
92. R. A. Horlick *et al.*, *Protein Engineering* **5**, 427 (JUL, 1992).
93. J. e. a. Hennecke, (Feb 18, 1999).
94. M. Iwakura, T. Nakamura, C. Yamane, K. Maki, *Nature Structural Biology* **7**, 580 (JUL, 2000).

95. M. Iwakura, T. Takenawa, T. Nakamura, *Journal of Biochemistry* **124**, 769 (OCT, 1998).
96. J. C. Martinez *et al.*, *Biochemistry* **38**, 549 (JAN 12, 1999).
97. K. Maki, M. Iwakura, *Biophysical Journal* **78**, 293a (JAN, 2000).
98. M. Lindberg, J. Tangrot, M. Oliveberg, *Nature Structural Biology* **9**, 818 (NOV, 2002).
99. C. Lee, E. J. Seo, M. H. Yu, *Biochemical and Biophysical Research Communications* **287**, 636 (SEP 28, 2001).
100. Z. Qian, C. J. Fields, S. Lutz, in *Chembiochem.* (2007), vol. 8, pp. 1989-1996.
101. R. Graf, H. K. Schachman, *Proc Natl Acad Sci USA* **93**, 11591 (Oct 15, 1996).
102. D. S. Wishart, B. D. Sykes, *Nuclear Magnetic Resonance, Pt C* **239**, 363 (1994).
103. J. Yao, J. Chung, D. Eliezer, P. E. Wright, H. J. Dyson, *Biochemistry* **40**, 3561 (MAR 27, 2001).
104. A. K. E. Svensson, J. A. Zitzewitz, C. R. Matthews, V. F. Smith, *Protein Engineering Design and Selection* (Jan 1, 2006).
105. K. S. Kim, J. A. Fuchs, C. K. Woodward, *Biochemistry* **32**, 9600 (Sep 21, 1993).
106. K. W. Plaxco, K. T. Simons, I. Ruczinski, B. David, *Biochemistry* **39**, 11177 (SEP 19, 2000).

107. J. N. Onuchic, Z. Luthey-Schulten, P. G. Wolynes, *Annu Rev Phys Chem* **48**, 545 (1997).
108. S. B. Ozkan, I. Bahar, K. A. Dill, *Nature Structural Biology* **8**, 765 (Sep, 2001).
109. S. S. Plotkin, J. N. Onuchic, *Proceedings of the National Academy of Sciences of the United States of America* **97**, 6509 (Jun 6, 2000).
110. N. D. Socci, J. N. Onuchic, P. G. Wolynes, *Proteins-Structure Function and Bioinformatics* **32**, 136 (Aug 1, 1998).
111. P. G. Wolynes, *Philosophical Transactions of the Royal Society of London Series a-Mathematical Physical and Engineering Sciences* **363**, 453 (Feb 15, 2005).
112. F. Chiti *et al.*, *Nature Structural Biology* **6**, 1005 (NOV, 1999).
113. V. F. Smith, C. R. Matthews, *Protein Science* **10**, 116 (JAN, 2001).
114. G. Bulaj, R. E. Koehn, D. P. Goldenberg, *Protein Sci* **13**, 1182 (May, 2004).
115. A. V. Cheltsov, M. J. Barber, G. C. Ferreira, *J Biol Chem* **276**, 19141 (Jun 1, 2001).
116. J. Osuna, A. Perez-Blancas, X. Soberon, *Protein Engineering* **15**, 463 (Jun, 2002).
117. L. Li, E. I. Shakhnovich, *Journal of Molecular Biology* **306**, 121 (FEB 9, 2001).
118. U. Heinemann, M. Hahn, *Prog Biophys Mol Biol* **64**, 121 (1995).

- 119. A. V. Cheltsov, W. C. Guida, G. C. Ferreira, *J Biol Chem* **278**, 27945 (Jul 25, 2003).
- 120. M. C. Shastry, V. R. Agashe, J. B. Udgaonkar, *Protein Sci* **3**, 1409 (Sep, 1994).
- 121. P. A. Jennings, P. E. Wright, *Science* **262**, 892 (Nov 5, 1993).
- 122. J. E. Shea, J. N. Onuchic, C. L. Brooks, 3rd, *Proc Natl Acad Sci U S A* **99**, 16064 (Dec 10, 2002).
- 123. D. K. Klimov, D. Thirumalai, *Proc Natl Acad Sci U S A* **97**, 2544 (Mar 14, 2000).
- 124. K. A. Dill, H. S. Chan, *Nature Structural Biology* **4**, 10 (Jan, 1997).
- 125. P. E. Leopold, M. Montal, J. N. Onuchic, *Proc Natl Acad Sci U S A* **89**, 8721 (Sep 15, 1992).
- 126. J. D. Bryngelson, P. G. Wolynes, *Proc Natl Acad Sci U S A* **84**, 7524 (Nov, 1987).
- 127. P. W. Shachi Gosavi, Patricia Jennings, and Jose Onuchic, *Proc Natl Acad Sci U S A* (2007).
- 128. S. Gosavi, L. L. Chavez, P. A. Jennings, J. N. Onuchic, *J Mol Biol* **357**, 986 (Mar 31, 2006).
- 129. F. Delaglio *et al.*, *Journal of Biomolecular Nmr* **6**, 277 (Nov, 1995).

- 130. T. D. G. a. D. G. Kneller.
- 131. S. A. Greenfeder *et al.*, *J Biol Chem* **270**, 22460 (Sep 22, 1995).
- 132. A. J. Wolfson, M. Kanaoka, F. T. Lau, D. Ringe, *Protein Engineering* **4**, 313 (Feb, 1991).
- 133. A. J. Wolfson *et al.*, *Biochemistry* **32**, 5327 (May 25, 1993).
- 134. C. C. Arico-Muendel, A. Patera, T. C. Pochapsky, M. Kuti, A. J. Wolfson, *Protein Engineering* **12**, 189 (Mar, 1999).
- 135. Y. Chi *et al.*, *Biochemistry* **40**, 7746 (Jun 26, 2001).
- 136. S. Srisailam *et al.*, *Journal of Biological Chemistry* **278**, 17701 (May 16, 2003).
- 137. C. Liu, J. A. Gaspar, H. J. Wong, E. M. Meiering, *Protein Sci* **11**, 669 (Mar, 2002).
- 138. K. B. Murray, W. R. Taylor, J. M. Thornton, *Proteins-Structure Function and Genetics* **57**, 365 (Nov 1, 2004).
- 139. A. G. Murzin, A. M. Lesk, C. Chothia, *J Mol Biol* **236**, 1369 (Mar 11, 1994).
- 140. T. Kiefhaber, A. M. Labhardt, R. L. Baldwin, *Nature* **375**, 513 (Jun 8, 1995).
- 141. K. Akasaka, A. Naito, M. Imanari, *Journal of the American Chemical Society* **113**, 4688 (Jun 5, 1991).
- 142. M. Adler, H. A. Scheraga, *Biochemistry* **27**, 2471 (Apr 5, 1988).

- 143. C. Frieden, S. D. Hoeltzli, I. J. Ropson, *Protein Science* **2**, 2007 (Dec, 1993).
- 144. S. Koide, H. J. Dyson, P. E. Wright, *Biochemistry* **32**, 12299 (Nov 23, 1993).
- 145. P. Schanda, V. Forge, B. Brutscher, *Proceedings of the National Academy of Sciences of the United States of America* **104**, 11257 (Jul 3, 2007).
- 146. J. Balbach *et al.*, *Nature Structural Biology* **2**, 865 (Oct, 1995).
- 147. X. J. Miao, R. Freeman, *Journal of Magnetic Resonance Series A* **116**, 273 (1995).
- 148. J. Cavanagh, *Protein NMR spectroscopy : principles and practice* (Academic Press, San Diego, 1996), pp. xxiii, 587.
- 149. C. A. Dinarello, S. M. Wolff, *N Engl J Med* **328**, 106 (Jan 14, 1993).